THE UNIVERSITY
of EDINBURGH

Role of S-nitrosylation in plant salt stress

Nurun Nahar Fancy

Doctor of Philosophy

THE UNIVERSITY
of EDINBURGH

May 2017

Abstract

Salinity stress is one of the main challenges for crop growth and production. The estimated loss of crop yield due to salinity stress is up to 20% worldwide each year. Plants have evolved an array of mechanisms to defend themselves against salinity stress. A key aspect of plant responses to salinity stress is the engagement of a nitrosative burst that results in nitric oxide (NO) accumulation. A major mechanism for the transfer of NO bioactivity is S-nitrosylation which is a modification of the reactive thiol group of a rare but highly active cysteine residue within a protein through the addition of a NO moiety to generate an S-nitrosothiol (SNO). S-nitrosylation can result in altered structure, function and cellular localisation of a protein. Our findings suggest that S-nitrosylation is a key regulator of plant responses to salinity stress.

Glutathione (GSH), a tripeptide cellular antioxidant, is S-nitrosylated to form S-nitrosoglutathione (GSNO), which functions as a stable store of NO bioactivity. Cellular GSNO levels are directly controlled by S-nitrosoglutathione reductase (GSNOR), thereby, regulating global SNO levels indirectly. The absence of this gene results in high levels of SNOs. In *Arabidopsis*, previous research has shown that loss-of-function mutation in *GSNOR1* results in pathogen susceptibility (Feechan et al., 2005). In our study, we investigated salt tolerance in *gsnor1-3* plants. We have found that this line is salt sensitive at various stages of their life cycle. Interestingly, classical salt stress signalling pathways are fully functional in *gsnor1-3* plants. We have also explored non-classical pathways involved in salt tolerance. Autophagy is a cellular catabolic process which is involved in the recycling and degradation of unwanted cellular materials under stressed and non-stressed conditions. We have demonstrated that *gsnor1-3* plants have impaired autophagy during salt stress. An accumulation of the autophagy marker NBR1 supports the lack of autophagosome formation. We hypothesised

that S-nitrosylation might regulate upstream nodes of autophagosome formation.

Our study demonstrated that at least one key player involved in autophagosome biogenesis is regulated by S-nitrosylation. ATG7, an E1-like activating enzyme, which regulates ATG8-PE and ATG12-ATG5 ubiquitin like conjugation systems, is S-nitrosylated *in vitro* and *in vivo*. S-nitrosylation of ATG7 impairs its function *in vitro*. We showed that S-nitrosylation of ATG7 is mediated by GSNO. Interestingly, ATG7 is also transnitrosylated by thioredoxin (TRX), another important redox regulatory enzyme. We suggest that similar mechanisms might exist *in planta.* Finally, work in this study revealed that S-nitrosylation of Cys558 and Cys637 cause the inhibition of ATG7 function. In aggregate, this study revealed a novel mechanism for the redox-based regulation of autophagy during salt stress.

Lay Summary

Salt stress is one of the main threats to crop production. Plants possess a plethora of mechanisms to defend against salt stress. Among various mechanisms, plants deploy stress signalling by modifying protein molecules. One of the protein modifications is S-nitrosylation, a post-translational modification which involves the attachment of a nitric oxide group (NO) to the thiol (SH) group of a cysteine residue within a protein to generate an S-nitrosothiol (SNO). Another important mechanism involved in plant salt tolerance is autophagy, a cellular catabolic process which involves degradation of intracellular materials to recycle cellular nutrient. Work presented in this thesis revealed that S-nitrosylation plays an important role during plant salt stress. We have also demonstrated that autophagy is negatively regulated by S-nitrosylation of a core autophagy protein. In addition, the findings of this thesis can potentially be translated into crop plants and humans, as many of the mechanisms studied are conserved in other eukaryotes. Therefore, novel regulatory mechanisms uncovered in this work may provide benefits in the context of food security and biomedical applications.

Declaration

I hereby declare that except where explicitly stated in the text*, the work presented here is my own and has not been submitted in any form for any degree at this or any other university.

4th May 2017

Nurun Nahar Fancy

*Data shown in Figure 6-3B, Figure 6-4B and Figure 7-2 were produced by Ann-Kathrin Bahlmann (MSc project student). Permission has been gained for inclusion in this thesis.

Acknowledgements

Firstly, I would like to thank the Darwin Trust of Edinburgh for funding my PhD. My sincere thanks to Edinburgh Association of University Women for and the Charles Wallace Bangladesh Trust for financial support in the fourth year of my PhD.

My sincere thanks to my supervisor, Professor Gary Loake for his encouragement and support throughout my PhD.

I thank Professor Andrew Hudson, my second supervisor for his good advice that improved my research.

Thanks to all former and present members of the Loake lab, Manda, Adil, Priya, Eun-Jung, Wai, Kyonga, Yan, Minghui, Rabia, Rumana, Michael, Rafael, Suzy, Yuan, Beimi, Qiaona, Jibril, Samuel, Helmi, Akmal.

A very special thanks to Debbie for our friendship. Special thanks to Juan-Carlos for checking my thesis, Kalim for his valuable suggestions, Saima for all our scientific/non-scientific chatting over lunch, Marisol for your encouragement and moral support, Rice for that we grew up together as PhD students. Thanks to Shawkat, Tereza and Anka for helping me in my project work.

I thank to all the IMPS staff, without their help, we could not continue our research.

I would like to express my greatest gratitude to my husband Mahedi Hasan for all his support, encouragement and patience during this period and his immense help to run our family smoothly. The person without whom my life and PhD would have been meaningless is our loving daughter Maahnoor for being such a good kid.

I would like to thank my parents, my sister, my parents-in-law and their whole family for believing in me. Without their support, I would not be where I am now.

Finally, I would like to express my sincere gratitude to the Almighty Allah for blessing me with such good people around and giving me the strength to carry on my passion and dream.

Contents

List of Figures

List of Tables

Publication

List of abbreviations

ABA	Abscisic acid
ABF/AREB	ABRE binding factor/protein
ABRE	ABA responsive element
AD	Adenylation domain
AIM	ATG8-interacting motif
ANOVA	Analysis of variance
AP2/ERF	Apetala2/Ethylene response factor
APX	Ascorbate peroxidases
ATG	Autophagy
AVP	Vacuolar H^+-translocating pyrophosphatase
BST	Biotin switch technique
bZIP	Basic leucine zipper
CA	Concanamycin A
CAT	Catalases
CBF/DREB	C-repeat binding factors/ dehydration responsive element binding
CBL	Calcineurin B-like protein
CDPK	Calcium-dependent protein kinase
CIPK	CBL-interacting protein kinase
CL	Crossover loop
CTD	C-terminal domain
Cys	Cysteine
DTT	Dithiothreitol
ECTD	Extreme C-terminal ATG7-specific domain
FT-ICR	Fourier transform-ion cyclotron resonance
GABA	Gamma-aminobutyric acid
GPX	Glutathione peroxidase
GSH	Glutathione
GSNO	S-nitrosoglutathione
GSNOR	S-nitrosoglutathione (GSNO) reductase
GST	Glutathione S-transferase
H_2O_2	Hydrogen peroxide
HK1	Histidine kinase receptor protein
HKT	High-affinity K^+ transporter
HRP	Horseradish peroxidase.
IPTG	Isopropyl β-D-1-thiogalactopyranoside
KDa	Kilo Dalton
KORC	K^+ outward-rectifying conductance
LB	Luria-Bertani media
LEA	Late embryogenesis abundant
LTG	Lysotracker green

MBP	Maltose binding protein
MDC	Monodansylcadaverine
NaASC	Sodium ascorbate
NBR1	Neighbour of BRCA1
NEDD8	Neural precursor cell expressed, developmentally down-regulated8
nESI	Nano-electrospray ionisation
NHX	Na^+/H^+ exchanger
Ni:NOR	Nitrite:NO oxidoreductase
NO	Nitric oxide
NO_2^-	Nitrite
NO_3^-	Nitrate
NOA1	NO-Associated protein 1
NORC	Nonselective outward-rectifying conductance
NOS	NO synthase
NPR1	Nonexpressor of PR1
NR	Nitrate reductases
NSCC	Nonselective cation channel
NTD	N-terminal domain
NTRA	Thioredoxin reductase A
$O_2^{\bullet-}$	Superoxide radicals
$OH^{\bullet}$	Hydroxyl radicals
$ONOO^-$	Peroxynitrite
OST1/SnRK2.6	Open stomata 1/SNF1-related protein kinase 2.6
OTS1/2	Overly tolerant to salt 1/2
P5CS1	Δ-1-pyrroline-5-carboxylate synthetase
PAD2	Phytoalexin deficient 2
PAGE	Polyacrylamide gel electrophoresis
PAS	Pre-autophagosomal structure
PE	Phosphatidylethanolamine
PLP	Pyridoxal-5-phosphate
PM-NR	Plasma membrane-bound NR
PP2C	Protein phosphatase 2C
PTM	Post-translational modification
RD22	Responsive to dehydration 22
RNS	Reactive nitrogen species
ROS	Reactive oxygen species
SA	Salicylic acid
SAE1/SAE2	SUMO activating enzyme 1/ SUMO activating enzyme 2
SDS	Sodium dodecyl sulphate
SEM	Standard error of mean
SNF1	Sucrose non-fermenting 1
SNO	S-nitrosothiol
SOD	Superoxide dismutase

SOS	Salt overly sensitive
SUMO	Small ubiquitin-like modifier
TF	Transcription factors
TRXh5	Thioredoxin h5
TSPO	Tryptophan-rich sensory protein/translocator
Ub	Ubiquitin
Ubl	Ubiquitination like
UBP16	Ubiquitin-specific protease 16
VTC2	Vitamin C2
XDH	Xanthine dehydrogenase/oxidase

Chapter-1

1 Introduction

1.1 *Arabidopsis thaliana* as a model plant

Arabidopsis thaliana is currently the most widely used model organism in plant biology. It is a small flowering plant and a member of the *Brassicaceae* family, which includes other cultivated species such as mustard, cabbage and radish (Al-Shehbaz and O'Kane, 2002; Pigliucci, 2002). Although of no major agronomic value, *Arabidopsis* offers important advantages for basic research in genetics and molecular biology because of having a relatively small genome, rapid reproduction, ease of cultivation and diploid nature. Also, the 125 Mb has been sequenced and annotated (The Arabidopsis Genome Initiative, 2000) and extensive genetic and physical maps of all five chromosomes are now available. Furthermore, the life cycle is short about eight weeks from germination to seed maturation (Koornneef and Meinke, 2010). Seed production is prolific and the plant can easily be cultivated in restricted space using limited resources. *Arabidopsis* can be efficiently transformed utilising *Agrobacterium tumefaciens* using varying techniques among which the most common is the floral dip method (Bechtold and Pelletier, 1998; Clough and Bent, 1998). Providentially, a large number of mutant lines and genomic resources are already available for this plant. Such advantages have made *Arabidopsis* a model organism for studies of the cellular and molecular biology of flowering plants especially dicots. The Arabidopsis Information Resource (TAIR) is a common platform for collecting and making available much of the information arising from research on *Arabidopsis* (https://www.arabidopsis.org/index.jsp).

1.2 Plant abiotic stress

Crop productivity is affected by various abiotic stresses such as high salinity, drought, high temperature and low temperature (Nakashima et al., 2009). The estimated yield loss per annum ranges from 51% to 82% worldwide due to abiotic stresses (Athar and Ashraf, 2009). To survive, plants respond to these stresses at the biochemical, molecular, cellular and physiological level employing a complex network for perception and transmission of stress signals to initiate cellular responses through changes in gene expression, enzyme activity and transport of molecules across membranes (Boyer, 1982; Mittler, 2006; Nakashima et al., 2009). The perception of a stress signal induces the expression of a variety of genes in plants (Bartels and Sunkar, 2005; Kreps et al., 2002). The products of these genes are thought to maintain cellular stability, promote stress tolerance and regulate gene expression through signal transduction pathways during stress (Shinozaki et al., 2003).

1.3 Salinity, ionic and osmotic stress in plants

Salinity stress is one of the most serious limiting factors for crop growth and production in arid regions. Estimated losses of crop yield due to salt stress are about 20% worldwide each year (Athar and Ashraf, 2009). About 23% of the world's cultivated land is saline and 37% is sodic (Khan and Duke, 2001). Salt-affected soils contain sufficient concentrations of soluble salts to reduce the growth of most plant species. In this context, salt-tolerant plants have evolved to grow on these soils with a wide range of adaptations. However, most agronomic important crops are salt-sensitive (Tester and Davenport, 2003).

High salinity affects plants in two distinct phases- osmotic and ionic stress. Firstly, high concentrations of salts in the soil disturb the capacity of roots to extract water and high concentrations of salts within the plant itself is toxic (Munns and Tester, 2008). Together, these effects reduce plant growth, development, yield and survival. During initial exposure to

salinity, plants experience water stress due to osmotic shock, which in turn reduces the expansion of growing leaf and decrease the emergence of new leaves. Thus, the initial response due to osmotic shock is immediate and severe. During long-term exposure to salinity, plants experience ionic stress, which can lead to premature senescence of adult leaves and thus a reduction in the photosynthetic area available to support continual growth (Läuchli and Grattan, 2007). High salt concentrations, usually sodium chloride, cause osmotic stress by decreasing water potential within the plant, which immediately causes stomatal closure and reduces cell expansion in young leaves and root tips. Subsequently, ions, in particular, sodium (Na^+), accumulate in the leaf blade and in the photosynthetic tissues, affecting photosynthetic components such as enzymes, chlorophylls, and carotenoids. These effects, in turn, lead to secondary stresses such as oxidative stress and nutritional disorders (Parihar et al., 2015).

1.3.1 Salt stress sensing and signalling

In the context of NaCl stress, plants have developed sensory mechanisms for both the osmotic component and the ionic component, specifically Na^+, of the stress. Though it is evident that these sensory components are distinct, the molecular elements are yet to be identified. One possible candidate for an osmotic sensor in *Arabidopsis* is the histidine kinase receptor protein HK1 which senses changes in osmolarity in cells caused by external stimuli and subsequently transduces the stress signals through a protein phosphorylation cascade (Tran et al., 2007; Urao et al., 1999). Plants show a rapid increase in cytosolic calcium ion (Ca^{2+}) levels, which act as a second messenger, within seconds of NaCl or mannitol exposure indicating that Ca^{2+} channels might be coupled with osmotic sensors (Knight et al., 1997). Recently, a hyperosmolality-gated calcium-permeable channel OSCA1 was discovered in a genetic screen in *Arabidopsis* which functions in osmosensing and is responsible for $[Ca^{2+}]_i$

increases induced by external stimuli in plants (Yuan et al., 2014). Other second messengers such as reactive oxygens species (ROS) and reactive nitrogen species (RNS) are also salt and osmotic stress inducible and are linked to Ca^{2+} signalling (Tuteja and Sopory, 2008; Jiang et al., 2013). Increased Ca^{2+} levels further activate downstream kinases including calcium-dependent protein kinases (CDPKs), calcineurin B-like proteins (CBLs) and CBL-interacting protein kinases (CIPKs). In addition, the cuticle is thought to function as an osmotic stress signalling mediator that induces abscisic acid (ABA) biosynthesis (Wang et al., 2011) (**Fig. 1-1A**).

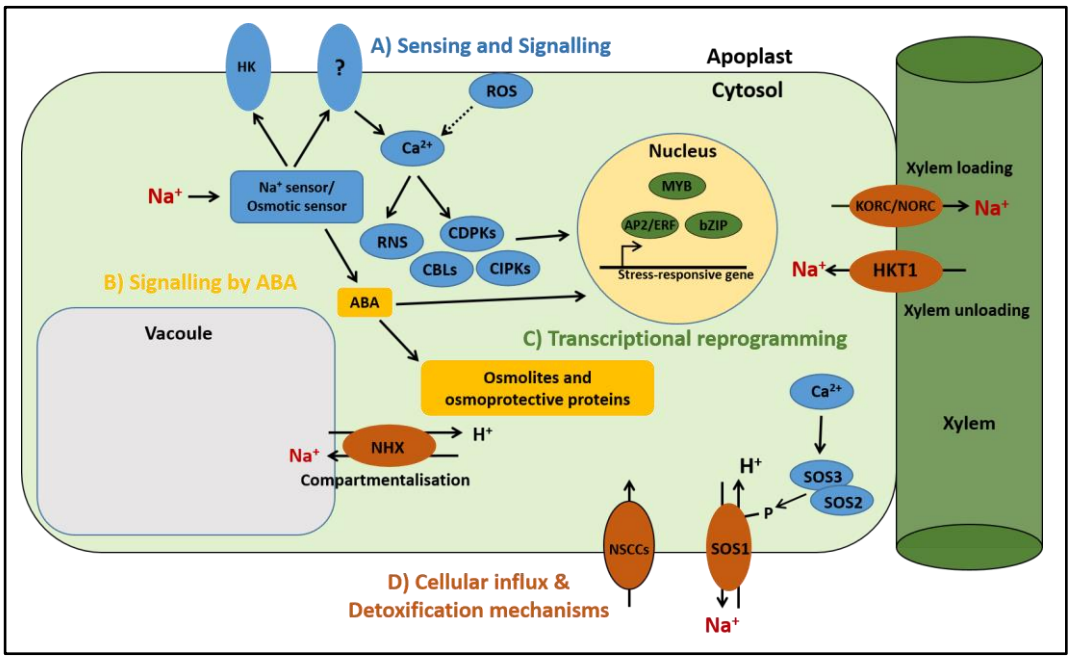

Figure 1-1. Schematic diagram of components of the salt stress response mechanisms in plant root cells.

A) Na^+ enters the cell via NSCCs and is sensed by an unidentified sensory mechanism. At the next step, Ca^{2+}, ROS, RNS and hormone signalling cascades are activated. CDPKs, CBLs and CIPKs are part of the Ca^{2+} signalling pathway, which can alter the global transcriptional profile of the plant. **B)** ABA biosynthesis is induced upon salt stress which regulates the production of osmolites and osmoprotective proteins as well as transcriptional reprogramming. **C)** Members of several transcription factor families are expressed differentially modulating expression of important stress-responsive genes. **D**) Finally, these early signalling pathways

result in expression and activation of cellular detoxification mechanisms, including HKT, NHX, and the SOS Na^+ transport mechanisms as well as osmotic protection strategies. ABA, abscisic acid; HK, histidine kinase; NSCCs, nonselective cation channels; ROS, reactive oxygen species; RNS, reactive nitrogen species, CDPKs, calcium-dependent protein kinases; CBLs, calcineurin B-like proteins; CIPKs, CBL-interacting protein kinases; AP2/ERF, Apetala2/Ethylene response factor; bZIP, basic leucine zipper; NHX, Na^+/H^+ exchanger; SOS, Salt overly sensitive; HKT, high-affinity K^+ transporter; KORC, K^+ outward-rectifying conductance; NORC, nonselective outward-rectifying conductance. Adapted and modified from (Deinlein et al., 2014).

1.3.2 Regulation by abscisic acid (ABA)

Salinity leads to abscisic acid (ABA) accumulation which is mediated by induction of ABA biosynthesis genes and suppression of ABA degradation (Zhu, 2002). The plant cuticle was shown to induce ABA biosynthesis and signalling during osmotic stress (Wang et al., 2011). Changes in the ABA levels regulate stomatal closure, water loss, lateral root elongation and induce the biosynthesis of osmolytes and osmoprotective proteins (**Fig. 1-1B**) (Zhu, 2002). These are simple sugars (mainly fructose and glucose), complex sugars (trehalose, raffinose, and fructans), quaternary ammonium derivatives (glycine betaine, β-alanine betaine, proline betaine) and amino acids (proline, GABA(gamma-aminobutyric acid), alanine), polyamines and proteins from the late embryogenesis abundant (LEA) superfamily (Zhu, 2001; Deinlein et al., 2014). These molecules have the capacity to maintain low intracellular osmotic potential, scavenge ROS and preserve the activity of enzymes with minimal effect on pH or charge balance (Bohnert and Jensen, 1996; Deinlein et al., 2014). In this context, a loss-of-function mutation in proline biosynthetic gene *Arabidopsis P5CS1* (*Δ-1-pyrroline-5-carboxylate synthetase*), confers salt hypersensitivity (Deinlein et al., 2014).

1.3.3 Transcriptional reprogramming during salt stress

It is evident that salt-responsive genes are under complex regulation. These genes can be categorised depending on their induction pattern. Early-response genes constitute genes

which are induced very quickly often within minutes of stress perception. On the other hand, delayed-response genes include genes that are activated within hours of stress perception. Usually, the early-response genes encode transcription factors (TF) that activate downstream delayed-response genes (Zhu, 2002). Early-response genes include CBF/DREB (C-repeat binding factors/dehydration responsive element binding) (AP2, apetala2 family), RD22 (responsive to dehydration 22) (MYC family), MYBs (myeloblastosis) and ABF/AREB (ABRE-binding factor/protein where ABRE, ABA-responsive element) (bZIP, basic leucine zipper family) while RD29 is a delayed response gene. These genes are all rapidly induced by both ABA-dependent or ABA-independent mechanisms during stress (**Fig. 1-1C**) (Nakashima et al., 2009).

1.3.4 Na^+/K^+ homeostasis

Plants deal with salinity and associated ion toxicity by various detoxification processes to re-establish normal cellular functions (Deinlein et al., 2014). Salt-tolerant plants differ from salt-sensitive ones by having a low rate of Na^+ and Cl^- transport to leaves. The ability to compartmentalise these ions into vacuoles is another way to prevent their build-up in the cytoplasm and thus avoid salt toxicity (Munns and Tester, 2008).

Na^+ influx into root cells occurs via nutrient channels and transporters including calcium-permeable nonselective cation channels (NSCCs), class I HKT (high-affinity K^+ transporter) and cation/H^+ antiporter. On the other hand, xylem loading of Na^+ from stellar cells is controlled by outward-rectifying K^+ channels KORC (K^+ outward-rectifying conductance) and NORC (nonselective outward-rectifying conductance) before being transported to aerial plant tissues (**Fig. 1-1D**). Salt tolerance involves the maintenance of K^+ level and distribution thereby balancing the toxic effects of Na^+ accumulation. Thus, manipulation of Na^+/K^+ influx/efflux mechanisms may provide significant insight into

generating salt tolerant plant.

One of the most important components in Na^+/ K^+ homoeostasis is HKT which plays a major role in root-to-shoot Na^+ partitioning. HKTs are categorised into two distinct subgroups, class I and II which regulate largely Na^+-selective transport and Na^+-K^+ co-transport respectively (Platten et al., 2006). Loss-of-function mutation in *AtHKT1;1*, a class I HKT, was shown to cause Na^+ overaccumulation and hypersensitivity in leaves but a reduction in root Na^+ during salt stress (Rus et al., 2001; Berthomieu et al., 2003; Mäser et al., 2002). Recently, it has been confirmed that AtHKT1;1 is involved in Na^+ unloading from the xylem and influx into root cells, reducing the net Na^+ influx into the shoot, thereby protecting leaves from Na^+ toxicity (**Fig. 1-1D**) (Davenport et al., 2007). *AtHKT1;1* expression can be regulated negatively by plant hormone cytokinin and the ABI4 (ABA-insensitive4) transcription factor (Mason et al., 2010; Shkolnik-Inbar et al., 2013). In aggregate, xylem parenchyma-localized class I HKT transporters confer salt tolerance by protecting photosynthetic organs from Na^+ accumulation.

During salt stress, ion homoeostasis is mediated by a Salt Overly Sensitive (SOS) signal pathway (**Fig. 1-1D**). The SOS pathway components were first discovered in *Arabidopsis* constituting three main proteins. *SOS1* encodes a plasma membrane Na^+/H^+ antiporter which plays a critical role in sodium extrusion (Shi et al., 2002a). The mechanism involves sensing of the salinity stress by SOS1 antiporter after the increase of cytosolic Ca^{2+}, reversible phosphorylation and protein interactions with other two proteins known as SOS2 and SOS3. *SOS3* encodes a calcineurin B-like (CBL) protein, a Ca^{2+} -binding protein that functions as a calcium sensor for salt tolerance. *SOS2* encodes a Serine/Threonine (Ser/Thr) protein kinase known as the CBL-interacting protein kinase (CIPK). Salt stress elicits a transient increase of Ca^{2+} that is sensed by SOS3 then SOS2 interacts with and is activated by SOS3 (Liu et al., 2000;

Halfter et al., 2000). The SOS2/SOS3 kinase complex phosphorylates and activates SOS1. The full activity of SOS1 depends on the SOS2/SOS3 complex (Zhu, 2002). Overexpression of *Arabidopsis* plasma membrane Na^+/H^+ antiporter *SOS1* was shown to improve plant tolerance to salt by limiting Na^+ accumulation (Shi et al., 2003). Recently, *SOS4* and *SOS5* have also been identified and characterised. *SOS4* encodes a pyridoxal (PL) kinase that is involved in the biosynthesis of pyridoxal-5-phosphate (PLP), an active form of vitamin B6 (Shi et al., 2002b). SOS5 has been shown to be a putative cell surface adhesion protein that is required for normal cell expansion. Under salt stress, the normal growth and expansion of a plant cell become even more important and SOS5 helps in the maintenance of cell wall integrity and architecture (Mahajan et al., 2008). In addition, other Na^+ efflux mechanisms may exist particularly Na^+-translocating ATPase which is found only in bryophytes but absent in flowering plants (Munns and Tester, 2008; Rodríguez-Navarro and Benito, 2010).

The compartmentalization of Na^+ into vacuoles provides an efficient mechanism to minimise the toxic effect of Na^+ in the cytosol. The transport of Na^+ into vacuoles is mediated by NHX1 (Na^+/H^+ exchanger), a vacuolar Na^+/H^+ antiporter (**Fig. 1-1D**) by using the electrochemical gradient of protons (H^+) generated by the vacuolar H^+-translocating enzymes, H^+-ATPase and H^+-pyrophosphatase (PP_iase). Na^+ can be passively leaked into the cytosol from vacuoles, possibly via tonoplast nonselective cation channels, requiring constant resequestration of Na^+ into vacuoles. In this context, the overexpression of *AtNHX1* resulted in transgenic *Arabidopsis* that were able to grow in a high salt concentration possibly due to higher Na^+ translocation into vacuoles (Apse et al., 1999). Further, leakage of Na^+ from vacuoles back to the cytosol can be minimised by vacuolar H^+-translocating pyrophosphatase (AVP), which can generate a H^+ gradient across the vacuolar membrane, in turn increasing the pumping of Na^+ into the vacuole by NHX1 (Munns and Tester, 2008).

1.3.5 ROS and RNS production during salt stress and cellular antioxidant systems

A secondary aspect of salt stress is the production of ROS, including superoxide radicals ($O_2^{\bullet -}$), hydrogen peroxide (H_2O_2), and hydroxyl radicals ($OH^{\bullet}$). ROS may be a product of chloroplast and mitochondrial metabolism during stress and can also be produced by other processes. ROS cause oxidative damage to cellular components (Halliwell and Gutteridge 1986). Plants use low molecular mass antioxidants such as ascorbic acid and reduced glutathione (GSH) and employ a diverse array of enzymes such as superoxide dismutase (SOD), catalases (CAT), ascorbate peroxidases (APX), glutathione S-transferase (GST), and glutathione peroxidase (GPX) to scavenge ROS. Transgenic tobacco plants overexpressing both GST and GPX displayed improved seed germination and seedling growth under salt stress (Apse and Blumwald, 2002).

Another important aspect of salt stress is the production of RNS, specifically, nitric oxide (NO) which has emerged as an important molecule in plant salt stress responses. The role of NO during salt stress will be discussed in details in later sections of this chapter.

1.3.6 Other regulatory mechanisms

Other less explored but notable mechanisms in salt tolerance involve post-translational modifications (PTM): phosphorylation, ubiquitination and SUMOylation. MAPK (mitogen-activated protein kinase) cascade includes three sequential molecular components to regulate phosphorylation: MAPK kinase kinase (MAPKKK), MAPK kinase (MAPKK) and MAP kinase (MAPK). Salinity or high-osmolarity-induced MAPK cascade has been shown to be involved in cell wall biosynthesis and cell growth and differentiation during salt stress (Parihar et al., 2015). *Ubiquitin-specific protease16 (UBP16)* has also been shown to be involved in salt tolerance. An absence of UBP16 function results in Na^+ accumulation in leaf tissue leading to salt hypersensitivity suggesting a role for ubiquitinylation and deubiquitinylation in salt

tolerance (Deinlein et al., 2014). Similarly, deSUMOylation by SUMO protease OTS1/2 (overly tolerant to salt1/2) was shown to be significant for salt tolerance by maintaining the cellular balance of SUMOylation (Conti et al., 2009).

1.4 NO synthesis in plants during salt stress

Cytosolic nitrate reductases (NR) encoded by *NIA1* and *NIA2* genes are thought to be the most common sources of NO in *Arabidopsis* with NIA2 showing the bulk NR activity (Wilkinson and Crawford, 1991). Primarily, NR reduces nitrate (NO_3^-) to nitrite (NO_2^-) in an NAD(P)H-dependent manner (Crawford, 1995). However, *in vitro* and *in vivo* experiments has established that NR is also able to reduce NO_2^- to NO and its derivative peroxynitrite ($ONOO^-$) (Dean and Harper, 1988; Rockel et al., 2002). *Arabidopsis* double NR mutant *nia1 nia2* is unable to accumulate NO or to mediate some NO responses (Bright et al., 2006). NR was reported to be involved in NO production during salt stress in orange (*Citrus aurantium*) (Ziogas et al., 2013). However, NO_3^- is the preferable substrate for NR, thus it is likely that NO will be produced at low levels by NR under typical conditions when the cellular NO_3^- level is 50-100 times higher than that of NO_2^-. However, under anaerobic conditions during hypoxia, due to the accumulation of NO_2^-, it is possible that NO can be generated at relatively higher levels (Rockel et al., 2002; Mur et al., 2012). It is also evident that, in *Nicotiana tabacum* roots, a plasma membrane-bound NR (PM-NR) is associated with a nitrite:NO oxidoreductase (Ni:NOR). The mitochondrial electron transport system possibly by cytochrome c oxidase and/or reductase and peroxisomal xanthine dehydrogenase/oxidase (XDH) are two other possible reductive pathways for NO production (Gupta et al., 2011).

In animal systems, NO is produced by three NO synthase (NOS) enzymes through the process of oxidising arginine to generate citrulline and NO (Mayer and Hemmens, 1997). In this context, NO production was reported through NOS-like activity during salt stress in olive

(*Olea europaea*) (Valderrama et al., 2007). In addition, the use of NOS inhibitors indicated the presence of NOS-like activity in chloroplasts and peroxisomes in many plant species, however, the analysis of numerous plant genomes failed to identify genes encoding NOS enzymes in land plants (Cueto et al., 1996; Delledonne et al., 1998; Barroso et al., 1999; Corpas et al., 2004; Jeandroz et al., 2016). In this context, a GTPase encoded by *AtNOA1* (*Arabidopsis thaliana* NO-Associated protein 1) has been suggested to be involved indirectly in NO production. *atnoa1* plants were shown to have a reduced endogenous NO level (Vitecek et al., 2008; Zemojtel et al., 2006; Moreau et al., 2008). Interestingly, *atnoa1* plants have been reported to be NaCl sensitive due to enhanced accumulation of Na^+ and reduced accumulation of K^+ leading to a greater Na^+ to K^+ ratio in shoots than wild type plants during NaCl stress (Zhao et al., 2007). Interestingly, genome analysis of the algae *Ostrococcus tauri* revealed the presence of a NOS-like enzyme (Derelle et al., 2006; Foresi et al., 2010). NO synthesis by other oxidative pathways has also been reported in plant as well. Polyamines like spermine and spermidine were shown to trigger rapid NO production *in planta* (Tun et al., 2006). In this context, exogenous application of spermidine was reported to increase tolerance to salinity in tomato (*Solanum lycopersicum*) possibly by inducing greater NO production (Li et al., 2015). In addition, under aerobic conditions, exogenous hydroxylamine application to NR-deficient tobacco cell cultures resulted in the release of NO (Rümer et al., 2009). Nevertheless, though NO production during salinity is evident, the major source(s) are still to be confirmed.

1.5 NO based reactions

NO is a highly diffusible gas which uncharged and relatively short-lived in its radical form due to an unpaired electron in its outer orbital. Due to this property NO can interact with a wide variety of targets including proteins, lipids and nucleic acids (Corpas et al., 2011;

Hong et al., 2008; Toledo and Augusto, 2012). The scavenging of superoxide anion (O_2^-) by NO leads to the formation of powerful oxidant, peroxynitrite ($ONOO^-$) which is extremely toxic for animal cells but not for plant cells (Delledonne et al., 2001). Molecular oxygen (O_2) can also interact with NO to form nitrogen dioxide (NO_2). At low NO concentration, the scavenging of hydroxyl radical (·OH) and high valent metal complexes confers an antioxidant property to NO (Wink et al., 2001). Further, NO is known as a strong inhibitor of lipid peroxidation and protein oxidation (Rubbo et al., 2000; Lam et al., 2008). In contrast, high levels of NO enhance superoxide production in mitochondria by inhibiting electron flow through cytochrome C oxidase (Millar and Day, 1996). Therefore, the dual effect of NO as an antioxidant or toxic compound depends mainly on its concentration ranging from nM to µM (Toledo and Augusto, 2012).

NO plays an important role in post-translational modifications (PTMs). The most important PTM by NO is S-nitrosylation, the attachment of a NO group to a protein thiol (SH) of the cysteine (Cys) residue to form an S-nitrosothiol (SNO) (Spadaro et al., 2010). However, S-nitrosylation is limited to rare, highly reactive, solvent exposed protein Cys thiol groups (Yu et al., 2014). S-nitrosylation also depends on the local concentration on NO in the cell (Toledo and Augusto, 2012). Often, the target Cys residues are surrounded by a consensus S-nitrosylation motif (Stamler et al., 1997). Interestingly, reactive Cys residues involved in S-nitrosylation are also subject to other reversible redox-based modification with varying levels of oxidation including S-sulphenylation (SOH), S-glutathionylation (GSH), S-thiolation (SS or disulphide formation) and S-sulphinylation (SO_2H) (**Fig. 1-2**) (Spadaro et al., 2010; Spoel and Loake, 2011). Another PTM mediated by NO is metal-nitrosylation. In this context, NO can bind to most transition metals in their ionic form such as iron (Fe^{2+} or Fe^{3+}), copper (Cu^{2+}) or zinc (Zn^{2+}) to form metal-nitrosyl complexes (M-NO) (Cooper, 1999). Metal-nitrosylation can effectively block the peroxidation of the metal thus preventing ROS production (Wink et al.,

2001). However, the interactions with iron within haem groups are biologically the most relevant (Cooper, 1999). Further, NO can also drive protein tyrosine (Tyr)-nitration, mediated by $ONOO^-$, which adds a nitro group ($-NO_2$) to a Tyr side chain (Radi, 2004; Rubbo and Radi, 2008).

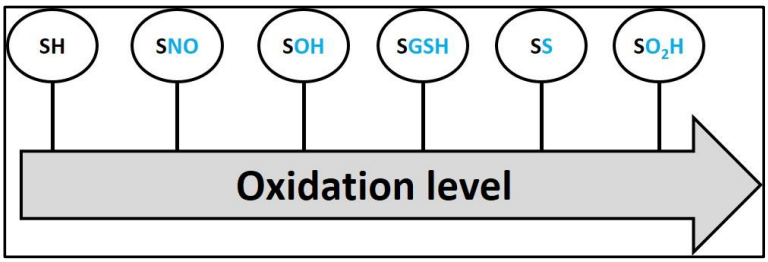

Figure 1-2. Redox states of cysteine thiol groups.

Schematic diagram showing different redox-based modifications of cysteine thiols and their relative oxidation levels. The cysteine modifications depicted are unmodified free thiol (SH), S-nitrosylation (SNO), S-sulphenation (SOH), S-glutathionylation (SGSH), disulphide (SS) and S-sulphination (SO_2H). Adapted from (Spadaro et al., 2010).

1.6 Specificity of NO as a signalling molecule

NO is readily soluble in water and even more soluble in hydrophobic solvents (Shaw and Vosper, 1977). Therefore, NO can pass through the hydrophobic double layer of biological membranes by simple diffusion, without any specialised membrane transporter, which confers unique biological properties to NO as a signalling molecule. Stimuli-triggered NO biosynthesis has evolved as an important signalling system in higher eukaryotes which necessitates specificity and reversibility of this signalling. NO function depends on its reactions with other signalling molecules and covalent chemical modifications of proteins. Thus, the rate, site and microenvironment of NO synthesis are potential determinants of the chemical reactions of NO and subsequent biological outcomes (Derakhshan et al., 2007). NO is found in several redox forms in the cell which can activate a sequence of events specific for

a given form. NO activity may also be limited to specific cells or cellular compartments due to the morphological and functional variation of cells and tissues (Arasimowicz and Floryszak-Wieczorek, 2007). Moreover, regulation and specificity of NO signalling are often controlled by its synthesis. Temporal and spatial variations of NO synthesis contribute to differential responses. Selective S-nitrosylation of a protein thiol may be achieved by positioning the thiol in proximity to a cellular source of NO reactivity. At least in animal cells, NO reactivity has been shown to be selectively channelled by NOS to a protein thiol by either direct binding of an NO-acceptor protein or indirect binding via a scaffold protein. NOS/target protein interactions are complex and suggest that coordinated evolution of NOS and target proteins occurred for enhancement of signalling selectivity (Derakhshan et al., 2007). Furthermore, during any stress, changes in the proteomics contribute to the generation of a set of S-nitrosylated proteins ensuing responses specific to that stress.

1.7 S-Nitrosylation as a post-translational modification

The covalent bond between thiol (SH) and NO in a nitrosothiol (SNO) group can be labile since it is light and redox sensitive (Gorren et al., 1996; Smith and Dasgupta, 2000). In addition, S-nitrosylation can control the activity or cellular localisation of a target protein (Yu et al., 2014). For instance, during pathogen infection in *Arabidopsis*, S-nitrosylation of NADPH oxidase (AtRBOHD) at Cys 890 inhibits its ability to synthesise reactive oxygen intermediates. Further, mutation of Cys 890 abolishes S-nitrosothiol-mediated regulation of AtRBOHD activity (Yun et al., 2011). A similar effect was observed for S-nitrosylation of the large subunit of ribulose-1,5-bisphosphate carboxylase/oxygenase (Rubisco) which leads to inhibition of its carboxylase activity under cold stress in *Brassica juncea* (Abat and Deswal, 2009). On the contrary, S-nitrosylation of cytosolic ascorbate peroxidase (APX), which is involved in the regulation of cellular hydrogen peroxide (H_2O_2) content, promotes its enzyme activity in pea

(*Pisum sativum*) under salt stress (Begara-Morales et al., 2014). Additionally, S-nitrosylation was shown to regulate the cellular localisation of proteins by changing the homoeostasis between monomer and oligomer formation in the case of the transcriptional coactivator, NPR1 (nonexpressor of PR1), a master regulator of salicylic acid (SA)-mediated defence genes. Upon pathogen infection, SA mediated monomerization of NPR1 leads to the translocation of this protein into the nucleus triggering expression of defence related genes. S-nitrosylation at Cys 156 favours NPR1 oligomerization thereby retaining this protein in the cytoplasm curbing SA signalling (Tada et al., 2008).

Post-translational modification typically includes the presence of a reversal mechanism to regulate its biological effect. Since the SNO bond is redox and light sensitive, denitrosylation is often mediated by metal ions, small antioxidant molecules such as ascorbate and tripeptide glutathione (GSH). GSH either interacts with NO or removes NO from protein SNOs to form S-nitrosoglutathione (GSNO). GSNO is the most abundant low-molecular mass (LMM) S-nitrosothiol (SNO) which functions as a stable store of NO bioactivity and by extension can donate its NO group to target Cys residues to produce high-molecular mass (HMM) SNOs in a process called S-transnitrosylation. HMM SNOs can also transfer NO to the thiol groups of other proteins through S-transnitrosylation between proteins. On the other hand, GSH can interact with specific thiol groups of proteins in a process known as S-glutathionylation (Yu et al., 2014). Thus, GSH, GSNO and total cellular protein SNOs are thought to be in dynamic equilibrium. Importantly, an enzyme termed GSNO reductase (GSNOR) can turn over GSNO into GSSG and ammonia (NH_3), where GSSG is further reduced to GSH by glutathione reductase (GSR) (**Fig. 1-3**). Thereby, GSNOR directly regulates GSNO levels and indirectly regulates total cellular SNOs (Feechan et al., 2005). Additionally, thioredoxins (TRX) have recently been shown to have both transnitrosylation and denitrosylation activity (Benhar et al., 2008; Kneeshaw et al., 2014; Wu et al., 2010, 2011).

Interestingly, S-nitrosylation by S-nitroso-CoA (SNO-CoA) has also recently been reported to occur in yeast. A specific SNO-CoA reductase has been identified, encoded by the alcohol dehydrogenase 6 (ADH6) gene, and deletion of this gene increases cellular S-nitrosylation and alters CoA metabolism. A similar system has also been proposed to function in mammals (Anand et al., 2014). However, a functional analogue of ADH6 has not been found to date in plants (Begara-Morales and Loake, unpublished data).

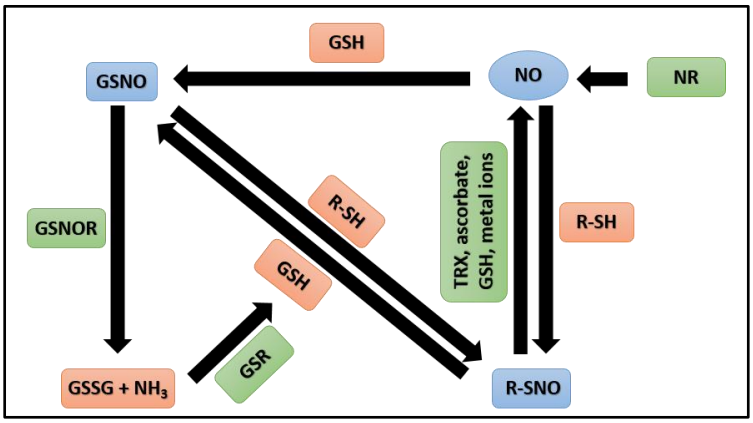

Figure 1-3. Regulation of S-nitrosylation by GSNOR.

GSNOR plays a central role in the homoeostasis of global cellular SNO and GSNO levels. NO generated predominantly from NR can directly S-nitrosylate GSH or any protein Cys thiol group (SH) to form GSNO or R-SNO respectively. R-SNO can be denitrosylated by antioxidant molecules ascorbate, GSH or metal ions and TRX. A protein R-SH group can be transnitrosylated by GSNO. GSNOR turns over GSNO to GSSG and ammonia (NH_3). GSSG is further reduced to GSH by GSR. NO, nitric oxide; NR, nitrate reductase; GSH, glutathione; GSNO, S-nitrosoglutathione; R-SH, protein thiol; R-SNO, S-nitrosothiol; GSNOR, S-nitrosoglutathione reductase; GSR, glutathione reductase; TRX, thioredoxin. Adapted and modified from (Fancy et al., 2016).

1.8 GSNOR in plants

In plants, the enzyme GSNOR regulates global S-nitrosylation. It is a key player in plant disease resistance. This enzyme in *Arabidopsis thaliana*, *GSNOR1* (AT5G43940) negatively regulates S-nitrosylation. In *Arabidopsis,* a loss-of-function (*gsnor1-3*) as well as a gain-of-

function mutant (*gsnor1-1*) have been identified and characterised in detail (Feechan et al., 2005). The loss-of function mutation in *GSNOR1* resulted in increased cellular SNO levels, while decreased SNO levels were observed in a gain-of-function mutant. Loss of GSNOR1 activity also resulted in compromised disease resistance against non-host, avirulent and virulent pathogens, whereas the *GNSOR1* over-express line showed increased resistance against virulent and non-host pathogens. The *gsnor1-3* line was shown to exhibit reduced and delayed SA-dependent gene expression after either pathogen infection or exogenous SA application as well as blocked SA accumulation. Increased GSNOR1 activity, on the other hand, resulted in accelerated SA-dependent gene expression. These findings show that GSNOR1 plays a role in both SA biosynthesis and SA signalling and hence regulates the disease resistance pathway (Feechan et al., 2005). The absence of GSNOR activity results in increased GSNO as well as increased protein SNO levels, however, GNSOR does not directly denitrosylate proteins (Fancy et al., 2016).

1.9 Role of nitric oxide (NO) and GSNOR in salt stress

Almost all abiotic stresses generate free radicals and other oxidants, particularly from the chloroplasts, mitochondria and peroxisomes, resulting in oxidative stress in terms of an increased level of reactive oxygen species (ROS) and reactive nitrogen intermediates (RNI) in plant cells (Mittler, 2002; Gould et al., 2003). ROS/RNI not only causes oxidative damage but also exerts some signalling responses, thus it is important for plants to regulate the concentration of ROS/RNI.

NO and S-nitrosylation plays an important role in different signal transduction pathways (Yu et al., 2014). NO has been observed to play important roles during salt stress in many plant species (Kopyra and Gwóźdź, 2003). Exogenous application of NO donors such as sodium nitroprusside (SNP) was shown to protect plants against salt stress by promoting

growth and providing protection from oxidative damage in rice (*Oryza sativa*) and cucumber (*Cucumis sativus*) (Uchida et al., 2002; Shi et al., 2007; Zhang et al., 2006). In addition, exogenous NO application has been shown to promote the maintenance of ion homoeostasis by increasing the activities of vacuolar H^+-ATPase and H^+-PPase and enhancing the Na^+/K^+ exchange in maize (*Zea mays*) (Zhang et al., 2006). In this context, exogenous NO was shown to enhance salt tolerance in reed (*Phragmites communis*) and poplar (*Populus euphratica*) calluses via increasing the expression of plasma membrane H^+-ATPase that is required for Na^+ homoeostasis and K^+ acquisition (Zhao et al., 2004; Zhang et al., 2007). On the other hand, the *Arabidopsis* mutant *atnoa1* (*Arabidopsis thaliana nitric oxide-associated 1*), defective in a GTPase, which has a reduced endogenous NO level and impaired NO signalling, was more sensitive to NaCl stress than wild type. Treatment with exogenous NO donor showed greater salt tolerance through attenuating the elevation of Na^+/K^+ ratio (Guo et al., 2003; Moreau et al., 2008; Zhao et al., 2007). Pre-treatment of seeds with the NO donor SNP has been reported to promote germination, root growth and increased antioxidant activity in the presence of NaCl (Kopyra and Gwóźdź, 2003; Fan et al., 2013; Zheng et al., 2009). ROS accumulation is one of the common biochemical changes during salt stress resulting in an imbalance of cellular redox status creating oxidative stress which can damage DNA, inactivate enzymes and cause lipid peroxidation. To control the level of ROS, plants have evolved the antioxidant defence system comprising both antioxidant enzymes and non-enzymatic constituents such as ascorbate and glutathione, which are responsible for scavenging accumulated ROS in plants under stress conditions (Abogadallah, 2010). Endogenous NO application has been shown to enhance the activities of antioxidant enzymes such as catalase (CAT), superoxide dismutase (SOD), ascorbate peroxidase (APX), peroxidases (POD), glutathione reductase (GR), guaiacol peroxidase (GPX) and dehydroascorbate reductase (DHAR) (Zheng et al., 2009; Fatma et al., 2016; Uchida et al., 2002; Ahmad et al., 2016). Further, exogenous NO was shown to

decrease the levels of Malondialdehyde (MDA), H_2O_2 and superoxide anion ($O_2^{\bullet-}$) (Zheng et al., 2009). Exogenous application of NO was also shown to enhance osmolyte accumulation during salt stress (Ahmad et al., 2016). Interestingly, NO recently has been shown to alleviate salt stress by interacting with sulphur (S) assimilation. Plants treated with exogenous NO and S showed enhanced S-assimilation, increased production of cysteine (Cys) and glutathione (GSH) (Fatma et al., 2016). In this context, NO was also shown to be endogenously generated during salt stress (Valderrama et al., 2007; Ziogas et al., 2013; Camejo et al., 2013; Begara-Morales et al., 2014).

In recent years, evidence is emerging that S-nitrosylation may play roles in the abiotic stress response. S-nitrosylated proteins formed under NaCl stress in orange were the first to be reported. Interestingly, however, the level of this modification was shown to be reduced following NaCl stress (Tanou et al., 2009; Ziogas et al., 2013; Camejo et al., 2013). Nonetheless, NO or H_2O_2 pre-treatment showed increased NaCl induced protein S-nitrosylation, which plays a protective role under salt stress conditions. S-nitrosylation, in this case, may prevent irreversible protein carbonylation provoked by ROS generated during salt stress. Another hypothesis is that ·NO prevents the formation of the most deleterious ROS, the ·OH hydroxyl radical, by forming metal nitrosyl complex with iron thereby preventing the Fenton reaction between iron and H_2O_2 (Tanou et al., 2009; Wink et al., 2001). In another study performed in *Arabidopsis* cell suspensions, transient NaCl stress has been shown to cause little changes in S-nitrosylation (Fares et al., 2011). On the contrary, total S-nitrosylation levels have been reported to be increased after salt stress in mustard (*Brassica juncea*) and in pea (Abat and Deswal, 2009; Begara-Morales et al., 2015).

S-nitrosylated proteins have been identified in respiratory/photorespiratory pathways and antioxidant systems during salt treatment, specifically the glycine dehydrogenase P

subunit, F1 ATPase β subunit and isocitrate dehydrogenase (ICDH), implying that this modification might regulate responses to abiotic stress (Camejo et al., 2013; Fares et al., 2011). A major H_2O_2 detoxification system, the ascorbate-glutathione cycle, is thought to play an important role during salt stress. Regulation of this cycle by S-nitrosylation has recently been reported in pea plants. APX and monodehydroascorbate reductase (MDAR) are two essential components of this pathway which are both induced at the transcriptional and translational level under 150 mM NaCl stress (Begara-Morales et al., 2014, 2015). Significantly, APX was found to be S-nitrosylated at Cys32 during NaCl stress and this modification increased the activity of this enzyme promoting the turnover of H_2O_2, leading to increased resistance to oxidative stress. In contrast, a substitution of Cys-32 for Ser (C32S), thereby hindering S-nitrosylation, resulted in the reduction of APX activity by abolishing its responsiveness to NO (Yang et al., 2015; Begara-Morales et al., 2014). On the other hand, MDAR was also found to be S-nitrosylated under salinity stress. Here, this modification was shown to inhibit MDAR enzyme activity (Begara-Morales et al., 2015).

In another study, Glyceraldehyde-3-phosphate dehydrogenase (GAPDH), a glycolytic enzyme, was found to interact directly with NtOSAK (*Nicotiana tabacum* osmotic stress-activated protein kinase) upon salt stress in tobacco BY-2 cells. It was proposed that a short salt exposure induced the S-nitrosylation of GAPDH, though this modification of GAPDH does not appear to alter its *in vivo* activity. Further, S-nitrosylation of GAPDH was found to neither modulate its interaction with NtOSAK nor the phosphorylation activity of NtOSAK (Wawer et al., 2010). However, it has been reported that S-nitrosylation of GAPDH triggers its nuclear localisation. During apoptotic stimulation, S-nitrosylation of GAPDH occurs which induces binding to an E3 ubiquitin ligase, SIAH1 (seven in absentia homolog 1) whose nuclear localisation mediates co-translocation of GAPDH and subsequent stabilisation of SIAH1 facilitating nuclear protein degradation by SIAH1 (Hara et al., 2005). Interestingly, a SIAH1

homolog is also present in several plant genomes (Herder et al., 2008). By extension, it is possible that during salt stress the S-nitrosylation of GAPDH serves as an apoptotic signal, mediating its translocation to the nucleus, facilitating nuclear protein degradation.

It has recently been reported that a knock down of GSNOR by RNAi results in enhanced sensitivity to sodic alkaline stress in tomato (*Solanum lycopersicum*), which was proposed to be resulted from excessive accumulation of NO and SNO during this stress (Gong et al., 2015). It is evident that NADPH oxidase-dependent (RBOHD-dependent) hydrogen peroxide production is induced during salt stress (Yang et al., 2007). Additionally, S-nitrosylation of NADPH oxidase (RBOHD) has been shown to be S-nitrosylated at Cys890 during biotic stress inhibiting its activity (Yun et al., 2011). In this context, a similar mechanism may exist during salt stress where S-nitrosylation of NADPH oxidase leads to its inhibition, thereby regulating hydrogen peroxide production.

Many MYB family transcription factors are involved in the regulation of abiotic stress responses in plants (Dubos et al., 2010). AtMYB2, an important transcription factor involved in both salt and drought stress, has been reported to be S-nitrosylated, inhibiting the DNA binding activity of this protein (Heine *et al.* 2004, Serpa *et al.* 2007). Similarly, environmentally induced changes in the redox state regulate the DNA binding activity of members of the G-group of bZIP transcription factors (Shaikhali *et al.* 2012). Recently, ABA induced S-nitrosylation of OST1/SnRK2.6 (open stomata 1/sucrose non-fermenting 1 (SNF1)-related protein kinase 2.6) has been reported in *Arabidopsis*. SnRK2.6 is a central component of ABA signalling. The S-nitrosylation of OST1/SnRK2.6 at Cys137 has been reported to inhibit its protein kinase activity *in vitro*. Further, a Cys137 to Ser (C137S) mutation prevented the inhibition of kinase activity by GSNO *in vitro*. Also, a knock out mutation of *GSNOR1* was shown to abolish the sensitivity to ABA-induced stomatal closure, thereby exhibiting

increased water loss relative to wild type plants. A C137S mutation in SnRK2.6 can partially rescue this phenotype. ABA induced S-nitrosylation of SnRK2.6 possibly functions as a negative feedback regulator of ABA signalling in plants (Wang et al., 2015).

Collectively, NO, S-nitrosylation and its regulatory enzyme GSNOR play vital roles in controlling salt tolerance in plants. The underpinning mechanisms might include the redox modification of ROS scavenging enzymes, respiratory/photorespiratory pathways and antioxidant systems.

1.10 Autophagy in plants

Autophagy is a catabolic process which involves the recycling of cytoplasmic contents during developmental transition or under stress conditions and this process is conserved among eukaryotes (Levine and Klionsky, 2004; Liu and Bassham, 2012). Autophagy is composed of different types, which includes: microautophagy, macroautophagy, chaperone-mediated autophagy, and organelle-specific autophagy, such as mitophagy, chlorophagy and pexophegy. However, plant autophagy mostly refers to macroautophagy, as this is the predominant form of autophagy observed (Li and Vierstra, 2012).

The distinct characteristic of autophagy is the formation of autophagosome, a double layer lipid membrane vesicle. Upon induction, proteins required for the autophagosome formation accumulate at a pre-determined site termed the pre-autophagosomal structure (PAS). Once the double layer lipid membrane starts to form around the cytoplasmic contents destined for degradation it is called phagophore. The phagophore then engulfs the contents into the circular vesicle, the autophagosome, which then delivers the cargo to the central vacuole. The outer membrane of the autophagosome fuses with the vacuolar membrane and all the contents of the autophagosome including the inner membrane are then degraded inside the vacuole by hydrolysis (**Fig. 1-4**) (Li and Vierstra, 2012).

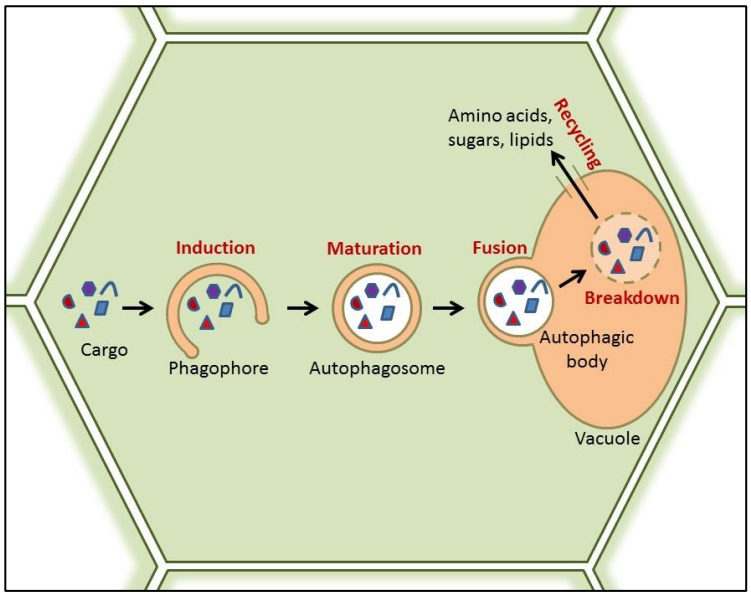

Figure 1-4. Autophagy involves autophagosome formation.

Autophagy is cellular catabolic process. Autophagy involves the formation of a double membrane structure, termed a phagophore, around the cargo which is destined for degradation. The phagophore matures into a double membrane circular vesicle called an autophagosome, which then fuses with the central vacuole in plant cells to release its cargo, with the inner membrane of the autophagosome forming an autophagic body. The outer membrane is fused with the tonoplast. Inside the vacuole the cargo along with the inner membrane of the autophagosome is degraded by hydrolases and other enzymes, enabling amino acids, sugars and lipids to be recycled back to the cytoplasm.

Although the core set of ***au**to**phag**y* (*ATG*) genes required for this process were initially identified in yeast, all of them are present in other eukaryotes. These genes can be categorised into different functional groups. Autophagy induction involves: the negative regulator-target of rapamycin (TOR) kinase; the positive regulator SNF1-related protein kinase 1 (SnRK1) which is known as sucrose non-fermenting 1 (SNF1) in yeast and AMP-activated protein kinase (AMPK) in mammal; and the ATG1-ATG13 kinase complex. Once induced, this complex directly or indirectly controls the activity of the nucleation of the phagophore at PAS by controlling ATG6 (Beclin1/VPS30) complex and phosphatidylinositol-3

kinase (PI3K) which decorates the phagophore with phosphatidylinositol-3-phosphate (PI3P). This then promotes lipid delivery to the developing phagophore by the ATG9-ATG2-ATG18 complex. The completion of autophagosome formation involves two ubiquitin-like conjugation systems to produce ATG8-phosphatidylethanolamine (ATG8-PE) conjugates and ATG12-ATG5:ATG16 complex (here, the dash represents a covalent interaction; colon represents a non-covalent interaction).

1.10.1 Autophagy induction

ATG-mediated autophagy has been modelled using evidence from multiple organisms including yeast and *Arabidopsis.* Interestingly, these components are conserved across kingdoms. Here we are presenting the model using *Arabidopsis* homologs for different components for simplification. Autophagy induction begins by sensing the nutritional and developmental status of the cell. The nutrient status specifically the ATP/AMP ratio affects the activity of several protein kinases including the TOR kinase and its target recognition cofactor RAPTOR, protein kinase A (PKA), and SnRK1 in *Arabidopsis.* It is becoming clear that TOR kinase and SnRK1/SNF1/AMPK play opposite roles during changes in nutritional status. The TOR kinase is mostly active during nutrient-rich conditions and regulates autophagy negatively. On the other hand, SnRK1 is a positive regulator of autophagy (Robaglia et al., 2012). Under nutrient-rich conditions, activated TOR kinase hyperphosphorylates ATG13 and hypophosphorylates ATG1 thereby repressing ATG1/ATG13 kinase complex assembly. During starvation, the drop in the ATP/AMP ratio is sensed by SnRK1 leading to hyperphosphorylation of ATG1 by SnRK1. At the same time, TOR kinase is inhibited resulting in hypophosphorylation of ATG13 (Liu and Bassham, 2010; Kim et al., 2011). The reversal in the phosphorylation status of ATG1 and ATG13 induces the association of ATG1 and ATG13 with each other and several other factors (ATG11p and ATG17p in yeast, and FIP200 (focal adhesion kinase family-

interacting protein of 200 kDa) and ATG101 in mammals) (**Fig. 1-5A**) (Li and Vierstra, 2012).

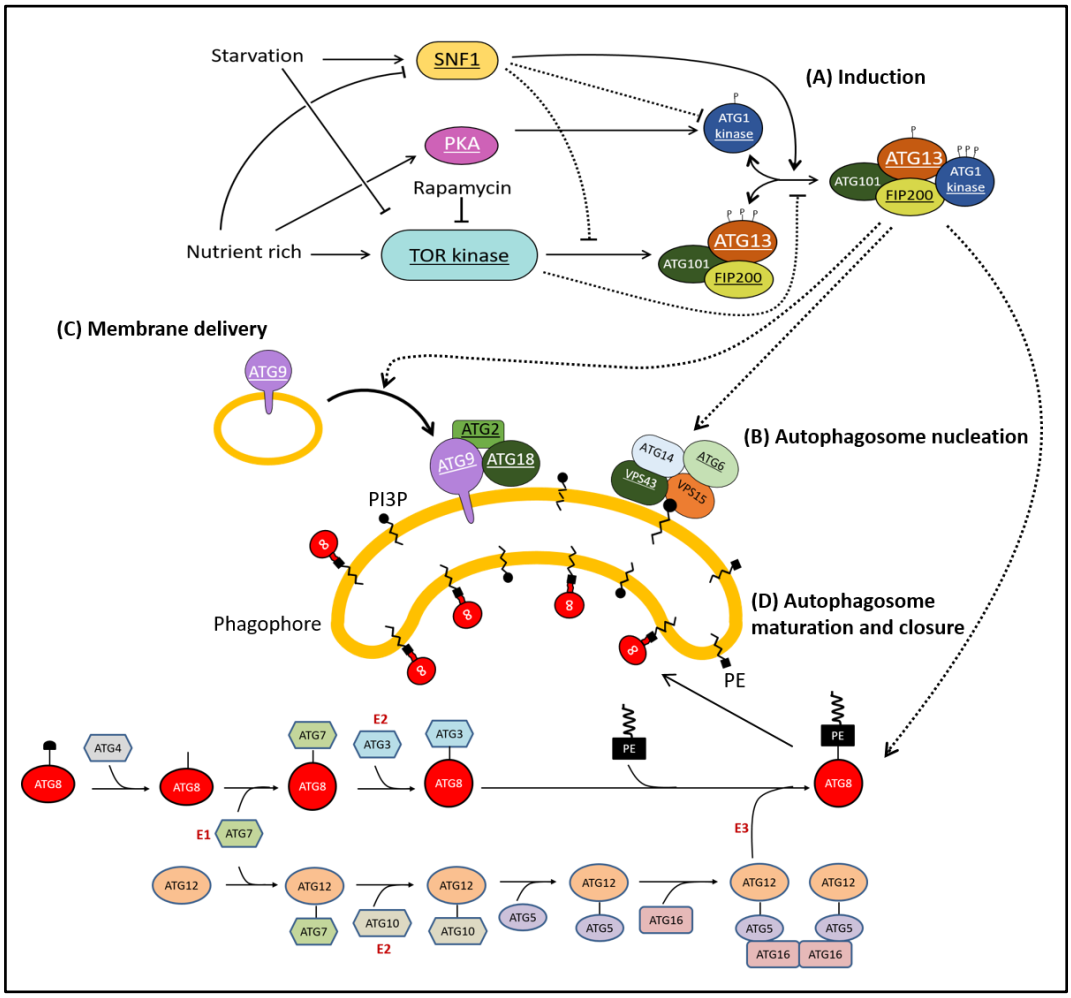

Figure 1-5. A schematic representative of the autophagy pathway.

A) Induction of the ATG pathway is regulated by the nutritional status of the cell. Under nutrient-rich conditions, the target of rapamycin (TOR) and other kinases induce hyperphosphorylation of the ATG13 subunit and hypophosphorylation of the ATG1 subunit of the ATG1/ATG13 kinase complex, promoting its dissociation. Under nutrient-poor conditions, these steps are reversed, thus allowing ATG1, ATG13, and the accessory subunits ATG101 and FIP200 to assemble. The activated ATG1/ATG13 kinase complex promotes: **B)** the ATG9-mediated delivery of lipids to the developing phagophore; **C)** the nucleation of the autophagosome in a process involving the VPS34 lipid kinase that adds phosphatidyl inositol-3 phosphate (PI3P) to the phagophore, and **D)** ATG12–ATG5:ATG16 conjugation (here, dash represents a covalent interaction; colon represents a non-covalent interaction) and lipidation

of ATG8 with phosphatidylethanolamine (PE). PKA, protein kinase A; SNF1, sucrose non-fermenting 1; VPS, vacuolar protein sorting. Arabidopsis and maize orthologs of the yeast ATG proteins are highlighted in colour. For step **A, B and C,** *Arabidopsis* proteins studied genetically are underlined. Adapted and modified from (Li and Vierstra, 2012).

1.10.2 Autophagy elongation

Upon assembly, the activated ATG1/ATG13 kinase complex (Ser/Thr kinase complex) directly or indirectly stimulates several steps related to autophagosome nucleation and elongation. One step involves the PI3K, vacuolar protein sorting 34 (VPS34), ATG6(VPS30/Beclin1), ATG14, VPS15 (Ser/Thr kinase) lipid kinase complex that decorates the phagophore with phosphatidylinositol-3-phosphate (PI3P). VPS15 is required for the membrane association of VPS34. ATG14 connects VPS34 and ATG6. PI3P most probably is involved in distinguishing the developing phagophore from other endomembrane compartments and recruiting proteins for the fusion of autophagosome with the tonoplast (**Fig. 1-5B**). Another step engages the transmembrane protein ATG9, which delivers lipids to the expanding phagophore in conjunction with the peripheral membrane proteins ATG2 and ATG18. The autophagosome membrane in yeast forms de novo, in mammals the sources are endoplasmic reticulum (ER), mitochondria and plasma membrane, however, in plants, the source of the autophagosome membrane is still unknown. ATG18 can bind to both ATG9 and PI3P thereby recruiting the ATG9 complex to the elongated phagophore with the help of ATG2, the ATG1-ATG13 kinase complex and the PI3K complex (**Fig. 1-5C**) (Yang and Klionsky, 2009; Xie and Klionsky, 2007).

1.10.3 Autophagosome maturation

The third step in phagophore elongation and maturation enabling complete autophasome formation involves two ubiquitin-like conjugation systems to generate ATG8-PE and ATG12-ATG5:ATG16 complex. ATG8-PE conjugation involves the ubiquitin like protein

ATG8, cysteine (Cys) protease ATG4, E1-like activating enzyme ATG7 and E2-like conjugating enzyme ATG3. In *Arabidopsis,* there are two ATG4, nine ATG8s, one ATG7 and one ATG3. ATG8 is usually synthesised as a long precursor which requires processing by the cysteine protease ATG4 to expose a conserved C-terminal glycine (Gly) residue which then reacts with the catalytic site Cys of ATG7 to form a thioester intermediate. ATG8 is then transferred to the catalytic site Cys of the conjugating enzyme ATG3. Finally, ATG8 is conjugated with the lipid molecule phosphatidylethanolamine (PE) to form ATG8-PE (**Fig. 1-5D**) (Ohsumi, 2001). Lipidated ATG8 then decorates both the inner and outer membranes of the autophagosome with equal preference. When the ATG8-PE containing outer membrane of the autophagosome fuses with the central vacuole, ATG8-PE decorates the membrane of the central vacuole while the ATG8-PE present in the inner membrane of the autophagosome is consumed by the central vacuole. The ATG8-PE conjugation is reversible and the ATG8-PE present on the membrane of the central vacuole can be cleaved by ATG4 to recycle free ATG. Due to the unique property of ATG8-PE to decorate the autophagosome, green fluorescent protein (GFP)-fused ATG8 has been widely used to monitor autophagy (Liu and Bassham, 2012; Xie and Klionsky, 2007). Recently, another interesting characteristic of ATG8 has been observed. Once ATG8-PE decorates the membrane of the phagophore, it serves as a docking site for ATG8-interacting proteins for phaogophore assembly, its closure and maturation to form the autophagosome and for selective cargo recruitment (**Fig. 1-6**). This unique property of ATG8 to interact with other proteins changed the perception of autophagy from one committed to bulk degradation to one that selectively sequesters and removes specific unwanted cargos. Recent studies have shown that Neighbour of BRCA1 (NBR1) in *Arabidopsis* contains an ATG8-interacting motif (AIM) and thus can serve as an adapter protein for specific cargos. NBR1 can bind to ubiquitinylated proteins destined for degradation and dock on to lipidated ATG8 inside the autophagosome before its closure (Li and Vierstra, 2012).

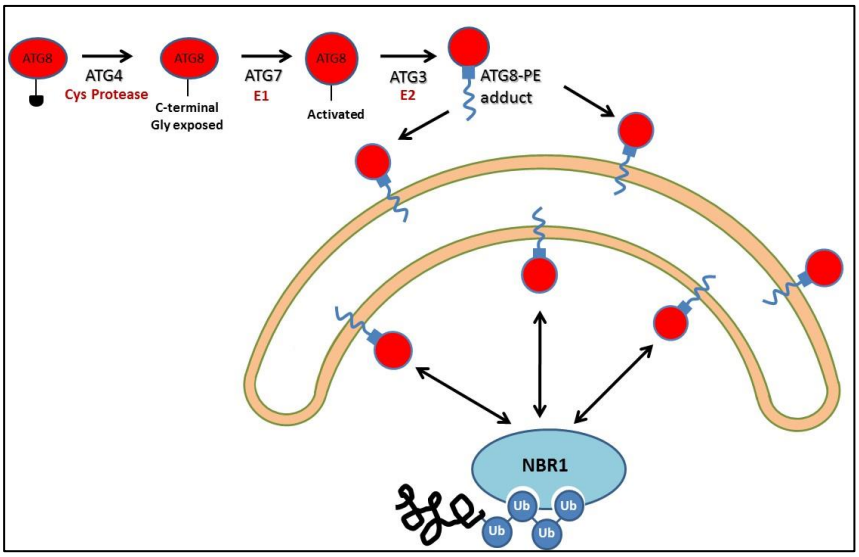

Figure 1-6. ATG8-PE decorates the phagophore outer and inner membrane and recruits other molecular players in autophagosome maturation.

The ATG8 conjugation system plays a role in autophagosome maturation. ATG8-PE adduct is formed by ATG7 and ATG3 activating and conjugating enzymes respectively. ATG8-PE decorates both the outer and inner membrane of the phagophore using the lipid part of the ATG8-PE adduct. ATG8 then recruits proteins that contain an AIM domain which takes part in autophagosome maturation. ATG8 also serves as a docking protein for adapter proteins like NBR1, which contains both an AIM and a ubiquitin binding domain. Ubiquitinylated proteins can bind to NBR1, which then interacts with ATG8 to be internalised by autophagosome. Thus, NBR1 serves as a selective marker for autophagy. PE, phosphatidylethanolamine; NBR1, neighbour of BRCA1; AIM, ATG8-interacting motif. Adapted and modified from (Li and Vierstra, 2012).

On the other hand, the second conjugation system includes the ubiquitin like protein ATG12 which is also activated by ATG7 and is transferred to the conjugating enzyme ATG10 and then conjugated to ATG5. The ATG12-ATG5 conjugates further interact with ATG16 to form a hexameric ATG12-ATG5:ATG16 complex, driven by the activity of the dimeric coiled-coil protein ATG16 (**Fig. 1-5D**). Recently, it has been shown that the ATG12-ATG5:ATG16 complex is essential for the lipidation of ATG8 (Liu and Bassham, 2012).

1.10.4 Autophagosome fusion with the tonoplast and subsequent degradation

Autophagosome translocation and fusion with the tonoplast is mediated via a v-SNARE type mechanism to release the internal vesicle as an autophagic body inside the vacuolar lumen. Finally, autophagic cargo is catabolized by different vacuolar hydrolases. These enzymes function optimally at acidic pH, making them collectively sensitive to several H^+-ATPase inhibitors, for example, concanamycin A (ConA) or E64d that raises vacuolar pH leading to the stabilisation of autophagic bodies. Consequently, ConA/E64d have become an essential tool for measuring autophagic flux in both yeast and plants *in vivo* (Liu and Bassham, 2012).

1.11 Autophagy during abiotic stress

Autophagy is known to be induced most commonly by nutrient deprivation (Doelling et al., 2002). Consequently, autophagy-defective plants display accelerated starvation induced chlorosis, since autophagy is required for nutrient recycling during starvation. In recent years, autophagy has also been shown to be a general response to a variety of abiotic stresses. Autophagy is induced in the presence of H_2O_2 or methyl viologen which cause oxidative stress. AtATG18a knock down plants are more sensitive to methyl viologen treatment and accumulate higher levels of oxidised proteins suggesting that autophagy is involved in the degradation of oxidised proteins (Xiong et al., 2007). Further, AtATG8 in *Arabidopsis* and OsATG10b in rice function effectively in response to salt stress and osmotic stress (Slavikova et al., 2005). Autophagy is also required for plant tolerance to drought and salt stress as autophagy-defective plants are sensitive to these stresses (Liu et al., 2009). In aggregate, autophagy plays a role in removing damaged/oxidised proteins or organelles during these cellular insults. ROS may function in the induction of autophagy by salt and osmotic stress. An NADPH oxidase inhibitor, which blocks ROS formation, was shown to

inhibit autophagy induction under high salt stress but not under osmotic stress. This implies that probably there are both NADPH oxidase dependent and independent pathways for regulating autophagy in plants (Liu et al., 2009; Shin et al., 2009). An abscisic acid–induced protein AtTSPO (tryptophan-rich sensory protein/translocator), involved in both salt and osmotic stress, has been shown to be selectively degraded by autophagy which indicates autophagy is involved in the responses to abscisic acid (Vanhee et al., 2011; Guillaumot et al., 2009). In addition, ER stress responses have been well characterised in animals and yeast (Liu et al., 2012), and autophagy has been suggested to play an important role in recovery from ER stress (Pu and Bassham, 2013). These stresses can create oxidation damage, leading to the accumulation of ROS and oxidised proteins (Xiong et al., 2007). Recently, it has been shown that autophagy-defective tomato plants show a compromised heat stress response. The knock down of *ATG7* and *ATG5* renders sensitivity to heat stress and accumulation of insoluble oxidised proteins in tomato plants (Zhou et al., 2014a). The knock down of NBR1, a selective autophagy substrate also shows accumulation of ubiquitinilated proteins, implying the inability to recycle oxidised proteins is responsible for heat sensitivity (Zhou et al., 2013, 2014b). The ability of autophagy to scavenge oxidised proteins and to regulate ROS levels suggests that autophagy is intimately involved in abiotic stresses.

1.12 Redox and NO regulation of Autophagy

The production of reactive oxygen species (ROS) and reactive nitrogen species (RNS) is one of the most important events during abiotic stress. However, no direct evidence of autophagy regulation by ROS and RNS have been shown in plants to date. Most of the evidence of autophagy regulation by ROS and RNS come from studies in animals and yeast. ROS are known to regulate autophagy under nutrient restricted conditions and superoxide ($O_2^{\bullet -}$) has been suggested to be the major ROS species involved in ROS-mediated autophagy

(Chen et al., 2009b; Scherz-Shouval et al., 2007). However, pharmacological evidence also showed that ROS, specially H_2O_2, is crucial for autophagy induction as the application of antioxidants blocks autophagy (Chen et al., 2009b).

AMPK, which is a redox sensitive protein is activated by H_2O_2 exposure leading to S-glutathionylation of reactive cysteines and by extension induces autophagy during starvation or stress induced H_2O_2 production (Zmijewski et al., 2010). Although there is a large amount of pharmacological data supporting redox regulation of autophagic signalling, the only redox-based mechanism demonstrated was that related to ATG4. It has been shown that starvation-induced H_2O_2 inhibits the hydrolysing activity of the human cysteine protease ATG4, thereby allowing autophagosomes to be correctly elongated (Scherz-Shouval et al., 2007). Recently, it has also been found that ATG4 is regulated by thioredoxin in yeast (Pérez-Pérez et al., 2014).

Although there are numerous reports for ROS regulation of autophagy, the specific roles of RNS and NO, and their mechanisms of action in autophagy remains unclear, especially in plants, where there is no current information. Protein S-nitrosylation plays vital physiological roles that are important in cellular homoeostasis along with a contribution to a broad spectrum of human diseases, such as heart failure and neurodegeneration (Foster et al., 2009). Nitrosative stress due to excess NO production plays a crucial role in neuronal cell death in the context of neurodegenerative diseases (Gu et al., 2010). It has been shown that overexpression of NOS isoforms resulting in increased NO, impairs autophagic flux. On the other hand, inhibition of NO synthesis induces autophagy and protects against neurodegeneration in models of Huntington's disease (HD) (Sarkar et al., 2011). In recent years, it has been shown that NO negatively regulates autophagy initiation and autophagic flux by S-nitrosylating BCL-2 (B-cell leukemia-2). This modification stabilises the BCL-2 interaction with Beclin-1, resulting in inhibition of Beclin-1 activity. Pre-treatments with

aminoguanidine, an NO inhibitor, resulted in increased autophagic flux (LC3-II/p62 upregulation). Further, a similar result was observed when a BCL-2 containing a C158A/C229A mutation was transfected. This study corroborated the regulatory role of BCL-2 by *S*-nitrosylation in autophagy (Wright et al., 2016). However, any direct evidence linking autophagy regulation by RNS and S-nitrosylation is yet to be found in plants.

1.13 Hypothesis, aims and objectives

S-nitrosylation is emerging as an important post-translational modification with regulatory roles in various cellular signalling pathways in both animals and plants. NO and S-nitrosylation function during stress in cellular signalling. It is now a well-established fact that GSNOR is a master regulator of cellular S-nitrosylation levels. In both animals and plants, the role of NO and S-nitrosothiols have been well established during plant-pathogen interactions. However, NO signalling via S-nitrosylation in abiotic stress remains largely unexplored. Therefore, the aim of this study was to uncover a possible role for S-nitrosylation during NaCl stress and if confirmed, to identify the associated molecular mechanism(s). We hypothesised that changes in NO/SNO levels in mutants dysregulated in NO production or S-nitrosylation may alter salt tolerance. By extension, post-translational modification may occur in the proteins involved in salt stress signalling pathways regulating plant salt tolerance.

In order to test this hypothesis, I will:

1. Utilise *Arabidopsis* mutants dysregulated in S-nitrosylation to determine if these lines are perturbed in NaCl tolerance.
2. Utilise *Arabidopsis* mutants dysregulated in NO production to determine if these lines are perturbed in NaCl tolerance.
3. Quantify the impact of salinity on different traits of plants.

4. Determine the expression of NaCl stress marker genes in dysregulated (S)NO lines during NaCl stress to identify possible associated signalling pathways/proteins regulated by S-nitrosylation.
5. Utilise mass-spectrometry, computer modelling and mutational analysis to identify the site(s) of S-nitrosylation during NaCl stress.
6. Formulate a model to explain the possible role of NO-mediated S-nitrosylation in the control of the NaCl tolerance.

Chapter-2

2 Materials and Methods

Unless otherwise stated, all chemicals and oligonucleotides used in this work were supplied by Sigma-Aldrich, UK, and all restriction enzymes were supplied by New England Biolabs (NEB), UK. Primer sequences are always written as 5' to 3'.

2.1 *Arabidopsis* seeds and growth conditions

Arabidopsis thaliana ecotype Columbia (Col-0) was used as the wild type plants. All used *Arabidopsis* mutant strains and transgenic lines were in Col-0 background and are outlined in **Table 2-1**. Seeds were stratified at 4-8°C in the dark for 2-4 days before moving to growth rooms. Seeds were placed on potting medium consisting of peat moss, vermiculite and sand (4:1:1), and then placed in a growth chamber and grown in long days (16 hours light and 8 hours dark) at 65% humidity and 22°C unless otherwise stated and illumination was provided by general fluorescent tube lighting at an intensity of 70-100 µmol $m^{-2}sec^{-1}$.

For aseptic growth, seeds were sterilised with 75% ethanol for 5 min, 10% (v/v) household bleach and a drop of Triton-X-100 for 20 minutes, washed 4 times in distilled water and maintained 2 days at 4-8°C in the dark to improve germination uniformity. Seeds were subsequently transferred to plates containing half strength MS (1/2 MS) basal salts supplemented with 0.3% (w/v) sucrose and 1% (w/v) agar, pH 5.8 where appropriate. Petri dishes were transferred to a growth chamber with 16 hours of light at 25°C and 8 hours of dark at 18°C.

Hydroponic system was set up following Gibeaut et al. 1997 and Conn et al. 2013. Seeds were stratified at 4-8°C in the dark for 2-4 days before placing on 0.6% agar-filled black seed holders. Seed holders were placed over trays containing water and seeds were covered with

clingfilm until germination. Germinated seeds were transferred to nutrient solution and grown in long days (16 hours light and 8 hours dark) at 65% humidity and 22°C and illumination was provided by general fluorescent tube lighting at an intensity of 70-100 µmol $m^{-2}sec^{-1}$.

Table 2-1. Plant lines used in this study.

Plant line name	Plant line type	Source
Col-0	Wild type	Loake lab
gsnor1-3	T-DNA insertion mutant	(Feechan et al., 2005)
par2-1	EMS mutant	(Chen et al., 2009a)
nox1/cue1-6	EMS mutant	(He et al., 2004; Li et al., 1995)
atg7-2	Transgenic	(Hofius et al., 2009)
GFP-ATG8a Col-0	Transgenic	(Thompson et al., 2005)
GFP-ATG8a *atg7-2*	Transgenic	(Thompson et al., 2005)
GFP-ATG8a *par2-1*	Transgenic	This study

2.2 Stress Treatments

For germination test, surface sterilized seeds were sown on 1/2MS plate containing different concentration of the following compound; NaCl (50 mM, 100 mM, 125 mM, 150 mM), KCl (50 mM, 100 mM, 125 mM, 150 mM), Mannitol (100 mM, 200 mM, 300 mM, 400 mM). Germinated seedlings were counted at 7 days after sowing. Appearance of green cotyledon was taken as the marker for germination.

For survival test and fresh weight measurement, after germination, 3-day-old seedlings from each line were carefully transferred to a fresh ½ MS agar plate supplemented with appropriate concentration of treatment component. After 7 days of growth on the treatment medium, seedlings which had green cotyledons were scored as survived and bleached

cotyledons were scored as dead. Fresh weight was taken per seedling in mg using Kern ABJ 120-4NM analytical balance.

For stress treatment for western blotting or microscopy, sterilized seeds were germinated in ½ MS agar plate. After 5-7 days of growth the seedlings were transferred to ½ MS agar plate supplemented with appropriate concentration of NaCl. The seedlings were then grown for 2-10 days before collecting for experiments.

For stress treatment on soil, four weeks old seedlings were irrigated from below with 200 mM aqueous NaCl solution in every 3 days for 14 days. Photographs were taken after that.

2.3 Determination of Sodium and Potassium content

The content of Na^+ and K^+ in shoot samples was analysed by the School of Geosciences, University of Edinburgh. 4-week-old soil grown plants were treated with or without 250 mM NaCl from below and shoot samples were collected at different time points. Shoot samples were dried in oven for 48 hours before grinding them into fine powder which were then sent to the School of Geosciences, University of Edinburgh for further analysis. Analysis was performed by research staff in the School of Geosciences. The digestion method was adapted from Chemical Analysis of Ecological Materials by Stewart E. Allen, Blackwell Publications. About 80 mg of ground dried sample was weighed and 2ml of concentrated sulphuric acid added and mixed well. 1.5 ml of 30% hydrogen peroxide were added and mixed well after the initial violent reaction. Samples were heated at 320°C for 6 hours and the resulting clear solution was subjected to Na^+ and K^+ were measurement using an iCE 3000 series Atomic Absorption spectrometer from Thermo Scientific of Cambridge England.

2.4 Measurement of abscisic acid (ABA) content

Abscisic acid was measured from plants treated with or without 250 mM NaCl by Miss Shuang Fang, Dr. Jinfang Chu in National Centre for Plant Gene Research (Beijing), Institute of Genetics and Developmental Biology, Chinese Academy of Sciences, Beijing, China and Dr. Yiqin Wang, State Key Laboratory of Plant Genomics, Institute of Genetics and Developmental Biology, Chinese Academy of Sciences, Beijing, China following the method described in (Fu et al., 2012). 4-week-old hydroponic grown (Gibeaut et al., 1997; Conn et al., 2013) plants were treated with or without 250 mM NaCl and shoot samples were collected at 0 hours and 5 hours. Samples were immediately frozen into liquid nitrogen and ground in fine powder using liquid nitrogen. 200 mg powdered samples per sample per replicate were then frozen in -80°C for 2 days before freeze dried. Freeze dried powder samples were then sent to China to our collaborators for ABA measurement. ABA was measured using ultra-high performance liquid chromatography-triple quadrupole mass spectrometry (UPLC-MS/MS) with negative electrospray ionization.

2.5 Total RNA extraction and cDNA synthesis

4-week-old hydroponic grown plants were treated with or without 250 mM NaCl and 100 mg leaf samples were collected at 0 hours to 24 hours. Samples were immediately frozen into liquid nitrogen and ground to fine powder using liquid nitrogen. RNA was extracted using QIAGEN RNeasy Plant Mini Kit following manufacturer's instruction. Before cDNA synthesis, RNA samples were quantified using a NanoDrop spectrophotometer (Thermo Scientific) and appropriate dilutions were made to ensure all samples contained equal amounts of RNA. Reverse transcription was performed using an Omniscript RT Kit (Qiagen) according to the manufacturer's instructions. Semi-quantitave RT-PCR was performed using the primers described in **Table 2-2**.

Table 2-2. Primers used for semi-quantitative RT-PCR.

Gene name	Primer Name	Primer Sequence	Tm (°C)	Cycle	Product length (bp)
RD22	rd22 F3	ATTGTGCGACGTCTTTGGAGTC	60	21	222
	rd22 R3	TCATCATCGCCTTGTGGCAGTA			
ERD1	ERD1 F	AGAGCTGTGAAGAGGTCCCG	60	23	180
	ERD1 R	CCAATCTCAGCATGGATTCTTCCG			
RD29a	rd29a F3	TCTGCTTTCTGGAACAGAGGATGT	60	23	346
	rd29a R3	GCGAATCCTTACCGAGAACAGAGT			
RD29b	rd29b F3	TTTCAGCAACAGAGGACGTGACTA	60	23	280
	rd29b R3	TTCGCGTCCTTGTCTTGATTTCTG			
RD26	RD26 RT F	GAAGGTGAGGCGGAGAGTG	60	23	110
	RD26 RT R	CCCGAAACTCTGAGTCAACCT			
ABF4	ABF4 F4	GGTTTTGCTGGGGCTGCAAA	52	25	284
	ABF4 R4	TCAATTTCGGCTTCCAGTTCCAATGTA			
DREB2a	Dreb2a F2	GACCTAAATGGCGACGATGT	52	25	146
	Dreb2a R2	TCGAGCTGAAACGGAGGTAT			
UBQ10	UBQ10 F	GATCTTTGCCGGAAAACAATTGGAGG ATGGT	52	25	500
	UBQ10 R	CGACTTGTCATTAGAAAGAAAGAGATA ACAGG			
Actin2	Actin2 F2	CACATTCCAGCAGATGTGGATCTC	52	25	249
	Actin2 R2	ACGCAGACGTAAGTAAAAACCCA			

2.6 Lysotracker green staining and confocal fluorescence microscopy

LysoTracker Green (LTG) fluorescence indicative of autophagy activity (Moriyasu et al., 2003; Liu et al., 2005) was detected by confocal microscopy. 5-day-old ½ MS grown seedlings were vacuum infiltrated with 1 mM LTG (DND-26, Molecular Probes, Inc.) at time points after NaCl stress and kept for an additional hour in darkness before visualization. Quantitation of

LTG stained autophagosome like structures was performed following the method described in (Liu et al., 2005). Confocal fluorescence microscopy was conducted using a Leica SP5 laser scanning confocal microscope at using 63X water objective (Leica Microsystem, UK). Excitation was at 480 nm and optical sections were collected with a GFP filter. Images were processed with LAS AF Lite for windows (Leica Microsystems). GFP-ATG8a Col-0 and GFP-ATG8a *atg7-2* transgenic lines were kindly provided by Prof. Richard Vierstra, Department of Genetics, University of Wisconsin, Wisconsin, USA. GFP-ATG8a Col-0 was crossed with *par2-1* and homozygous line was selected at F2 progeny using BASTA selection. Confocal microscopy was performed with or without the treatment of concanamycin A (CA). CA is a specific inhibitor for vacuolar-type ATPase (V-ATPase) usually used to visualise autophagic bodies inside the vacuole (Huss et al., 2002). During microautophagy, autophagosomes fuse with the vacuole for degradation mediated by vacuolar hydrolases. CA inhibits the V-ATPase thereby raising the pH of vacuole rendering inhibition to hydrolase mediated degradation of autophagic bodies facilitating visualisation (Thompson et al., 2005). 5-day-old ½ MS grown seedlings were treated with or without 150 mM NaCl for 48 hours before visualising with confocal microscopy as described previously. Seedlings with CA treatment were incubated with or without NaCl for 24 hours before vacuum infiltrating with CA followed by another 24 hours in NaCl stress in dark.

2.7 NBR1 protein analysis

For the analysis of total NBR1 protein accumulation, 5-day-old ½MS grown seedlings were transferred to ½MS agar plates containing 100 mM NaCl and incubated for 5-10 days. 100 mg samples were snap frozen in liquid nitrogen and mechanically ground before adding 100 µl of urea extraction buffer (4M urea, 100mM DTT, 1% Triton X-100, 1X Protease Inhibitor Cocktail (Sigma, St. Louis, MO, USA)). Protein extract was centrifuged for 15 min at 13000g at

4°C. The supernatants were collected, boiled on SDS-loading buffer (100mM Tris-HCl, pH 6.8, 20% glycerol, 4% SDS, 5 mM DTT and 1% Bromophenol blue) and separated on 10% SDS-PAGE gels. Immunoblot analysis was performed using a 1:500 dilutions of anti-NBR1 polyclonal antibody (anti-NBR1 antisera was kindly provided by Prof. Terje Johansen, University of Tromso, Norway). For insoluble NBR1 protein accumulation, seedlings samples were homogenized in tris extraction buffer (100 mM Tris-HCl pH 8.0, 100 mM DTT, 10 mM NaCl, 1 mM EDTA, 1% Triton X-100, 1X Protease Inhibitor (Sigma, St. Louis, MO, USA)). Soluble protein fraction was collected by centrifugation for 5 min at 2500g at 4°C. The pellets were resuspended in the aforementioned urea extraction buffer. Protein extract was centrifuged for 15 min at 13000g at 4°C before subjected to western blotting as above to detect NBR1 in the insoluble fraction.

2.8 Constructs for protein expression in *E. coli*

The coding sequence of the genes (**Table 2.4**) were amplified using Phire Hot Start II DNA Polymerase (ThermoFisher Scientific) from freshly synthetized cDNA of wild type *Arabidopsis* Col-0 accession. For restriction cloning method, restriction enzyme cutting sites were added to the primers. Restriction cloning was used for constructs were stated using appropriate restriction enzymes. Digested PCR products were ligated to appropriately digested expression plasmid using T4 ligase (NEB) and transformed into *E. coli* competent cells DH5α. Single colonies were first confirmed using colony PCR before isolating and extracting plasmid for verification by sequencing. For Gateway® (Invitrogen) cloning system primers (**Table2-3**) were designed to add the attb1 and attb2 sites according to the manufacturer protocol, thus allowing BP cloning using donor vector pDONR221. The PCR products were gel-purified and cloned into the pDONR221 vector using BP reaction according to the manufacturers' instructions. Constructs were transformed into chemically competent

E. coli DH5α using heat shock method and selected on Kanamycin plates. Single colonies were isolated, submitted to plasmid purification and validated by sequencing. Inserts from positive constructs were transferred by LR recombination from Gateway® cloning (Invitrogen) into the appropriate destination vectors **(Table 2-4**) Recombinant clones were selected on appropriate antibiotic plates and confirmed by sequencing.

Table 2-3. Primers used to make plasmid construct.

Amplicon	**Primer Name**	**Primer Sequence**
ATG7 C-terminal domain coding sequence	NotI-ATG7 CTD F4	ttttGCGGCCGCTCAGGTGAATCAGCTGAGACTGTACCT
	EcoRI-ATG7 R3	ttttGAATTCTTAAAGATCTACAGCTACATCGTCATCATCAGT
ATG7 C-terminal domain coding sequence	attB1(C)-ATG7(880-906) F	GGGGACAAGTTTGTACAAAAAAGCAGGCTTCATGTCAGGTGAATCAGCTGAGACTGTACCT
	attB2(K)-ATG7(2062-2094)-S-R	GGGGACCACTTTGTACAAGAAAGCTGGGTTTTAAAGATCTACAGCTACATCGTCATCATCAGT
ATG7 N-terminal domain coding sequence	attB1(C)-ATG7(1-26) F	GGGGACAAGTTTGTACAAAAAAGCAGGCTTCATGGCTGAGAAAGAAACTCCAGCAAT
	attb2(K)ATG7-NTD R	GGGGACCACTTTGTACAAGAAAGCTGGGTTTTATGAAAGTGTAATTGAGGCTTGACCAACA
ATG8a G132 exposed coding sequence	BamHI-ATG8a F2	aaaaGGATCCATGATCTTTGCTTGCTTGAAATTCGCA
	NotI-ATG8a R2	aaaaGCGGCCGCTCATCCAAAAGTGTTCTCTCCACTGT
ATG8a G132 exposed coding sequence	attB1(C)ATG8a-F	GGGGACAAGTTTGTACAAAAAAGCAGGCTTCATGATCTTTGCTTGCTTGAAATTCGCA
	attb2-ATG8a-G132-S-R	GGGGACCACTTTGTACAAGAAAGCTGGGTTTTATCATCCAAAAGTGTTCTCTCCACTGT
TRXh5 coding sequence	BamHI-TRX-h5 F1	aaaaGGATCCATGGCCGGTGAAGGAGAAGTGA
	NotI-TRX-h5-S-R1	ttttGCGGCCGCTCAAGCAGAAGCTACAAGACCACCAT

NTRA coding sequence	BamHI-AtNTRA F	aaaaGGATCCATGAGCCAGTCAAGATTCATTATAAA
	NotI-AtNTRA R	aaaaGCGGCCGCATCACTCTTACCCTCCTGAGA

*Gene specific sequences are underlined.

Table 2-4. Constructs generated in this study.

Gene name	vector name	Fusion tag	Construct
ATG7	pMalC5X	N-terminal MBP	pMalC5X-*ATG7*^{CTD}
	pETG40A	N-terminal MBP	pETG40A-*ATG7*^{CTD}
	pETG40A	N-terminal MBP	pETG40A-*ATG7*^{CTD} C558A
	pETG40A	N-terminal MBP	pETG40A-*ATG7*^{CTD} C637S
	pETG40A	N-terminal MBP	pETG40A-*ATG7*^{CTD} C558A C637S
	pETG40A	N-terminal MBP	pETG40A-*ATG7*^{CTD} C634S C637S
	pETG40A	N-terminal MBP	pETG40A-*ATG7*^{CTD} C558A C634S C637S
	pETG40A	N-terminal MBP	pETG40A-*ATG7*^{NTD}
	pGWB15	N-terminal 3XHA	pGWB15-*ATG7*^{FL}
	pGWB15	N-terminal 3XHA	pGWB15-*ATG7*^{CTD}
ATG8a	pET28a	N-terminal 6XHis	pET28a-*ATG8a*^{G132}
TRXh5	pET28a	N-terminal 6XHis	pET28a-*TRXh5*
TRXh5	pET28a	N-terminal 6XHis	pET28a-*TRXh5* C42S
NTRA	pET28a	N & C terminal dual 6XHis	pET28a-*NTRA*

2.9 Site-directed mutagenesis

All site-directed mutagenesis reactions were performed using the QuickChange Lightning Site-directed Mutagenesis Kit (Agilent Technologies) according to manufacturers' instructions. Two complementary primers were synthesized to each desired mutation (**Table 2-5**) and used in the PCR reaction following the conditions: 5 µL of 10x reaction buffer, 50 ng

of plasmid DNA, 125 ng of each complementary primer, 1µL of dNTP mix (10 mM), 3 µL of QuikSolution reagent, 2.5 U of Pfu Ultra HF DNA polymerase and distilled water to a final volume of 50 µL. The reaction parameters were as follow: 95°C 2 min, followed by 95°C for 50 sec, 52°C for 50 sec and 68°C for 4 min, 18 cycles finally 68°C for 5 min. After that, parental plasmids were digested with Dpn I (10 U) at 37°C for 5 min and the Dpn I-treated DNA was transformed into XL10-Gold ultracompetent cells. The mutated expression plasmid was purified and the mutated site was confirmed by DNA sequencing using appropriate primers.

Table 2-5. Primers used for site-directed mutagenesis of Cys residues of *ATG7*.

Mutation	Primer sequence
C558A	TGATCGAACTCTAGACCAACAAGCCACTGTTACACGCCC
	GGGCGTGTAACAGTGGCTTGTTGGTCTAGAGTTCGATCA
C637A	TCCAACAGCTGTACCGCTGCCTCTGAAACCGTGATATC
	GATATCACGGTTTCAGAGGCAGCGGTACAGCTGTTGGA
C637S	CAACAGCTGTACCGCTAGCTCTGAAACCGTG
	CACGGTTTCAGAGCTAGCGGTACAGCTGTTG
C634S C637S	TTGGTCAAGCTTCCAACAGCAGTACCGCTAGCTCTGAAACCGTGATAT
	ATATCACGGTTTCAGAGCTAGCGGTACTGCTGTTGGAAGCTTGACCAA

*Sites for mutation are underlined.

2.10 Recombinant protein expression and purification

E. coli BL21(DE3) cells were transformed with the appropriate constructs selected on LB agar plates supplemented with appropriate antibiotics. Single colonies were selected and grown overnight in 5 mL LB medium supplemented with antibiotic at 37°C and 250 rpm. Overnight cultures were diluted in 500 mL of LB medium also supplemented with antibiotic using 2 L conical flask and incubated at 37°C, 250 rpm until O.D. reached 0.6-0.7. IPTG was added at a range of 0.1-1 mM (details are given in **chapter 6**) and cultures were further

incubated for 1-4 hours. Cells were harvested by centrifugation at 6000 g for 15 minutes and pellet was stored at -20°C before proceeding to the purification step. Fusion proteins were purified by gravity-flow using appropriate affinity chromatography columns corresponding to the fusion tag according to the manufacturers' instructions. The fusion proteins were run in a SDS-PAGE gel and concentration was quantified. Finally, the proteins were stored at -80°C for later usage.

2.11 S-nitrosylation and denitrosylation assays

The biotin-switch technique (Jaffrey et al., 2001; Jaffrey and Snyder, 2001) was employed with minor modification to detect S-nitrosylation of recombinant proteins exposed to NO donors and endogenously modified proteins expressed in *Arabidopsis*.

For *in vitro* assays 15 µg of purified recombinant protein was equilibrated with buffer containing (250 mM HEPES pH7.7, 1 mM EDTA, 0.1 mM Neocuproine) before treating with different concentrations (10-500 µM) of NO donors (GSNO or CysNO) for 20 minutes in dark. Excess of NO donor was removed using Zeba™ Spin Desalting Columns (7K MWCO, 0.5 mL, ThermoFisher Scientific). Free thiols were blocked in four volume of blocking buffer (250 mM HEPES pH 7.7, 1 mM EDTA, 0.1 mM Neocuproine, 2.5% (w/v) SDS, 20 mM MMTS) for 20 minutes at 50°C. The blocking buffer was removed by precipitating proteins with two volumes of cold acetone. After one hour at -20°C, samples were centrifuged at 15000 g for 15 minutes at 4°C. Samples were washed two times with 70% acetone and resuspended in 30 µL of $HENS_{1\%}$ labelling buffer (250 mM HEPES, 1 mM EDTA, 0.1 mM Neocuproine,1% (w/v) SDS, 1 mM sodium ascorbate, 1 mM biotin-HPDP (N-[6-(biotinamido)hexyl]-3'-(2'-pyridyldithio)-propionamide)). Samples were incubated at room temperature for one hour in dark. Samples were run on a 12% non-reducing SDS-PAGE and submitted to western blots with an anti-Biotin antibody.

For the *in vitro* denitrosylation assay, recombinant $ATG7^{CTD}$ was incubated with 200 µM GSNO for 20 mins in the dark before removal of GSNO by Zeba desalting spin columns (Thermo Scientific). Reactions were set up in 100 µl volumes of HEN buffer (250 mM HEPES pH7.7, 1 mM EDTA, 0.1 mM neocuproine) containing 50 µM $ATG7^{CTD}$ and additional components at the following concentrations; 5 µM TRX5, 0.5 µM NTRA and 5 mM NADPH. Denitrosylation reactions were incubated at RT in the dark for 1 hr before samples were directly used for biotin switch technique described previously.

Endogenous S-nitrosylation of ATG7 was detected by *in vivo* BST. 5-day-old ½ MS grown seedlings were treated with or without 100 mM NaCl for five days. Samples were collected and snap frozen in liquid nitrogen before subjected to BST. 200 mg samples were homogenised in extraction buffer (250 mM HEPES pH7.7, 1 mM EDTA, 0.1 mM Neocuproine, 100 mM NaCl, 0.5% Triton X-100, 1X protease inhibitor cocktail) and samples were centrifuged at 13,000 rpm at 4°C for 15 minutes. Supernatant was collected and submitted to the biotin switch as described above, but omitting the addition of NO donors. Samples were blocked using the blocking buffer containing (250 mM HEPES pH 7.7, 1 mM EDTA, 0.1 mM Neocuproine, 5% (w/v) SDS, 100 mM NEM). After labelling with Biotin-HPDP, samples were precipitated and washed with acetone. Samples were air dried before resuspending in 200 µL of $H_{25}ENS_{1\%}$ (25 mM HEPES pH 7.7, 1 mM EDTA, 0.1 mM Neocuproine, 1% SDS) and submitted to streptavidin pull-down. Samples were subjected to pull down using streptavidin agarose beads. Before the pull-down step, 20 µL was taken from each sample, mixed with reducing protein loading buffer, heated for five minutes at 99°C and kept at -20°C. The remaining 180 µL were mixed with 1 mL of neutralisation buffer (25 mM HEPES, 1 mM EDTA, 0.1 mM Neocuproine, 100 mM NaCl, 0.5% Triton X-100). 20 µL of streptavidin beads, pre-washed and resuspended in 100 µL of neutralisation buffer, was added to each sample and incubated at 4°C on a rotating mixer overnight. Next morning, samples were washed five

times with 400 µL of wash buffer (25 mM HEPES, 1 mM EDTA, 0.1 mM Neocuproine, 600 mM NaCl, 0.5% Triton X-100) and resuspended in 20 µL of elution buffer (25 mM HEPES, 1 mM EDTA, 0.1 mM Neocuproine, 1%β-mercaptoethanol v/v). After 30 minutes at room temperature, beads were spun down for one minute at room temperature and maximum speed. Samples were collected and detected by western blot using an anti-ATG7 antibody.

2.12 *In vitro* assay for ATG7^{CTD}-ATG8a^{G132} thioester intermediates

For detecting ATG7^{CTD}-ATG8a^{G132} thioester intermediates, recombinant ATG7^{CTD} and ATG8a^{G132} were incubated in reaction buffer containing 50 mM HEPES pH 7.5, 150 mM NaCl, 1 mM ATP, and 1 mM $MgCl_2$ at 30°C for 2 hours. Reactions were incubated in the dark when NO donor was added. All the reactions were stopped by mixing with SDS sample buffer and analysed by SDS-PAGE and western blotting using anti-MBP antibody.

2.13 SDS-PAGE and western blots

Protein samples were mixed with a 6X stock of SDS sample buffer to a final concentration of 10 mM Tris-HCl pH 6.8, 2% SDS, 0.025%bromophenol blue and 8% glycerol with or without 10 mM dithiothreitol (DTT). Next, samples were heated at 95°C for 5 min before separating on gels of appropriate polyacrylamide percentage. Coomassie Blue staining, gels were washed in ddH2O before incubating in staining solution (0.1% Brilliant Blue R, 50%methanol, 10% acetic acid) for 30 min to one hour. Gels were then de-stained overnight in de-staining solution (30% methanol, 10% acetic acid) and photographed.

For western blots, proteins were transferred on to nitrocellulose membranes either overnight at a constant voltage of 20V or for 2-3 hours at 80V. Proteins were visualised on the membranes before blocking by staining with Ponceau S (0.1% Ponceau S, 5% acetic acid) for 1 min followed by rinses with PBS to remove background staining. Photographs were taken

before the stain was completely removed with PBST (PBS, 0.2% tween 20). After that, membranes were blocked for 1 hour at room temperature using 5% dried skimmed milk in PBST and incubated with primary antibodies **(Table 2-6)** either at 4°C overnight or for 1-2 hours at room temperature with the only exception of biotin switch where the membranes were blocked with 5% BSA (bovine serum albumin) in PBST. After washing the membrane to remove the excess of primary antibody, appropriate secondary antibodies **(Table 2-7)** coupled to horseradish peroxidase (HRP) were incubated with the membrane for 1 hour at room temperature. After another washing to remove the excess of secondary antibody SuperSignal West Pico/Dura Chemiluminescent Substrate (Thermo Scientific) was added to the membranes and bands were detected on X-ray films. All antibodies were diluted in 1% skimmed milk in PBST except for the anti-biotin HRP antibody which was diluted in 1% BSA in PBST.

Table 2-6. List of primary antibodies used.

Antibody name	Dilution use	Host species	Manufacturer	Product code
Anti-MBP HRP conjugated	1:10,000	mouse	NEB	E8032S
Anti-Biotin HRP conjugated	1:5,000	goat	Cell signalling	7075S
Anti-ATG7 unconjugated	1:1000	rabbit	abcam	ab99001
Anti-NBR1 unconjugated	1:500	rabbit	(Svenning et al., 2011)	

Table 2-7. List of secondary antibodies used.

Antibody name	Dilution use	Host species	Manufacturer	Product code
Anti-Rabbit IgG HRP conjugated	1:10,000	goat	abcam	ab205718

2.14 Identification of S-nitrosylation sites

20 µg purified recombinant protein was treated without or with NO donor (GSNO, 500 uM) for 20 minutes at room temperature to induce SNO formation. Samples were passed through column to remove excess GSNO. Alkylation was performed with 4X sample volume of 20 mM N-ethylmaleimide (NEM), 2.5% SDS to block non-S-nitrosylated free thiols. Samples were precipitated and washed with acetone. Dried samples were then sent to our collaborator Dr. David Clarke, School of Chemistry, University of Edinburgh for the detection of S-nitrosylation site(s) by LC-MS/MS. Samples were reduced with 50 mM DTT, 6M guandine-HCl, pH 7.5 before performing in solution digestion with trypsin. Digested samples were analysed by nESI (nano-electrospray ionisation) on FT-ICR (fourier transform-ion cyclotron resonance).

2.15 Protein structure modelling and analysis

Protein structures were viewed and analysed using PyMOL™ molecular graphics system (v. 1.7.4.4. Educational build, Schrödinger**,** LLC). The crystal structures of yeast free ATG7 and ATG7-ATG8 complex (Noda et al., 2011) were downloaded from the Protein Data Bank (http://www.rcsb.org/pdb) with the PDB codes 3VH2 and 3VH4 respectively. The predicted structure of *Arabidopsis* ATG7 was modelled using Phyre2 protein structure prediction (http://www.sbg.bio.ic.ac.uk/phyre2) (Kelley et al., 2015).

Chapter-3

3 Investigating the effect of salt and osmotic stress on *Arabidopsis thaliana gsnor1-3* and *nox1* plants

3.1 Introduction

Salt and drought stresses are the most common abiotic stresses for crop plants (Munns, 2002). Salt and drought stresses affect almost all aspects of plant physiology and metabolism (Zhu, 2002). Both stresses have some common features including osmotic stress. Salt stress can be distinguished from drought stress in creating Na^+ toxicity and K^+ deficiency apart from causing osmotic stress (Munns and Tester, 2008). High soil salt concentrations induce stress in plants in two distinct mechanisms. Firstly, they impede water extraction from the soil by root and secondly, a high concentration of salts within the plant result in toxicity (Munns and Tester, 2008). Plants respond to salt stress in two phases. The first phase is the osmotic phase where pressure is exerted by the high salt content of soil on the roots. The second phase is the ion specific phase, where the plant accumulates salt at toxic levels within the cells leading to cell death (Munns and Tester, 2008). The osmotic stress happens quickly and plants rapidly adjust the osmotic pressure of the cells as osmotic stress causes membrane disruption and enzyme dysfunction if persist for a longer period. The ionic stress progresses slowly with the accumulation of the toxic ions in the cells leading to perturbations of key cellular functions (Munns and Tester, 2008). There are several signs and symptoms of salt stress on plants. Salt stress particularly impairs germination and establishment of seeds, inhibits the vegetative growth, causes leaf chlorosis or leaf yellowing and finally affects reproduction and yields (Munns, 2002; Munns and Tester, 2008; Läuchli and Grattan, 2007).

A significant feature during salt stress is the rapid production of nitric oxide (NO), an important concentration dependent, redox-related signalling molecule (Neill et al., 2008; Yu et al., 2014). NO can directly or indirectly interact with a wide range of targets including proteins leading to the modulation of protein function and the reprogramming of gene expression (Fancy et al., 2016). The transfer of NO bioactivity can occur through a variety of potential mechanisms but chief among these is S-nitrosylation, the covalent attachment of NO group to a cysteine (Cys) thiol (SH) to form S-nitrosothiol (SNO) (Stamler et al., 1992). S-nitrosylation of the antioxidant tripeptide glutathione (GSH) forms S-nitrosoglutathione (GSNO). GSNO acts as the principal mobile reservoir of NO in the cell because GSNO can donate NO to other proteins in a process termed tansnitrosylation (Yu et al., 2014). Both NO and GSNO can S-nitrosylate cellular proteins containing rare, highly reactive, solvent exposed cysteine (Cys) residues to form protein SNOs (Yu et al., 2014). *Arabidopsis thaliana* S-nitrosoglutathione (GSNO) reductase (*GSNOR1*), turns over GSNO, thereby controlling total cellular concentrations of GSNO directly and protein SNO indirectly (Feechan et al., 2005). Loss-of-function mutations in *GSNOR1* results in elevated total cellular SNO concentrations while enhanced *GSNOR1* activity promotes the turnover of these metabolites in *Arabidopsis* (Feechan et al., 2005). Although there has been extensive research on the NO regulation of plant salt tolerance/susceptibility, there is little work on the role of *GSNOR1* in plant salt tolerance.

For this study, *Arabidopsis GSNOR1* loss-of-function mutant *gsnor1-3 and NO overproducer 1* (*nox1*) plants were used. In contrast with *gsnor1-3, nox1* plants have a high level of NO in leaves and roots (He et al., 2004; Feechan et al., 2005; Vitecek et al., 2008). However, recently it has been shown that NO can S-nitrosylate GSNOR1 leading to a reduction of activity (Frungillo et al., 2014). Thus, *nox1* plants may have a reduced GSNOR1 activity in conjunction with a high level of NO. Work presented in this chapter aims to investigate the

role of the *GSNOR1* gene and S-nitrosylation in the regulation of plant salt tolerance.

3.2 Effects of different salts on seed germination of *gsnor1-3* and *nox1* plants

Germination tests were performed to check the effects of four different salts (NaCl, KCl) on seed germination of different *Arabidopsis* lines (Col-0 as wild type, *gsnor1-3* & *nox1*) on ½MS agar plates. The following concentrations of salts were used for the experiment; NaCl (50 mM, 100 mM, 125 mM, 150 mM); KCl (50 mM, 100 mM, 125 mM, 150 mM); Experiment was done following the procedure described in **chapter 2.2**. In conjunction with NaCl, KCl is often used as salt stress indicator to differentiate between Na^+ and K^+ specific stress response (Affenzeller et al., 2009).

gsnor1-3 seeds showed increased sensitivity in the presence of both NaCl and KCl at the germination stage. The germination percentage of *gsnor1-3* seeds were lower than that of wild type and *nox1* plants in both NaCl and KCl (**Fig. 3-1A, B & Fig. 3-2A, B**). Statistical analysis of variance and Tukey's simultaneous tests for differences of means (two-way ANOVA, Minitab 17) showed that compared to wild type, *gsnor1-3* seeds have a significantly reduced germination percentage in 100 mM and 125 mM NaCl, whereas *nox1* plants did not show any significant difference (**Fig. 3-1C**). Thus, *gsnor1-3* seeds have 38% and 7% germination, in 100 mM and 125 mM NaCl, respectively, whereas the wild type line Col-0 showed 90% and 50% germination and *nox1* showed 65% and 48% germination in 100 mM and 125 mM NaCl respectively. Similarly, statistical analysis further showed that compared to wild type, *gsnor1-3* seeds have a significantly reduced germination percentage in 100 mM and 125 mM KCl, whereas *nox1* showed a significantly reduced germination only at 125 mM KCl (**Fig. 3-2C**). *gsnor1-3* seeds have 50% and 16% germination, whereas the wild type showed 93% and 68% and *nox1* has 71% and 13% germination in 100 mM and 125 mM KCl, respectively.

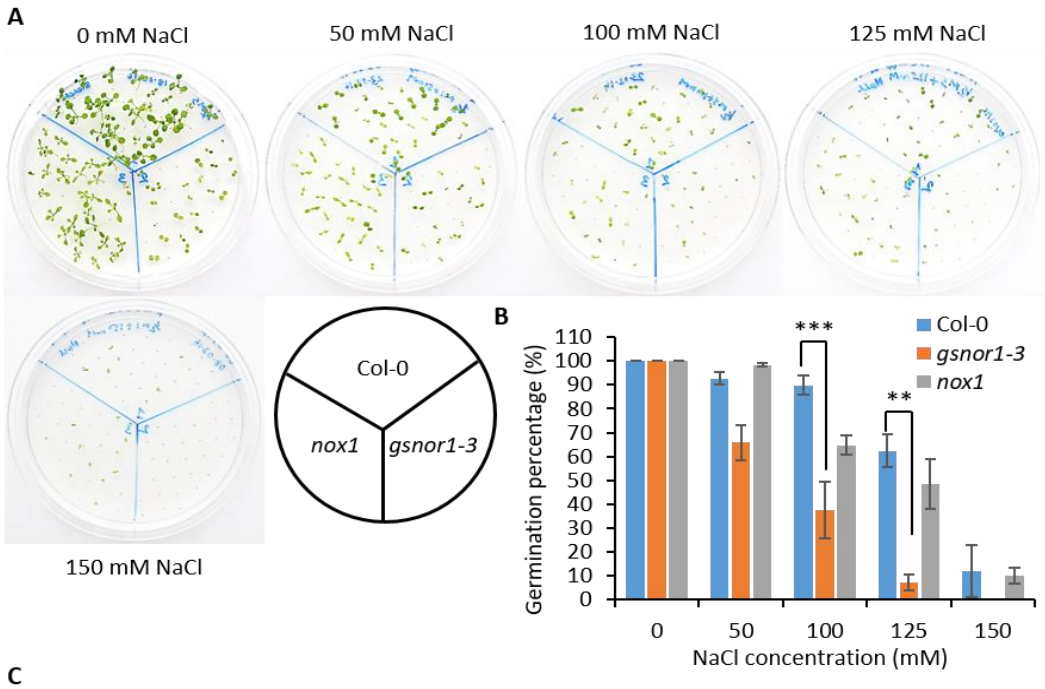

C

Two-way ANOVA & Tukey's Simultaneous Tests for Differences of Means

	0 mM		50 mM		100 mM		125 mM		150 mM	
	Significance	P-value	Significance	P-value	Significance	P-value	Significance	P-value	Significance	P-value
Col-0 & *gsnor1-3*	ns	1	ns	0.256	***	0.000	**	0.012	ns	0.998
Col-0 & *nox1*	ns	1	ns	1	ns	0.455	ns	0.991	ns	1
gsnor1-3* & *nox1	ns	1	ns	0.11	ns	0.334	**	0.011	ns	0.999

	0 mM & 50 mM		0 mM & 100 mM		0 mM & 125 mM		0 mM & 150 mM	
	Significance	P-value	Significance	P-value	Significance	P-value	Significance	P-value
Col-0	ns	1	ns	0.999	*	0.03	***	0.000
gsnor1-3	*	0.042	***	0.000	***	0.000	***	0.000
nox1	ns	1	ns	0.087	***	0.001	***	0.000

Figure 3-1. Sensitivity of *gsnor1-3* and *nox1* seeds to NaCl.

A) Surface sterilised seeds were placed on agar plates containing ½MS media supplemented with NaCl at the concentrations indicated. Germination was counted at the appearance of green cotyledon 7 days after the seeds were plated. **B)** The bar chart represents germination percentage calculated from 30 seeds. Values are mean ± SEM (n=4). **C)** Two-way ANOVA and Tukey simultaneous tests for differences of means performed by statistical package Minitab 17; SEM, standard error of mean; not significant (ns), $p > 0.05$; *, $p \leq 0.05$; **, $p \leq 0.01$; ***, $P \leq 0.001$. The threshold of family wise significance was set at 0.05.

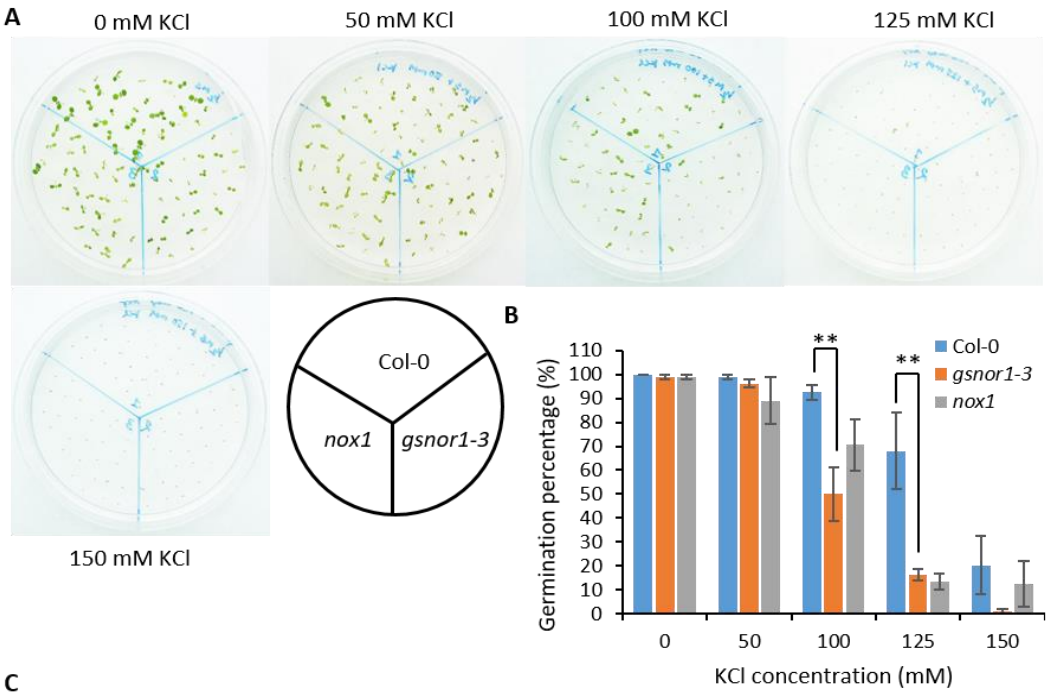

C

Two-way ANOVA & Tukey's Simultaneous Tests for Differences of Means

	0 mM		50 mM		100 mM		125 mM		150 mM	
	Significance	P-value	Significance	P-value	Significance	P-value	Significance	P-value	Significance	P-value
Col-0 & *gsnor1-3*	ns	1	ns	1	**	0.009	**	0.007	ns	0.738
Col-0 & *nox1*	ns	1	ns	0.999	ns	0.549	**	0.004	ns	1
gsnor1-3* & *nox1	ns	1	ns	1	ns	0.761	ns	1	ns	0.994

	0 mM & 50 mM		0 mM & 100 mM		0 mM & 125 mM		0 mM & 150 mM	
	Significance	P-value	Significance	P-value	Significance	P-value	Significance	P-value
Col-0	ns	1	ns	1	ns	0.28	***	0.000
gsnor1-3	ns	1	***	0.001	***	0.000	***	0.000
nox1	ns	0.999	ns	0.171	***	0.000	***	0.000

Figure 3-2. Sensitivity of *gsnor1-3* and *nox1* seeds to KCl.

A) Surface sterilised seeds were placed on agar plates containing ½MS media supplemented with KCl at the concentrations indicated. Germination was counted at the appearance of green cotyledon 7 days after the seeds were plated. **B)** The bar chart represents germination percentage calculated from 30 seeds. Values are mean ± SEM (n=4). **C)** Two-way ANOVA and Tukey simultaneous tests for differences of means performed by statistical package Minitab 17; SEM, standard error of mean; not significant (ns), $p > 0.05$; *, $p \leq 0.05$; **, $p \leq 0.01$; ***, $P \leq 0.001$. The threshold of family wise significance was set at 0.05.

3.3 Effect of different salts on the survival of *gsnor1-3* and *nox1* seedlings

After checking the germination, the effect of NaCl and KCl on the survival of *gsnor1-3* & *nox1* seedlings was tested on ½MS agar plates following the procedure described in **chapter 2.2**. It is important to note that the ages of the seedlings were synchronised before transferring them into new plates. *gsnor1-3* plants have a slower germination rate, so the seeds were plated before the wild type and *nox1* seeds. At three days post-germination, the seedlings were transferred to new plates containing given concentrations of NaCl and KCl. Seedlings for the control plates were transferred to fresh ½MS agar plates with no added NaCl or KCl. In the presence of different concentrations of NaCl (50 mM, 100 mM, 125 mM, 150 mM), and KCl (50 mM, 100 mM, 125 mM, 150 mM) the survival of *gsnor1-3* seedlings was lower than that of wild type (**Fig. 3-3A, B & Fig. 3-4A, B**). *nox1* showed some sensitivity at the seedling stage at 125 mM NaCl, 100 mM KCl and 125 mM KCl. Statistical analysis of variance and Tukey's simultaneous tests for differences of means (two-way ANOVA, Minitab 17) showed that compared to controls, *gsnor1-3* plants showed significantly reduced survival in the presence of 100 mM and 125 mM NaCl while *nox1* showed significantly reduced germination in only 125 mM NaCl (**Fig. 3-3C**). Wild type plants had 95.6% and 81.7% whereas *gsnor1-3* plants had 58.9% and 34.2% survival in 100 mM and 125 mM NaCl respectively. Similarly, compared to controls, both *gsnor1-3* and *nox1* plants showed reduced survival in the presence of 100 mM and 125 mM KCl (**Fig. 3-4C**).

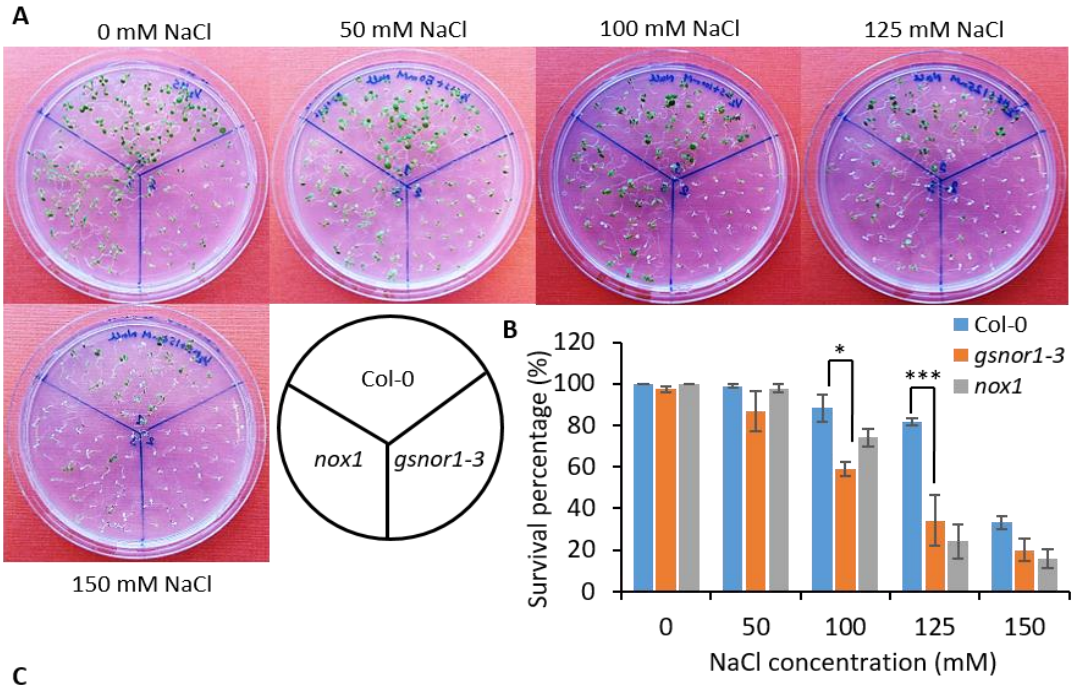

C

Two-way ANOVA & Tukey's Simultaneous Tests for Differences of Means

	0 mM		50 mM		100 mM		125 mM		150 mM	
	Significance	P-value	Significance	P-value	Significance	P-value	Significance	P-value	Significance	P-value
Col-0 & *gsnor1-3*	ns	1	ns	0.996	*	0.038	***	0.000	ns	0.957
Col-0 & *nox1*	ns	1	ns	1	ns	0.581	***	0.000	ns	0.756
gsnor1-3* & *nox1	ns	1	ns	0.998	ns	0.993	Ns	0.997	ns	1

	0 mM & 50 mM		0 mM & 100 mM		0 mM & 125 mM		0 mM & 150 mM	
	Significance	P-value	Significance	P-value	Significance	P-value	Significance	P-value
Col-0	ns	1	ns	1	ns	0.695	***	0.000
gsnor1-3	ns	0.997	**	0.011	***	0.000	***	0.000
nox1	ns	1	ns	0.186	***	0.000	***	0.000

Figure 3-3. Sensitivity of *gsnor1-3* and *nox1* seedlings to NaCl.

A) Sterilised seeds were placed on ½MS agar plates. Three days after germination the seedlings were transferred to agar plates containing ½MS media supplemented with NaCl at the concentrations indicated. Survival was counted at the presence of green cotyledon 7 days after seedling were transferred. Bleached cotyledons were scored as dead. **B)** The bar chart represents seedling survival percentage calculated from 30 seedlings. Values are mean ± SEM (n=4). **C)** Two-way ANOVA and Tukey simultaneous tests for differences of means performed by statistical package Minitab 17; SEM, standard error of mean; not significant (ns), $p > 0.05$; *, $p \leq 0.05$; **, $p \leq 0.01$; ***, $P \leq 0.001$.

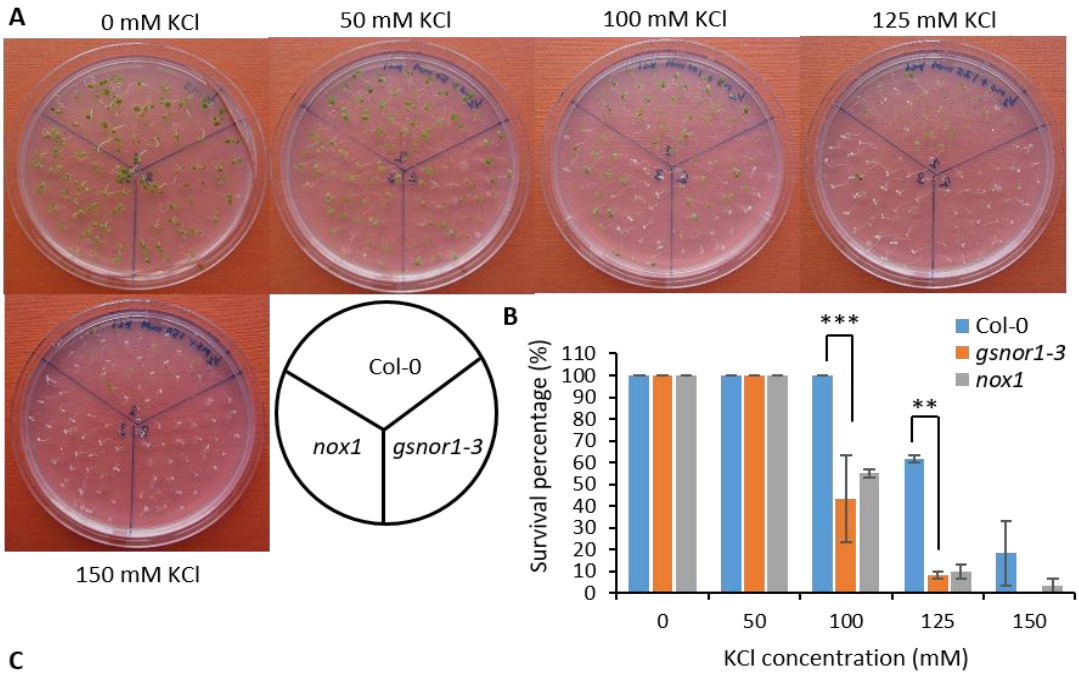

C

Two-way ANOVA & Tukey's Simultaneous Tests for Differences of Means

	0 mM		50 mM		100 mM		125 mM		150 mM	
	Significance	P-value	Significance	P-value	Significance	P-value	Significance	P-value	Significance	P-value
Col-0 & *gsnor1-3*	ns	1	ns	1	***	0.001	**	0.002	ns	0.793
Col-0 & *nox1*	ns	1	ns	1	*	0.012	**	0.003	ns	0.933
gsnor1-3* & *nox1	ns	1	ns	1	ns	0.99	ns	1	ns	1

	0 mM & 50 mM		0 mM & 100 mM		0 mM & 125 mM		0 mM & 150 mM	
	Significance	P-value	Significance	P-value	Significance	P-value	Significance	P-value
Col-0	ns	1	ns	1	*	0.042	***	0.000
gsnor1-3	ns	1	***	0.001	***	0.000	***	0.000
nox1	ns	1	*	0.012	***	0.000	***	0.000

Figure 3-4. Sensitivity of *gsnor1-3* and *nox1* seedlings to KCl.

A) Sterilised seeds were placed on ½MS agar plates. Three days after germination the seedlings were transferred to agar plates containing ½MS media supplemented with KCl at the concentrations indicated. Survival was counted at the presence of green cotyledon 7 days after seedling transfer. Bleached cotyledons were scored as dead. **B)** The bar chart represents seedling survival percentage calculated from 30 seedlings. Values are mean ± SEM (n=3). **C)** Two-way ANOVA and Tukey simultaneous tests for differences of means performed by statistical package Minitab 17; SEM, standard error of mean; not significant (ns), $p > 0.05$; *, $p \leq 0.05$; **, $p \leq 0.01$; ***, $P \leq 0.001$.

3.4 *gsnor1-3* plants had more fresh weight reduction compared to wild type plants in the presence of NaCl

At seedling stage, another growth parameter- seedling fresh weight- was tested following the procedure described in **chapter 2.2**. In the presence of different concentrations of NaCl (50 mM, 100 mM, 125 mM, 150 mM), the fresh weight of *gsnor1-3* was lower than that of control plants (**Fig. 3-5A**). It should be noted that *gsnor1-3* has lower fresh weight compared to wild type even under control conditions. Statistical analysis of variance and Tukey's simultaneous tests for differences of means (two-way ANOVA, Minitab 17) showed that compared to controls, *gsnor1-3* seedlings have significantly less fresh weight at 100 mM and 125 mM NaCl, whereas wild type seedlings have reduced fresh weight only at a higher concentration of NaCl (**Fig. 3-5B)**. Interestingly, *nox1* did not show any fresh weight reduction in any concentration of NaCl.

3.5 Mannitol has negative effects on seed germination of *gsnor1-3* plants

Mannitol is deployed as a well-established test sugar for osmotic stress (Tholakalabavi et al., 2013; Neto et al., 2004). Germination tests were performed to check the effects of mannitol on seed germination of different *Arabidopsis* lines (Col-0, *gsnor1-3* & *nox1*) on ½MS agar plates containing different concentrations of mannitol following the procedure described in **chapter 2.2**. *gsnor1-3* seeds showed increased sensitivity under mannitol stress at germination. In the presence of different concentrations of mannitol (100 mM, 200 mM, 300 mM, 400 mM), *gsnor1-3* plants showed reduced germination than that of wild type and *nox1* (**Fig. 3-6A, B**). Statistical analysis of variance and Tukey's simultaneous tests for differences of means (two-way ANOVA, Minitab 17) showed that compared to wild type, *gsnor1-3* seeds have a significantly reduced germination percentage in 300 mM mannitol, whereas *nox1* plants did not show any significant difference (**Fig. 3-6C**). *gsnor1-3* seeds have

66% and 0% germination, whereas the wild type line Col-0 showed 100% and 66% germination and *nox1* showed 90% and 66% germination in 200 mM and 300 mM mannitol, respectively.

A

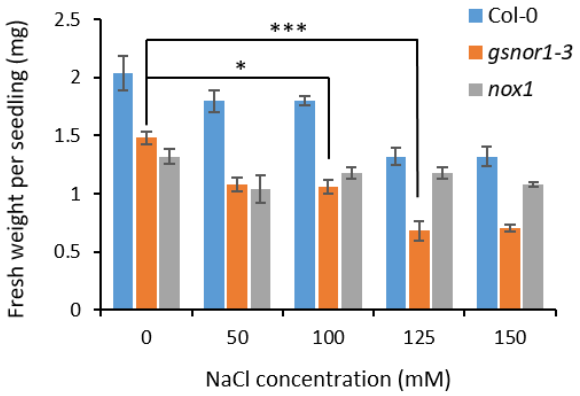

B

Two-way ANOVA & Tukey's Simultaneous Tests for Differences of Means

	0 mM		50 mM		100 mM		125 mM		150 mM	
	Significance	P-value	Significance	P-value	Significance	P-value	Significance	P-value	Significance	P-value
Col-0 & *gsnor1-3*	***	0.001	***	0.000	***	0.000	***	0.000	***	0.000
Col-0 & *nox1*	***	0.000	***	0.000	***	0.000	***	0.000	ns	0.787
gsnor1-3* & *nox1	ns	0.99	ns	1	ns	0.999	**	0.008	ns	0.124

	0 mM & 50 mM		0 mM & 100 mM		0 mM & 125 mM		0 mM & 150 mM	
	Significance	P-value	Significance	P-value	Significance	P-value	Significance	P-value
Col-0	ns	0.787	ns	0.787	***	0.000	***	0.000
gsnor1-3	ns	0.083	*	0.054	***	0.000	***	0.000
nox1	ns	0.567	ns	0.997	ns	0.997	ns	0.787

Figure 3-5. Fresh weight of *gsnor1-3* and *nox1* seedlings in the presence of NaCl.

Sterilised seeds were plated on ½ MS agar plates. Three days after germination the seedlings were transferred to agar plates containing ½MS media supplemented with NaCl at the concentrations indicated. Fresh weights were taken in mg per seedling using analytical balance. The bar chart represents mean fresh weight ± SEM (n=5). **B)** Two-way ANOVA and Tukey simultaneous tests for differences of means performed by statistical package Minitab 17; SEM, standard error of mean; not significant (ns), $p > 0.05$; *, $p \leq 0.05$; **, $p \leq 0.01$; ***, $P \leq 0.001$.

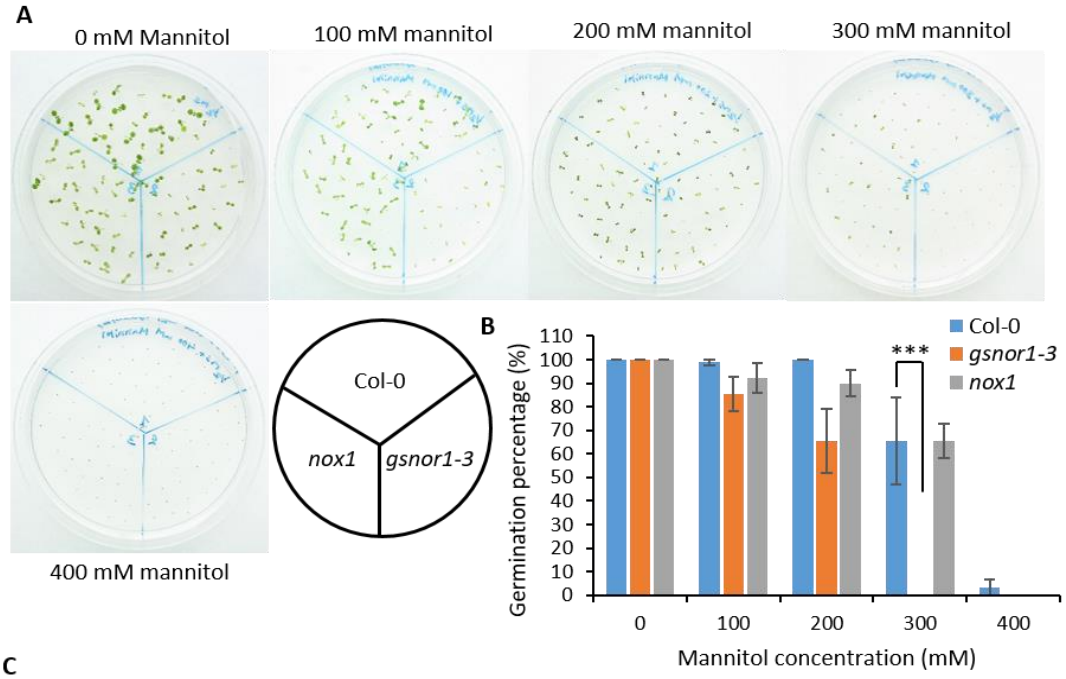

C

Two-way ANOVA & Tukey's Simultaneous Tests for Differences of Means

	0 mM		100 mM		200 mM		300 mM		400 mM	
	Significance	P-value	Significance	P-value	Significance	P-value	Significance	P-value	Significance	P-value
Col-0 & *gsnor1-3*	ns	1	ns	0.984	ns	0.073	***	0.000	ns	1
Col-0 & *nox1*	ns	1	ns	1	ns	0.999	ns	1	ns	1
gsnor1-3* & *nox1	ns	1	ns	1	ns	0.47	***	0.000	ns	1

	0 mM & 100 mM		0 mM & 200 mM		0 mM & 300 mM		0 mM & 400 mM	
	Significance	P-value	Significance	P-value	Significance	P-value	Significance	P-value
Col-0	ns	1	ns	1	ns	0.073	***	0.000
gsnor1-3	ns	0.971	ns	0.073	***	0.000	***	0.000
nox1	ns	1	ns	0.999	ns	0.073	***	0.000

Figure 3-6. Sensitivity of *gsnor1-3* and *nox1* seeds to mannitol.

A) Surface sterilised seeds were placed on agar plates containing ½MS media supplemented with mannitol at the concentrations indicated. Germination was counted at the appearance of green cotyledons 7 days after the seeds were plated. **B)** The bar chart represents germination percentage calculated from 30 seeds. Values are mean ± SEM (n=3). **C)** Two-way ANOVA and Tukey simultaneous tests for differences of means performed by statistical package Minitab 17; SEM, standard error of mean; not significant (ns), $p > 0.05$; *, $p \leq 0.05$; **, $p \leq 0.01$; ***, $P \leq 0.001$.

3.6 NaCl negatively affects *gsnor1-3* plants at vegetative stage on soil

It is important to test the salt response of plants under both transpiring and transpiration limited conditions since the former one have a major influence on Na^+ transport and tolerance (Munns and Tester, 2008). Thereby, we tested whether *gsnor1-3* plants show any phenotype at vegetative stage under transpiring condition. Plants were grown on soil and four-weeks-old plants were irrigated with 200 mM NaCl every 4 days for 14 days. After 14 days, *gsnor1-3* plants showed increased necrosis and leaf chlorophyll loss compared to both wild type and *nox1* plants (**Fig. 3-7**). The necrosis initially appeared in the older leaves.

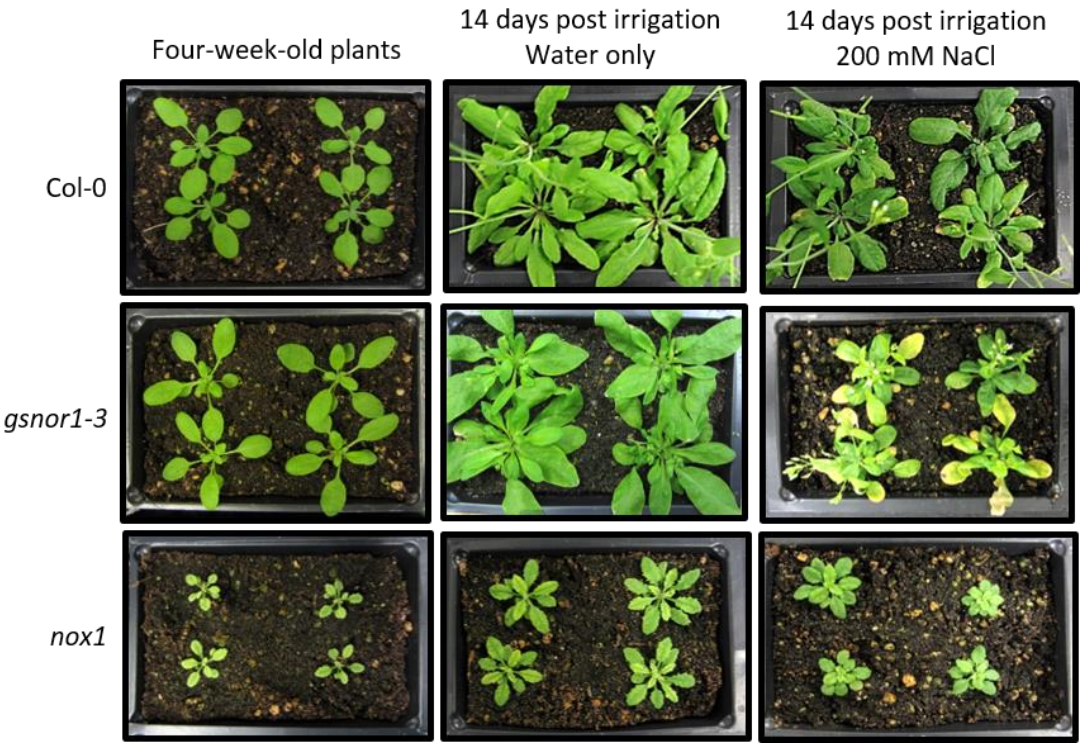

Figure 3-7. Sensitivity of *gsnor1-3* and *nox1* plants to NaCl at vegetative stage.

A) Cold stratified seeds were placed in the soil for 7 days for germination before transferring them to larger pots. 200 mM aqueous NaCl solution was applied from below every 4 days for 14 days to four-week-old seedlings. Photographs were taken before and after stress.

3.7 Discussion

GSNOR activity is essential for the maintenance of redox homoeostasis in plants. GSNOR enzyme indirectly controls total levels of protein S-nitrosylation and is necessary for plants biotic stress responses (Feechan et al., 2005). In addition, some studies have shown the importance of *GSNOR* in plant abiotic stress response (Leterrier et al., 2011; Corpas et al., 2011). Studies have shown an increase in GSNOR activity under salinity stress (Ziogas et al., 2013; Camejo et al., 2013). GSNOR activity was also shown to be increased under both high and low temperature stress in pea (*Pisum sativum*) and pepper (*Capsicun annuum*) (Airaki et al., 2012; Corpas et al., 2008). GSNOR activity is induced upon arsenic stress as well (Leterrier et al., 2012). Interestingly, *GSNOR* transcript and enzyme activity were shown to be reduced under high temperature in sunflower (*Helianthus annuus*) (Chaki et al., 2011). A recent study showed that suppression mutation in *GSNOR* using RNAi results in susceptibility to sodic alkaline (soil containing $NaHCO_3$ and Na_2CO_3) stress in tomato (*Solanum lycopersicum*) (Gong et al., 2015). In addition, in *Arabidopsis,* loss of GSNOR1 function results in a higher level of endogenous S-nitrosylation, renders insensitivity to ABA-induced stomatal closure, thereby exhibiting increased water loss relative to wild type plants during water stress. The same study showed that abscisic acid (ABA) induced S-nitrosylation of OST1/SnRK2.6 (Open Stomata 1/Sucrose non-fermenting 1 (SNF1)-Related Protein Kinase 2.6) might function as a negative feedback regulator of ABA signalling in plants during water stress (Wang et al., 2015). Further, *hot5/gsnor1*, primarily identified in a genetic screen for thermotolerance/susceptibility and *nox1* plants were shown to have decreased heat acclimation which suggests that high NO/SNO levels may impair thermotolerance in plants (Hong et al., 2003; Lee et al., 2008; He et al., 2004). Thus, accumulating data suggests, *GSNOR1* may regulate plant abiotic stress. However, salt tolerance in the context of S-nitrosylation and *GSNOR1* remains unclear.

Our data demonstrated that loss-of-function of *GSNOR1* in *Arabidopsis* renders susceptibility to salt stress in three different stages (seed germination, seedling and vegetative) of the plant life cycle. *gsnor1-3* plants showed significantly reduced germination, decreased survival rate and fresh weight reduction in the presence of NaCl compared to wild type plants. Adult plants also showed increased leaf necrosis, which first appeared in the older leaves, compared to wild type plants under NaCl stress.

KCl treatment is commonly used in conjunction with NaCl treatment to provide an initial indication of the salt or ion specificity of any observed differences in growth (Shi et al., 2002b; Affenzeller et al., 2009). KCl also provides initial indication as to whether the response is due to cation (Na^+, K^+) toxicity or anion (Cl^-) toxicity (Munns and Tester, 2008). In this context, *gsnor1-3* plants showed reduced germination and survival under KCl stress. Our result showed that the sensitivity is to cation toxicity but not associated with anion (Cl^-) toxicity. The sensitivity of *gsnor1-3* plants in the presence of mannitol indicates that this line is also sensitive to osmotic stress.

Previous research has shown that the ion-specific phase of the plant salt stress response begins with the accumulation of salt at toxic concentrations in the old leaves leading to necrosis or death of older leaves (Munns and Tester, 2008; Munns et al., 1995). Further, it is particularly important to investigate salt tolerance in transpiring conditions because, in the transpiration-limited conditions, the primary effect of salinity would be osmotic and is often unrelated to the extent of shoot Na^+ accumulation. On the contrary, in transpiring conditions, salt tolerance is related to shoot Na^+ levels (Munns and Tester, 2008). In this context, when four-weeks old plants grown in transpiring conditions were treated with aqueous NaCl solution, *gsnor1-3* plants showed increased sensitivity to the treatment compared to wild type plants resulting in higher leaf necrosis in the older leaves. New leaves emerged and leaf

necrosis appeared in older leaves first due to Na^+ accumulation in *gsnor1-3* plants which indicates that the sensitivity is not due to osmotic stress alone but may be due to both initial osmotic shock and prolonged Na^+ toxicity. Although in this chapter, we have used only *gsnor1-3* plants, use of another allele, for example, *par2-1* or *hot5* will further reconfirm the observed phenotype.

Interestingly, though *nox1* plants showed a significant reduction in survival rate in the presence of NaCl and KCl in agar plates, the germination rate was not lower than that of the wild type line in any of the treatments. In addition, the fresh weight of *nox1* plants did not reduce significantly compared to controls. It is evident that *nox1* plants have higher levels of endogenous NO (He et al., 2004; Hu et al., 2014). Previous research has shown that exogenous NO application enhances seed germination in salt and drought stress (Zhang et al., 2010). The high level of endogenous NO may render enhanced germination of *nox1* plants in the presence of NaCl. It is evident that the first sign of osmotic shock due to a high concentration of salt is reduced growth rate (Munns and Tester, 2008). Since *nox1* plants did not show any significant reduction in fresh weight, it indicates that *nox1* plants may have increased osmotic shock tolerance. This hypothesis is further supported as *nox1* plants germinated well in the presence of mannitol and have a continual growth in the presence of 200 mM NaCl in soil. In contrast, *nox1* showed significantly reduced survival at the seedling stage in agar plates however it did not show any leaf necrosis in the vegetative stage during prolonged NaCl treatment. Our hypothesis is that this apparently different results might arise from the differences in the experimental setup since in agar plates there are higher levels of relative humidity than in the ambient environment. We hypothesised that *nox1* responds differentially to salt stress in transpiring and transpiration-limited conditions.

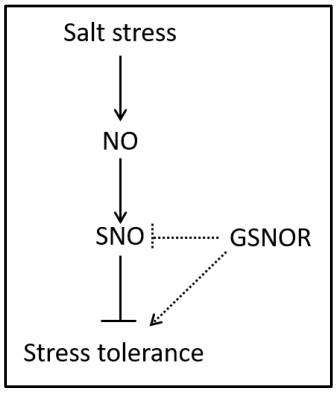

Figure 3-8. A model for salt stress regulation by GSNOR and S-nitrosylation.

Simplified schematic diagram showing that GSNOR positively regulates plant salt tolerance. NO, nitric oxide; SNO, S-nitrosothiol; GSNOR, S-nitrosoglutathione reductase.

Collectively, our data suggest that a high level of endogenous NO/SNO and loss of *GSNOR1* function has a negative effect on salt tolerance in plants at multiple stages of the life cycle (**Fig. 3-8**). This sensitivity is possibly due to both osmotic stress and ion toxicity. In the next chapters, the mechanism of this sensitivity during salt stress in plants with impaired NO/SNO regulation will be further investigated. In **chapter 4**, the regulation of classical salt stress signalling mechanisms in *gsnor1-3* plants will be studied.

Chapter-4

4 Investigating the regulation of classical salt response mechanisms in *gsnor1-3* plants

4.1 Introduction

Plants have adapted several mechanisms to deal with salt stress. The response to salt stress can be broadly divided into three main categories. Osmotic stress is the first phase of salt stress, which immediately reduces cell expansion in root tips and young leaves and causes stomatal closure. Plants insensitive to osmotic stress exhibit greater leaf growth and stomatal conductance, which is beneficial only when there is sufficient supply of water in the soil (Munns and Tester, 2008). The second mechanism involved in salt tolerance is the exclusion of Na^+ from leaves. Na^+ exclusion by roots prevents Na^+ accumulation at a toxic concentration within leaves. Toxic levels of Na^+ accumulation result in the death of older leaves (Munns and Tester, 2008). The third approach for plants to cope with salt stress is to compartmentalise Na^+ and Cl^- at the cellular and intracellular level to avoid toxic concentrations within the cytoplasm. Toxicity occurs with long term salt stress after leaf Na^+ or in some species Cl^- increases to high concentrations in the older leaves (Munns and Tester, 2008). NHX1, a Vacuolar Na^+/H^+ antiporter was reported to be involved in Na^+ translocation into the vacuole in *Arabidopsis* (Apse et al., 1999). Similarly, *SOS1* is a plasma membrane Na^+/H^+ importer, involved in the efflux of Na^+ from the cell and the regulation of long-distance Na^+ movement in plants (Shi et al., 2002a). In addition, class I HKTs play a major role in Na^+ unloading from the xylem leading to a net reduction of Na^+ influx into the photosynthetic organs (Munns and Tester, 2008).

Another component of the plant salt tolerance is abscisic acid (ABA). ABA plays an important role in stress response as well as seed development and germination (Cutler et al., 2010). Plant survival during salt and drought stress is linked with ABA-mediated adaptive responses. ABA plays a role in the first phase of salt stress when a high concentration of salt in the soil causes osmotic shock. This stress triggers the accumulation of ABA, which in turn activates various stress associated genes that are thought to function in the accumulation of osmoprotectants, LEA (late embryogenesis abundant) proteins, signalling and transcriptional regulation (Bartels and Sunkar, 2005).

Transcriptional reprogramming is one of the most important responses to abiotic stress. High salinity and dehydration treatments were reported to result in increased expression of 194 and 277 genes, respectively (Seki et al., 2002). 141 genes of the salt stress-inducible genes are also induced by dehydration, highlighting a possible overlapping between dehydration and salt stress probably due to the osmotic shock phase of both stresses. In the same experiment, 40 transcription factor genes were identified as high salinity, dehydration or cold-inducible genes. These include members from DREB, ERF, Zn-finger, WRKY, Myb, bHLH, bZIP, NAC and HDZIP protein family (Seki et al., 2002). This transcriptional reprogramming was observed in both ABA-dependent or ABA-independent gene families (Seki et al., 2002; Kreps et al., 2002).

In the previous chapter, we have shown that *gsnor1-3* plants are more sensitive to salt stress. In this chapter, we have explored the classical salt tolerance mechanisms to compare the regulation between wild type and *gsnor1-3* and to investigate the possible mechanism for salt sensitivity in *gsnor1-3* plants.

4.2 Na^+/K^+ homoeostasis pathways are functional in *gsnor1-3* plants

Maintenance of Na^+/K^+ homoeostasis in plants is achieved by several pathways which include Na^+ exclusion from photosynthetic tissues, Na^+ retrieval from xylem and compartmentalization of Na^+ and Cl^- at the cellular and intracellular level. Loss-of-function mutation in the *Arabidopsis HKT1;1* has been shown to overaccumulate Na^+ in the shoot (Mäser et al., 2002). In addition, an unresponsive *SOS* pathway in plants results in accumulation of Na^+ ions and a decrease of K^+ ions creating Na^+ ion toxicity. *SOS* mutants show a significant increase in Na^+ ion contents in shoot tissues compared to wild type plants (Shi et al., 2002b, 2002a). To check if the ion homoeostasis pathways are functional in *gsnor1-3* plants, the amount of Na^+ and K^+ was quantified in plants treated with 250 mM NaCl solution by atomic absorption ion analysis following the procedure described in **chapter 2.3**. The *gsnor1-3* line did not show increased accumulation of Na^+ compared to wild type plants (**Fig. 4-1A)**. The decrease of K^+ ion content was also similar to the wild type line (**Fig. 4-1B)**. There was no significant difference in the K^+/Na^+ ratio between wild type and *gsnor1-3* suggesting that *gsnor1-3* plants have functional ion homoeostasis pathways (**Fig. 4-1C)**.

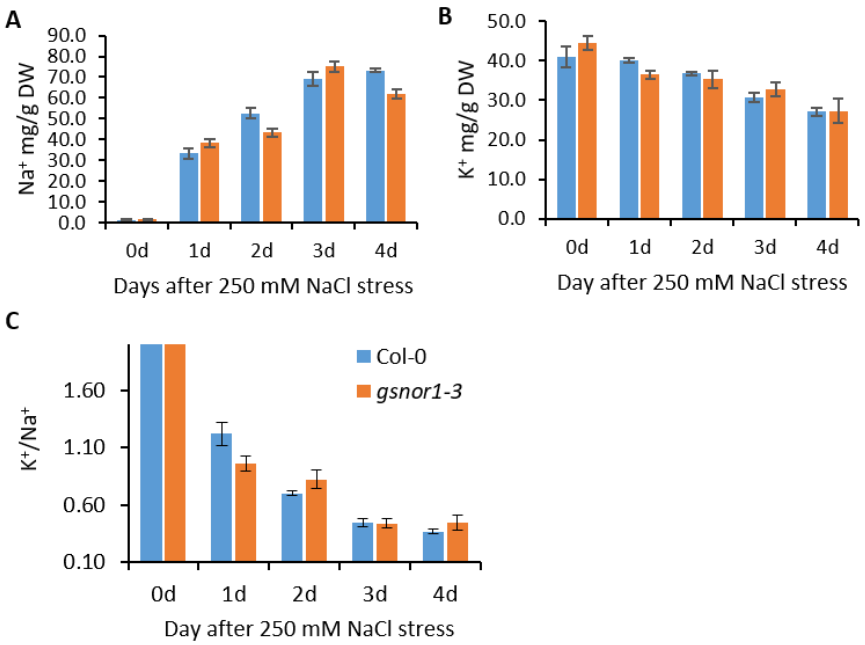

Figure 4-1. Na^+ and K^+ contents in wild type and *gsnor1-3* plants.

Four-week-old soil-grown plants were treated with 250 mM aqueous NaCl solution from below. Shoot samples were collected at the days indicated. 80 mg dried samples were used per genotype per time point. Ions were measured using an atomic absorption spectrophotometer iCE3000. A) Na^+ content, B) K^+ content, C) K^+/Na^+. The bar chart is representing means ± SEM (n=3). SEM, standard error of mean; DW, dry weight.

4.3 ABA content in *gsnor1-3* after salt stress

Next, we tested the ABA content in *gsnor1-3* plants before and after salt stress. For this experiment, we used hydroponics grown plants to mediate a rapid and homogeneous salt stress response under transpiring conditions. Four-week-old hydroponics grown plants were treated with a nutrient solution containing 250 mM NaCl. Shoot samples were collected at 0 and 5 hours. Samples were immediately frozen in liquid nitrogen, ground in fine powders and freeze dried. Samples were taken in triple biological replicates. ABA was measured using ultra-high performance liquid chromatography–triple quadrupole mass spectrometry (UPLC-MS/MS) with negative electrospray ionisation following the procedure described in **chapter 2.4** (Fu et al., 2012). The basal ABA levels in wild type and *gsnor1-3* were 2.2 and 2.1 pg/mg

of fresh weight respectively. After 5 hours of NaCl treatment, the levels of ABA increased to 9.2 and 14.2 pg/mg of fresh weight respectively (**Fig. 4-2**). The level of ABA in *gsnor1-3* plants was significantly higher compared to wild type according to two-way ANOVA performed followed by Tukey's simultaneous test for differences of means using Minitab 17.

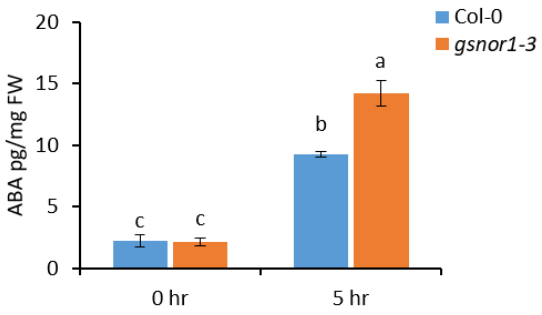

Figure 4-2. ABA content in wild type and *gsnor1-3* plants.

Four-week-old hydroponic grown plants were treated with a nutrient solution containing 250 mM NaCl. Shoot samples were collected at times indicated. 200 mg fresh leaf samples were used per sample. ABA was measured using ultra-high performance liquid chromatography–triple quadrupole mass spectrometry (UPLC-MS/MS) with negative electrospray ionisation. The Bar chart is representing means ± SEM (n=3). Two-way ANOVA and Tukey simultaneous tests for differences of means performed by statistical package Minitab 17; Means that do not share a letter are significantly different at P value ≤ 0.005. The threshold of family wise significance was set at 0.05. SEM, standard error of mean; FW, fresh weight.

4.4 Transcriptional changes in *gsnor1-3* during salt stress

Gene expression levels of several abiotic stress marker genes were carried out using semi-quantitative RT-PCR in wild type Col-0 and *gsnor1-3* plants. Four-week-old hydroponic grown plants were treated with a nutrient solution containing 250 mM NaCl. Leaf samples were then collected at 0 1, 2 3, 4 and 24 hours and immediately frozen in liquid nitrogen. RNA was extracted using RNeasy® plant mini kit (QIAGEN) following manufacturer's instruction. cDNA was synthesised using High-Capacity cDNA Reverse Transcription Kit (Applied

Biosystems™) following manufacturer's instruction. Detailed procedure and primer sequences are given in **chapter 2.5**. Tested marker genes included both early responsive genes, late responsive genes and genes from both ABA-dependent and ABA-independent pathways. In aggregate, these marker genes showed no consistent difference in expression level between wild type Col-0 and *gsnor1-3* plants (**Fig. 4-3**).

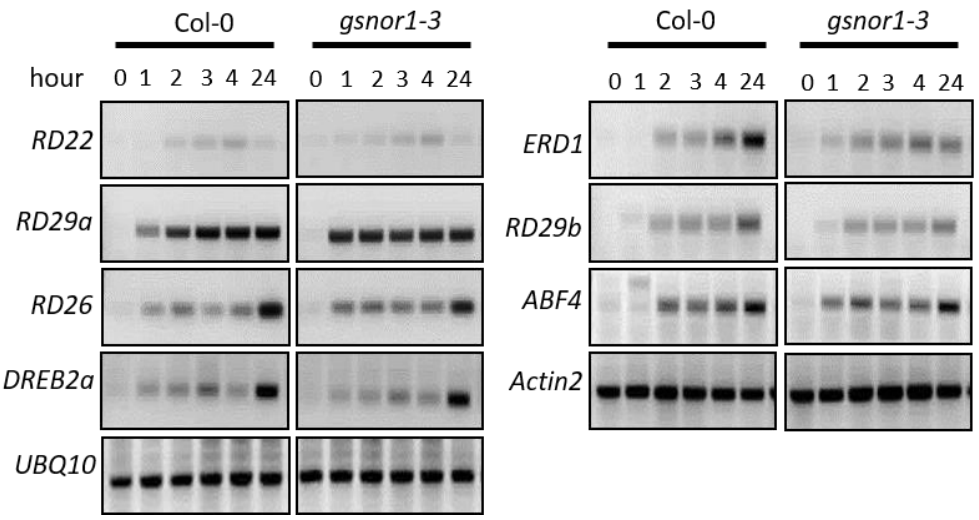

Figure 4-3. Salt stress induced marker gene expression in *gsnor1-3* plants using semi-quantitative RT-PCR.

Four-week-old hydroponic grown plants were treated with a nutrient solution containing 250 mM NaCl. Leaf samples were collected at times indicated (hours post treatment) and RNA was extracted for cDNA synthesis and RT-PCR analysis of the given genes. *Actin2* and *UBQ10* expression were analysed as constitutively expressed house-keeping control genes.

4.5 Discussion

Our initial hypothesis was that *gsnor1-3* plants may be impaired in ion homoeostasis as they showed sensitivity in the presence of NaCl and KCl. Previous studies have shown that *Arabidopsis* plants with defective ion homoeostasis, specifically loss-of-function mutations in class I *HKT* or *SOS* pathway, tend to have an accumulation of Na^+ and a low K^+ content, thus a

lower K^+/Na^+ ratio (Shi et al., 2002b, 2002a, 2003). However, *gsnor1-3* plants showed a similar level of Na^+ and K^+ contents and K^+/Na^+ ratio as wild type plants, implying that *gsnor1-3* has functional ion homoeostasis pathways.

NO-mediated S-nitrosylation has been reported to regulate the biosynthesis of and signalling by salicylic acid (SA), rendering susceptibility to pathogen infection (Feechan et al., 2005). Further, it was reported that knocking out of *GSNOR1* might impair auxin signalling, resulting in loss of apical dominance in *gsnor1-3* plants (Shi et al., 2015). Interestingly, Wang et al (2015) reported that S-nitrosylation of sucrose nonfermenting 1 (SNF1)-related protein kinase 2.6 (SnRK2.6) at Cys 137, inhibits its catalytic activity, at least *in vitro. gsnor1-3* plants showed constitutive S-nitrosylation of SnRK2.6 resulting in an inhibition of ABA-induced stomatal closure (Wang et al., 2015). SnRK2s are central components of the ABA pathway. Stress-induced ABA production leads to the inhibition of protein phosphatase 2Cs (PP2Cs), negative regulators of ABA signalling, resulting in the activation of SnRK2s which then phosphorylate a number of downstream effectors to regulate various physiological processes specifically stomatal closure, root growth and the induction of stress-responsive genes (Cutler et al., 2010). Thereby, inhibition of SnRK2 activities by S-nitrosylation may lead to reduced stress gene expression leading to sensitivity to salt stress. We hypothesised that the salt sensitivity of *gsnor1-3* plants might be due to reduced biosynthesis of ABA or impaired ABA signalling. Interestingly, *gsnor1-3* plants have similar basal levels of ABA as wild type. There was also an increase in ABA content indicating that the ABA biosynthetic pathway is not negatively regulated by S-nitrosylation. *gsnor1-3* plants have significantly higher levels of ABA compared to wild type under stress condition. It was reported previously that ABA triggers NO generation followed by the stomatal closure (Bright et al., 2006). In contrast, NO was shown to induce ABA biosynthesis during oxidative stress (Zhang et al., 2011). While this controversial data needs further clarification, we see a small increase in ABA biosynthesis in

gsnor1-3, possibly due to an increase in total SNOs leading to a variation in oxidation status of the cell.

Next, we examined if the ABA signalling in *gsnor1-3* plants is affected by salt stress. S-nitrosylation of transcription factors or any signalling pathway component may lead to an impact on transcriptional reprogramming. Previous research has shown that *RD22, ERD1, RD29a, RD29b, RD26, ABF4 and DREB2a* genes are inducible by salt stress (Kreps et al., 2002; Zhu, 2002). Among these marker genes, *DREB2a* is an ABA-independent stress-inducible gene, while the rest of the genes are ABA-dependent (Shinozaki and Yamaguchi-Shinozaki, 2007). Interestingly, the expression patterns of all the genes in *gsnor1-3* are comparable to that of wild type plants. This data demonstrates that the salt stress signalling pathway downstream to ABA is not directly affected by S-nitrosylation. Surprisingly, as it has been reported that SnRK2.6 S-nitrosylation inhibits its catalytic activity, it would be expected that the downstream signalling pathway will also be affected. However, in our experimental conditions, no inhibition of ABA-dependent gene expression was observed.

In summary, in this chapter, we have explored classical signalling pathways for salt stress responses to test whether S-nitrosylation may regulate any of these signalling mechanisms. We found that *gsnor1-3* plants have functional pathways for regulating Na^+/K^+ homoeostasis. Also, *gsnor1-3* plants have a functional ABA biosynthetic and cognate signalling pathway. Finally, expressions of salt stress response genes were unaffected by increased levels of cellular S-nitrosylation. All these data suggest that there is an alternative mechanism, probably regulated by S-nitrosylation, that confers *gsnor1-3* plants more sensitivity to salt stress than wild type plants. In our next chapter, we will explore whether non-classical mechanism in salt stress signalling such as autophagy is regulated by S-nitrosylation.

Chapter 5

5 Investigating the role of autophagy during salt stress in *gsnor1-3* plants

5.1 Introduction

Autophagy is a macromolecule degradation pathway to recycle cellular nutrients and to degrade toxic components during developmental programmes or in response to stress. A key feature of autophagy is the formation of the autophagosome, a double-membrane vesicle structure. After autophagy induction, the autophagosome encloses the components to be degraded. Later, the autophagosome fuses with the central vacuole to deliver the cargo (Liu and Bassham, 2012). More than 30 ***a**u**t**opha**g**y* (*ATG*) genes are already identified in yeast and *Arabidopsis*. One of the core components of autophagosome formation is ATG7, a ubiquitin-like activating enzyme (E1) which regulates two ubiquitin like conjugation systems ATG8 and ATG12 (Liu and Bassham, 2012). Many autophagy deficient mutants are characterised in *Arabidopsis* including *atg7-2,* a loss-of-function mutant which results in the absence of autophagosomes (Doelling et al., 2002; Thompson et al., 2005).

Autophagy can be bulk and selective. Bulk autophagy involves the sequestering of the whole cytoplasm, sometimes even organelles into the autophagosome to deliver them into the central vacuole for degradation. On the other hand, selective autophagy is involved in removing specific cargos when appropriate (Johansen and Lamark, 2011). Both bulk and selective autophagy share one of the components of the core ATG-mediated autophagic system, ATG8, a small ubiquitin like protein family of around 15 KDa molecular weight. During autophagy, the ATG machinery generates ATG8-PE (PE, phosphatidylethanolamine) adducts which coat the autophagosome membrane (Shpilka et al., 2011; Liu and Bassham, 2012). This ATG8 provides a docking platform for proteins that are important for the maturation of

autophagosome and for selective recruitment of proteins to be degraded via ATG8-interacting motifs (AIMs). One particular AIMs containing protein in plants is NBR1 (Neighbour of BRCA1) which is a selective autophagic substrate that binds to ATG8. NBR1 also serves as an autophagic cargo receptor and an adaptor protein for other ubiquitinylated proteins destined for degradation. Thus, an accumulation of NBR1 serves as a marker for defective autophagosome formation (Li and Vierstra, 2012; Svenning et al., 2011).

There are several techniques to monitor autophagy in plant cells. The most extensively used technique is the use of fluorescence confocal microscopy. Autophagosomes can be visualised using fluorescence dye specifically lysotracker green (LTG) or monodansylcadaverine (MDC). These fluorescence dyes can efficiently stain the autophagosomes due to their internal acidic environment surrounded by double membranes (Contento et al., 2005; Moriyasu et al., 2003). Another popular fluorescence marker to visualise autophagosomes is GFP fused ATG8 (Thompson et al., 2005; Contento et al., 2005). During autophagy, ATG8 are activated and conjugated to phosphatidylethanolamine (PE) via a ubiquitin like conjugation system. This ATG8-PEs or the lipidated ATG8s then coat the outer and inner membrane of autophagosomes. Thus, GFP-ATG8 serves as a powerful marker for autophagosome formation. Autophagosomes are normally visualised as spherical dot-like structures upon labelling with a size range of 0.5 to 1 µm in diameter (Merkulova et al., 2014). However, the fluorescent dyes may often stain other acidic organelles or the autophagosomes may not be *a priori* acidic in nature thereby the use of both fluorescent dyes and GFP-ATG8 is necessary.

In *Arabidopsis*, multiple abiotic stresses, including nutrient deficiency, salt, drought, oxidative and other stresses induce autophagy (Xiong et al., 2007, 2005; Liu et al., 2009). All these stresses cause protein oxidation leading to oxidation stress. Thereby, the ability of

autophagy to scavenge oxidised proteins is crucial to defend against abiotic stress (Xiong et al., 2007). Additionally, NO and S-nitrosylation are thought to have important roles during abiotic stress. Thus, in this chapter, we sought to investigate the potential regulation of autophagy by protein S-nitrosylation during salt stress in *Arabidopsis*.

5.2 *gsnor1-3* plants have less autophagosome formation during NaCl stress

To determine the level of autophagosome formation, fluorescence confocal laser scanning microscopy was undertaken in NaCl-stressed root and roots of non-stressed seedlings following the procedure described in **chapter 2.6**. Lysotracker green (LTG), a fluorescent dye that is retained in acidic vacuoles, was used to specifically stain the autophagosomes due to the acidic nature of this vesicle. In wild type line Col-0, the number of autophagosomes increased significantly after NaCl stress. However, the number of autophagosomes in *gsnor1-3* plants did not increase in this stress**.** LTG staining of the autophagy deficient mutant *atg7-2* also showed no autophagosome like structures demonstrating that LTG is specific to autophagosomes (**Fig. 5-1A**). Autophagosomes were quantified and compared between different plant lines. Statistical analysis confirmed that the autophagosome number in *gsnor1-3* plants was significantly lower compared to that of wild type plants under NaCl stress (**Fig. 5-1B**).

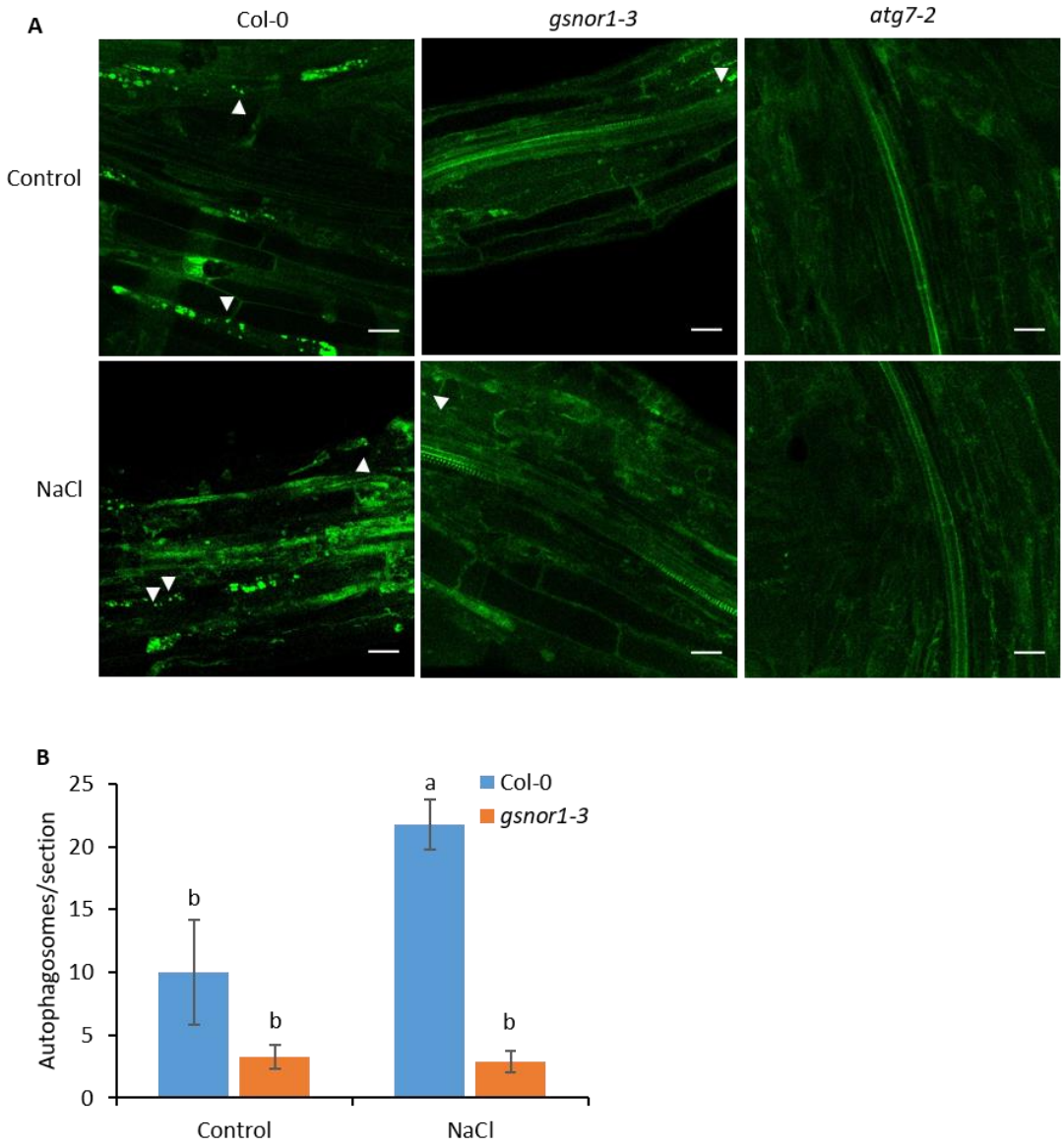

Figure 5-1. Induction of autophagy in *gsnor1-3* plants during NaCl stress visualised by LTG staining.

Five-day-old seedlings were transferred to control MS plates or to MS plates containing 150 mM NaCl for 24 hours followed by LTG staining and observed using fluorescence confocal laser scanning microscopy. **A)** Images showing autophagosomes with or without NaCl treatments of the given genotypes. Arrowheads indicate LTG-stained autophagosomes. Scale bar = 50 µm. **B)** The number of LTG-stained autophagosomes per root section was counted and the average number determined for 10 seedlings per treatment. Values are mean ± SEM (n=10). Two-way ANOVA and Tukey simultaneous tests for differences of means performed by statistical package Minitab 17; Means that do not share a letter are significantly different at P value ≤ 0.001. SEM, standard error of mean.

We also used the GFP-ATG8a transgenic *Arabidopsis* line to further confirm the level of autophagosomes formation during NaCl stress. We utilised GFP-ATG8a reporter in both a Col-0 and autophagy deficient mutant *atg7* background. The transgenic lines were kindly provided by Prof. Richard Vierstra (Thompson et al., 2005). To understand the potential role of S-nitrosylation in autophagy regulation, we crossed the GFP-ATG8a Col-0 line with an EMS mutagenized loss-of-function line of *GSNOR1*, *par2-1* (*paraquat resistant 2-1*) (Chen et al., 2009a). We avoided the *gsnor1-3* line since this was a T-DNA insertion mutant and the GFP-ATG8a expression was under a constitutive cauliflower mosaic virus *35S* promoter (CaMV *35S*). The combination of two T-DNAs often leads to the silencing of transgenes. We selected the GFP-ATG8a *par2-1* progeny with BASTA resistance up to the F3 generation to generate a homozygous line for both transgene and the *par2-1* mutation. Finally, we used the transgenic GFP-ATG8a *par2-1* line for fluorescence confocal laser scanning microscopy to visualise autophagosomes. Briefly, sterilised seeds were germinated on ½ MS agar plates for five days and transferred to ½ MS agar plates containing 150 mM NaCl from a further two days. All the samples were visualised with or without the treatment of concanamycin A (CA), a vacuolar H^+-ATPase inhibitor. Application of CA leads to the inhibition of vacuolar degradation of autophagic bodies by raising internal pH thereby facilitates visualisation

In the wild type line Col-0, the number of autophagosomes increased significantly after NaCl stress. Conversely, the number of autophagosomes in *par2-1* plants was similar to that of wild type plants in the absence of NaCl, thus the number of autophagosomes did not increase under NaCl stress**.** The autophagy deficient mutant *atg7-2* was used as a negative control for autophagosome formation, which showed no autophagosome like structures before and after NaCl stress (**Fig. 5-2A**). Autophagosomes were quantified and compared between different plant lines. Statistical analysis of variance and Tukey's simultaneous tests for differences of means (two-way ANOVA, Minitab 17) showed that compared to wild type,

par2-1 plants have a significantly reduced autophagosome formation under NaCl stress (**Fig. 5-2B**). A similar result was found in the sample treated with Concanamycin A, demonstrating that reduced autophagosome formation was not due to a higher rate of autophagosome degradation (**Fig. 5-3**). Autophagy is a catabolic process that involves cellular nutrient recycling and is indispensable during stress responses. Thereby, inhibition of autophagy can be detrimental to plant stress responses.

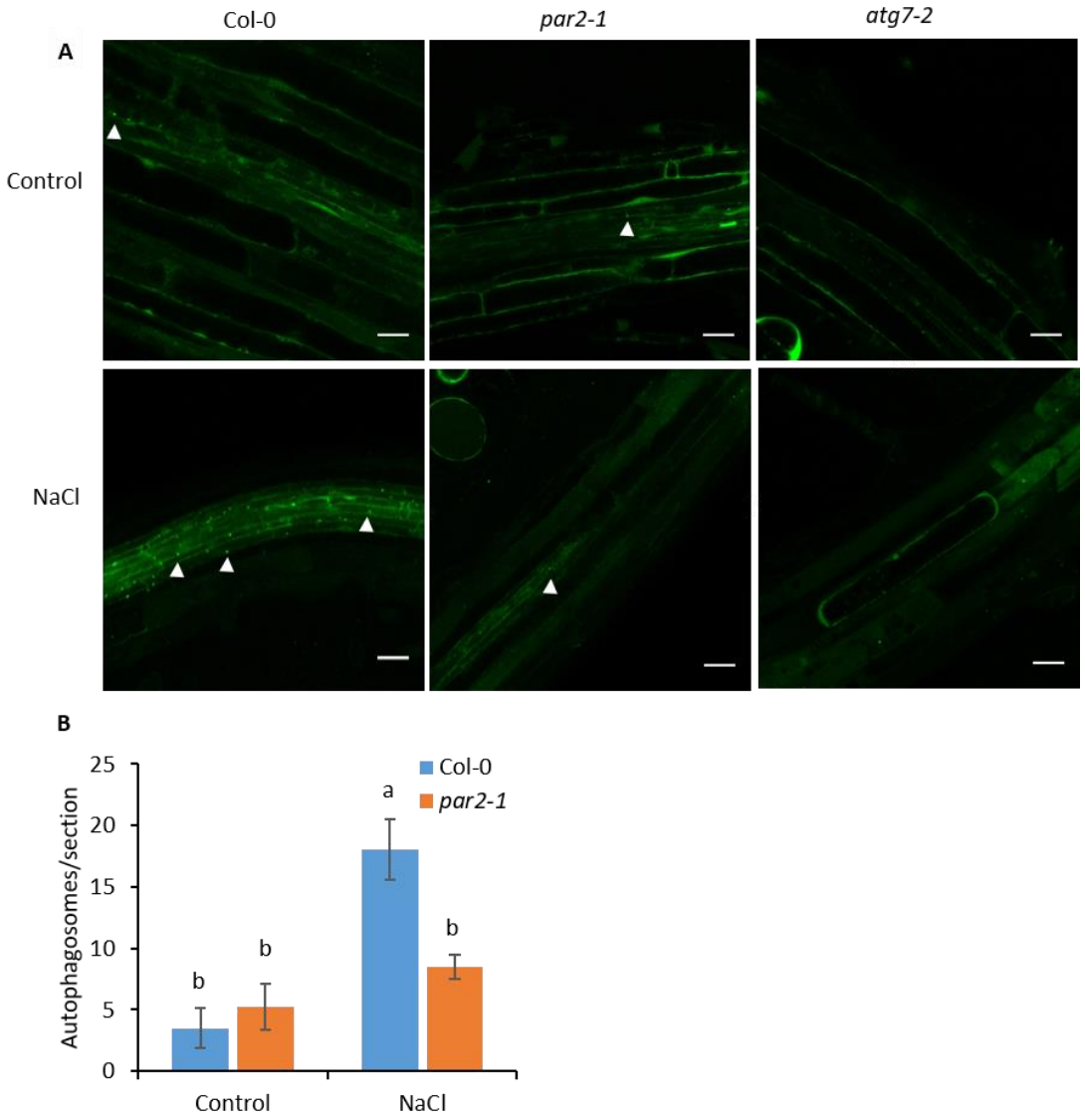

Figure 5-2. Induction of autophagy in *par2-1* plants during NaCl stress visualised by GFP-ATG8.

Five-day-old seedlings were transferred to control MS plates or to MS plates containing 150 mM NaCl for 48 hours. Roots were visualised by fluorescence confocal microscopy of GFP. **A)** Images showing autophagosomes with or without NaCl treatments of GFP-ATG8a plants in the given genetic backgrounds. Arrowheads indicate autophagosomes. Scale bar = 50 µm. **B)** The number of autophagosomes per root section was counted and the average number determined for 10 seedlings per treatment. Values are mean ± SEM (n=10). Two-way ANOVA and Tukey simultaneous tests for differences of means performed by statistical package Minitab 17; Means that do not share a letter are significantly different at P value ≤ 0.001. SEM, standard error of mean.

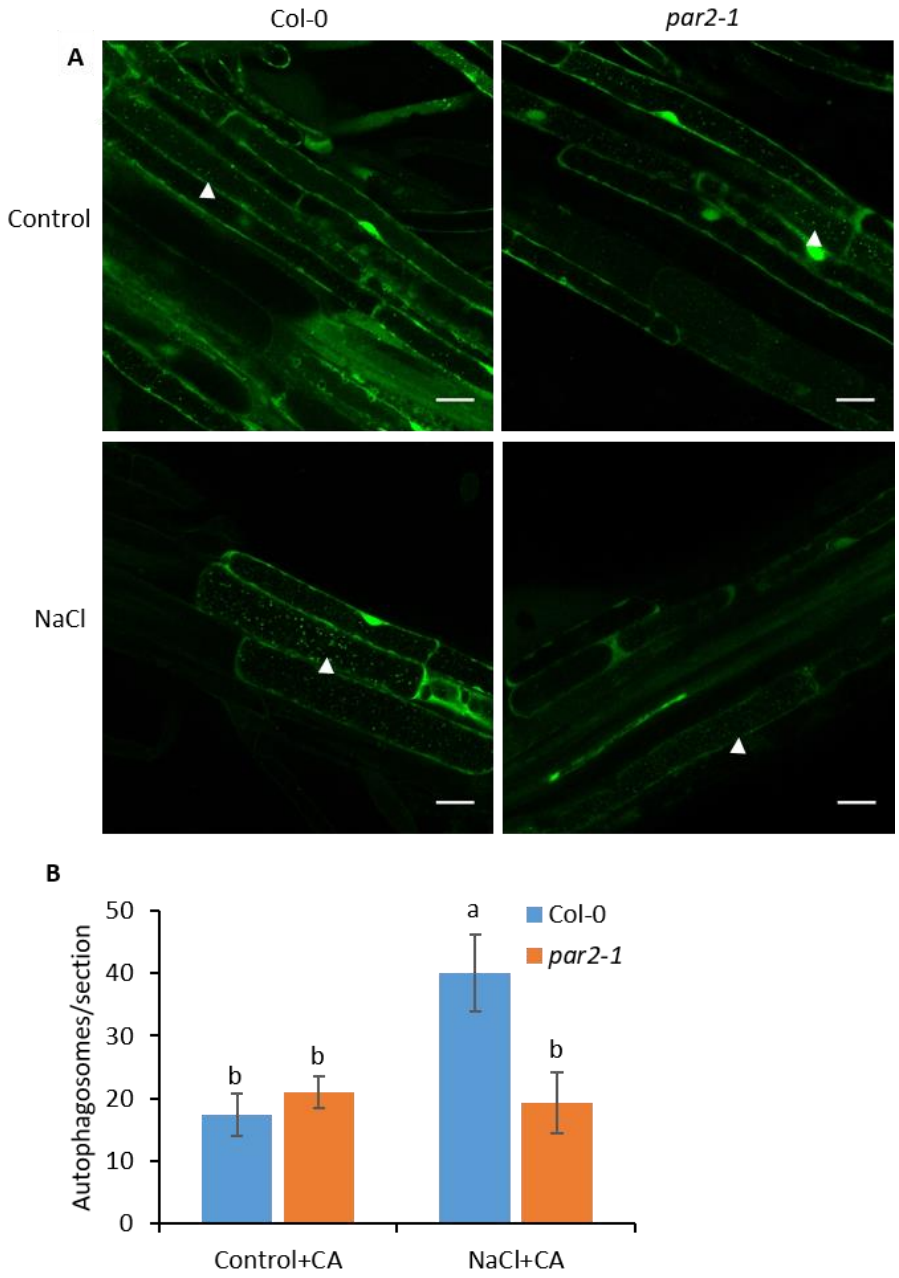

Figure 5-3. Induction of autophagy in *par2-1* plants during NaCl stress visualised by GFP-ATG8 in the presence of concanamycin A (CA).

Five-day-old seedlings were transferred to control MS plates or to MS plates containing 150 mM NaCl for 24 hours and then incubated for an additional 12 to 16 h with 0.5 μm concanamycin A (+CA) with or without 150 mM NaCl in ½ MS liquid media. Roots were visualised by fluorescence confocal microscopy of GFP. **A)** Images showing autophagosomes with or without NaCl treatments of GFP-ATG8a plants in the given genetic backgrounds. Arrowheads indicate autophagosomes. Scale bar = 50 µm. **B)** The number of

autophagosomes per root section was counted and the average number determined for 10 seedlings per treatment. Values are mean ± SEM (n=10). Two-way ANOVA and Tukey simultaneous tests for differences of means performed by statistical package Minitab 17; Means that do not share a letter are significantly different at P value ≤ 0.001. SEM, standard error of mean.

5.3 Accumulation of NBR1 indicates a lack of autophagy during NaCl stress in *gsnor1-3* plants

NBR1 is an adapter protein which carries other proteins to the autophagosome and interacts with the ATG8 via an AIM domain during the autophagosome formation process. Either lack of autophagosome formation or inhibition of autophagosome formation results in the accumulation of cytosolic NBR1 leading to insoluble NBR1 aggregates. Thus, NBR1 serves as a marker for inhibition of autophagosome formation. Western blotting was performed to detect NBR1 protein in total protein extracts before and after 100 mM NaCl stress for 10 days in Col-0 and *gsnor1-3* using an antibody against NBR1 (anti-NBR1 antisera was kindly provided by Prof. Terje Johansen) following the procedure described in **chapter 2.7**. *atg7-2* plants were included as an autophagy deficient mutant which was shown to accumulate constitutive cytosolic NBR1 (Svenning et al., 2011). In the wild type line, NBR1 can be seen as a single band corresponding to its molecular weight of 76.1 KDa. After NaCl stress in wild type the band appears to be ~15 KDa larger, corresponding to the size expected ATG8 conjugated to NBR1. Whereas, in *gsnor1-3* the signal of NBR1 in *gsnor1-3* was stronger compared to wild type. *atg7-2* plants showed higher accumulation of NBR1 due to a defective autophagy pathway. These results demonstrate there is an accumulation of NBR1 after NaCl stress (**Fig. 5-4A**) and the autophagy pathway is defective in *gsnor1-3* plants (**Fig. 5-1**).

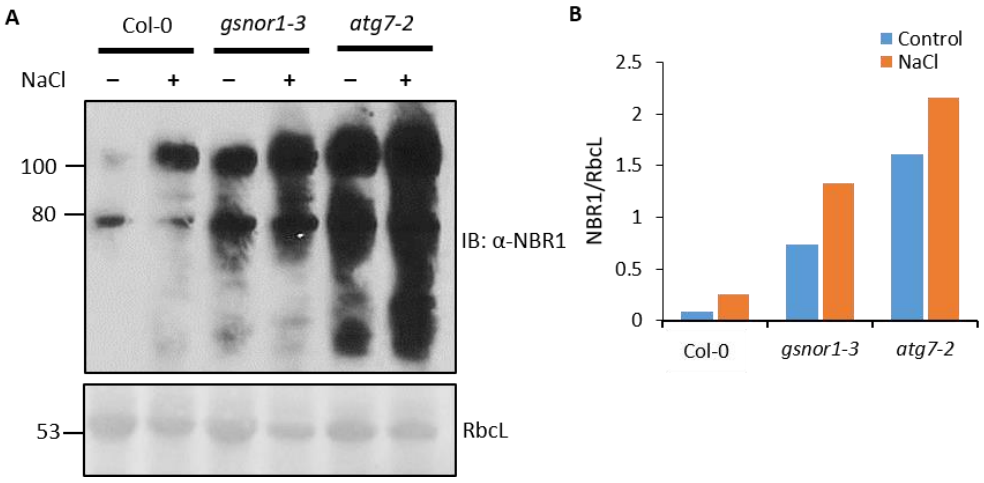

Figure 5-4. NBR1 accumulation in *gsnor1-3* plants during NaCl stress suggests a lack of autophagosome formation.

A) Seedlings of the indicated phenotypes were grown on MS medium for five days before transferring on control MS agar plate or MS agar plate containing 100 mM NaCl. Samples were collected 10 days of stress period. Western blot analysis of the total NBR1 cargo receptor protein was performed. Panceau S-stained Rubisco large subunit (RbcL) was used as a loading control. **B)** ImageJ was used to measure the signal intensity. The signal intensity ratio of NBR1 and RbcL was taken to normalise the signal which showed increased accumulation of NBR1 in *gsnor1-3* plants in normal condition compared to wild type. The NBR1 content further increased after 10 days of NaCl stress.

Prolonged accumulation of NBR1 leads to the formation of insoluble aggregates so different time lengths of stress were applied to check the onset of accumulation of NBR1 and at five days after stress, NBR1 accumulation was seen in the insoluble protein fraction extracted from *gsnor1-3* (**Fig. 5-5**). To further assess if NBR1 accumulation is a direct response to NaCl stress, stressed seedlings were transferred to fresh MS plates after five days of stress for a recovery period of two days. After two days of recovery from stress, seedlings were collected for extraction of insoluble protein fraction and western blotting to detect NBR1. Indeed, the withdrawal of stress had a direct effect on the accumulation of NBR1 protein in

gsnor1-3 plants. After stress withdrawal, the accumulated insoluble aggregate of NBR1 was reduced to the level prior to NaCl stress (**Fig. 5-6**). This result demonstrates that the accumulation of NBR1 in *gsnor1-3* during NaCl stress was a direct effect of the stress.

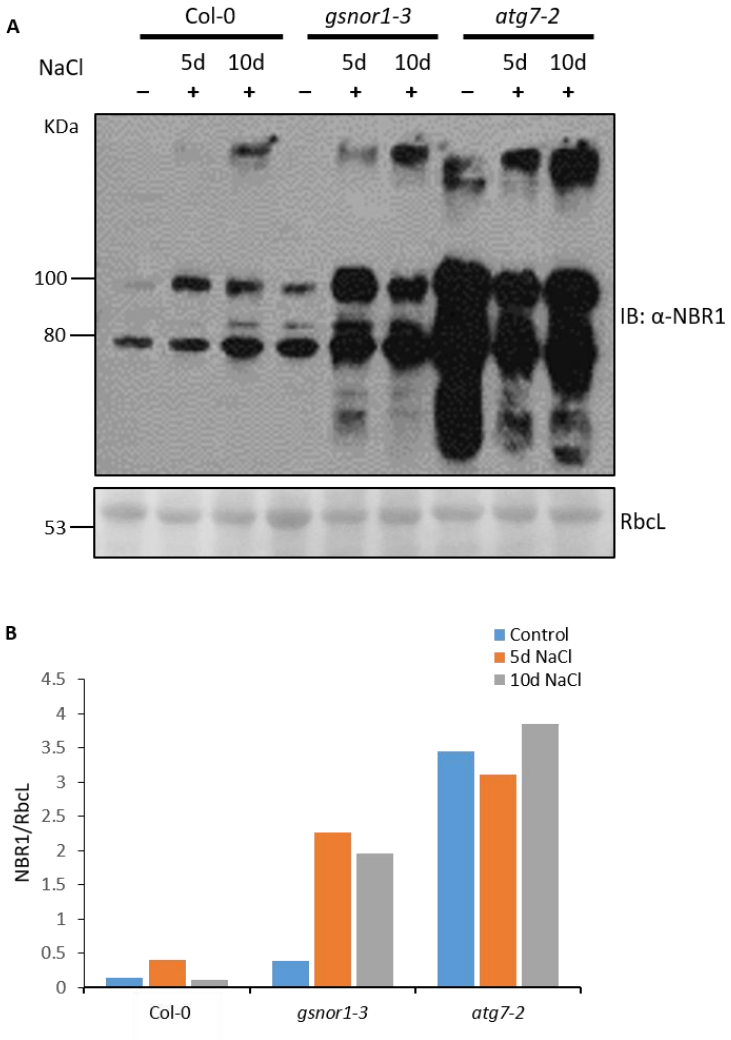

Figure 5-5. Early NBR1 accumulation in *gsnor1-3* plants during NaCl stress suggests a lack of autophagosome formation.

A) Seedlings of the indicated phenotypes were grown on MS medium for five days before transferring to control MS agar plates or MS agar plate containing 100 mM NaCl. Samples were collected at the days indicated. Western blot analysis of the NBR1 cargo receptor protein in the insoluble protein fraction was performed. Panceau S-stained Rubisco large subunit (RbcL) was used as a loading control. **B)** ImageJ was used to measure the signal intensity.

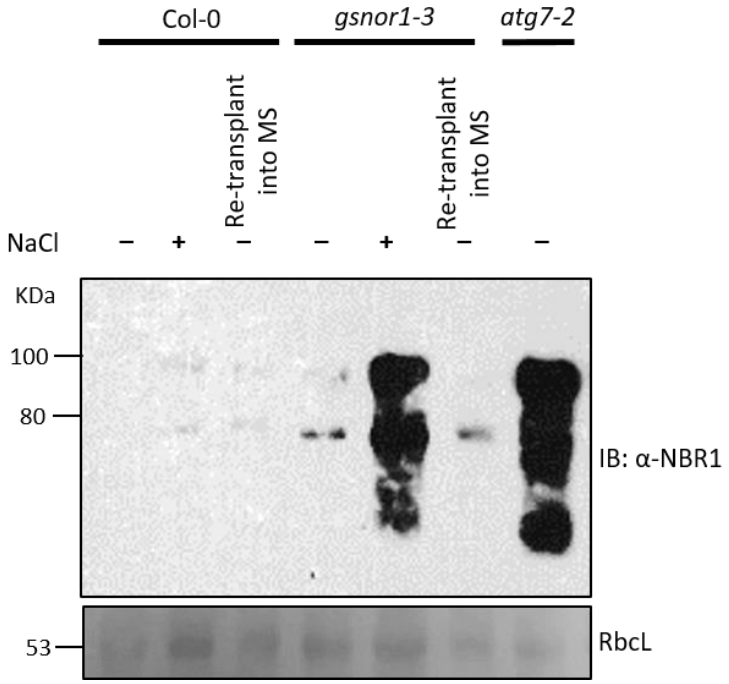

Figure 5-6. Withdrawal of NaCl stress restores the basal level of insoluble NBR1 protein in *gsnor1-3* plants.

A) Seedlings of the indicated phenotypes were grown on MS medium for five days before transferring to control MS agar plates or MS agar plates containing 100 mM NaCl. Half of the treated samples were re-transplanted into fresh MS agar plate for recovery from the stress. Seedlings were grown for further two days for recovery before collecting for western blot. Western blot analysis of the NBR1 cargo receptor protein in the insoluble protein fraction was performed. Panceau S-stained Rubisco large subunit (RbcL) was used as a loading control.

5.4 Discussion

Autophagy is a dynamic cellular recycling process involving the degradation of the intracellular component that is conserved across the kingdom. Autophagy is a basal process, however, autophagy induction has been observed in plants by various environmental stimuli, both biotic and abiotic, though the exact nature and the components of this induction remain still unknown. Autophagy is induced in both salt and drought stress and ROS (reactive oxygen species) production is one of the common characteristics in both of these stress responses

(Zhou et al., 2013; Liu et al., 2009; Munns, 2002). In this context, autophagy has been shown to be regulated by the level of ROS. Another important feature of salt and drought stress is the production of RNS (reactive nitrogen species) especially the production of NO leading to the post-translational modification termed S-nitrosylation. NO has been shown to have negative effects on autophagy in animal systems especially during neurodegenerative diseases (Sarkar et al., 2011), although the molecular details remain to be established. Further, there is a lack of knowledge of autophagy regulation by NO or S-nitrosylation in the context of plants signalling to date. A possible role for the regulation of plant autophagy by NO or S-nitrosylation during abiotic stress was therefore explored. In this chapter, we have demonstrated that autophagy is regulated by SNO during NaCl stress. So, the homoeostasis of NO/SNO during abiotic stress may play an important role in the regulation of autophagy.

Autophagy was found to be induced by increased autophagosome formation in wild type plants during NaCl stress, as measured by the LTG staining of autophagosomes. On the other hand, in *gsnor1-3* plants autophagosome formation did not increase under NaCl stress (**Fig. 5-1, Fig. 5-2, Fig. 5-3**). This data demonstrates that there is reduced autophagosome formation in *gsnor1-3* plants during NaCl stress. Along with the autophagosome specific fluorescence dye, LTG, we have also used GFP-ATG8a that serves as a specific marker for autophagosomes, in three different genetic backgrounds: Col-0 wild type, *par2-1* and the autophagy deficient *atg7.* Fluorescence confocal microscopy of these transgenic lines confirmed that autophagosome formation is reduced in a high S-nitrosylation background during NaCl stress. It was previously reported that autophagy deficient mutants are susceptible to both salt and drought stress. An *Arabidopsis* RNAi-*AtATG18a* plants were found to be hypersensitive to NaCl and mannitol treatment at the germination stage which also showed significant growth reduction compared to wild type plants during salt and drought stress (Liu et al., 2009). In another study, it has been reported that the autophagy deficient

mutants *atg5* and *atg7* showed enhanced sensitivity to salt and drought stress (Zhou et al., 2013). In the light of the previous reports and our results, it is evident that autophagy is strongly involved during abiotic stress, specifically salt and drought stress and an absence of autophagy during these stresses results in increased susceptibility to these environmental insults.

NBR1 is a selective autophagy substrate, but at the same time, it acts as a cargo receptor for degradation of other substrates (Svenning et al., 2011). In recent years, NBR1 has been established as an important marker for selective autophagy and accumulation of NBR1 was reported in autophagy deficient *atg2, atg7* and *atg18a* plants and thus an accumulation of NBR1 protein serves as a marker for reduced autophagosome formation (Hackenberg et al., 2013; Coll et al., 2014; Svenning et al., 2011). Moreover, NBR1 was found be involved in the degradation of ubiquitinylated proteins (Kirkin et al., 2009). In this context, *atg5*, *atg7*, and *nbr1* mutants were reported to have increased accumulation of highly ubiquitinated, insoluble proteins resulting in compromised heat tolerance (Zhou et al., 2013, 2014a). Collectively, this evidence suggests an important role of NBR1-mediated selective autophagy in response to abiotic stress, probably integral to the clearance of damaged and unwanted proteins which form ubiquitinylated protein aggregates during stress.

A western blot experiment to detect the NBR1 content during NaCl stress confirmed the presence of accumulated NBR1 in *gsnor1-3* plants compared to wild type. The autophagy deficient loss-of-function mutant *atg7-2* shows a blockage in autophagosome formation leading to the accumulation of NBR1 at basal levels compared to wild type. Our data demonstrate that *gsnor1-3* has a higher level of total basal NBR1 that was further increased during NaCl stress, suggesting an inhibition of autophagy during NaCl stress. We also showed an accumulation of insoluble NBR1 in *gsnor1-3* plants during salt stress. Withdrawal of NaCl

stress restores the basal insoluble NBR1 level suggesting that the accumulation of NBR1 in *gsnor1-3* plants was due to the inhibition of autophagy during NaCl stress.

Altogether, the microscopy and western blot results imply that *gsnor1-3* plants have reduced autophagy during NaCl stress. We showed that autophagy is impaired in a high S-nitrosylation background suggesting a possible regulation of autophagy by this PTM. Further, impaired autophagy in *gsnor1-3* plants results in the failure of clearance of the damaged and/or oxidized proteins, evident from NBR1 accumulation and thus renders susceptibility to salt stress. In my next chapter, the mechanism of this inhibition of autophagy in *gsnor1-3* plants by S-nitrosylation will be demonstrated.

Chapter 6

6 *In vitro* regulation of ATG7 by S-nitrosylation

6.1 Introduction

Under typical plant growth conditions, macroautophagy, hereafter termed, autophagy, degrades unwanted and damaged cytoplasmic contents (Liu et al., 2009). After induction, an autophagosome forms around the cytoplasmic contents targeted for degradation, which is then delivered to the central vacuole for the breakdown. Autophagosome formation requires two ubiquitin-like conjugation systems. Most of the uncovered mechanistic details have been derived from yeast, however, autophagy components are largely conserved across kingdoms (Liu and Bassham, 2012; Li and Vierstra, 2012). These systems involve two ubiquitin like proteins ATG8 and ATG12, both proteins are activated by an E1-like activating enzyme ATG7. ATG8 protein is synthesised as a long precursor which requires processing by cysteine protease ATG4. After the C-terminus is cleaved to expose a conserved glycine (Gly) residue, it is then bound to the catalytic site cysteine (Cys) in ATG7 via a thioester link in an ATP-dependent manner. Activated ATG8 is then transferred to an E2-like conjugating enzyme ATG3 via trans-thioesterification. Finally, ATG8 is conjugated to the membrane lipid phosphatidylethanolamine (PE) to form ATG8-PE (Xie and Klionsky, 2007). On the other hand, after activation by ATG7 in a manner similar to ATG8, ATG12 is transferred to the E2-like conjugating enzyme ATG5. The ATG12-ATG5 conjugate then non-covalently interacts with a coiled-coil protein ATG16. Both ATG8-PE and ATG12-ATG5:ATG16 (here, the dash represents a covalent interaction and the colon represents a non-covalent interaction) complexes are bound to the pre-autophagosomal structure (PAS) for recruiting more proteins required for the expansion of the semi-circular double membrane structure, the phagophore, into a

circular double membrane vesicle, the autophagosome. ATG8-PE is found to be bound to both the inner and outer membrane of the autophagosome. Thus, ATG7 plays a central role in both of the ubiquitin-like conjugation systems which are essential for autophagosome formation (Liu and Bassham, 2012; Li and Vierstra, 2012). As an ubiquitin (Ub)-like activating enzyme E1, ATG7 shares some features with E1 antecedents MoeB, as well as other canonical E1 enzymes for ubiquitin (Ub), NEDD8 (neural precursor cell expressed, developmentally downregulated), and SUMO (small ubiquitin-like modifier) in that all these E1 enzymes function via a conserved catalytic site Cys residue (Lake et al., 2001; Lee and Schindelin, 2008; Lois and Lima, 2005; Walden et al., 2003). Despite this, ATG7 has evolved to be a non-canonical E1 which provides the unique recognition features of two different Ub-like proteins (ATG8 and ATG12) and two distinct E2-like enzymes (ATG3 and ATG12 respectively) (Noda et al., 2011).

The ATG7 loss-of-function mutant lacks autophagosome formation (Thompson et al., 2005). In **chapter 5**, it was shown that there is a lack of autophagosome formation in *gsnor1-3* plants, in this chapter, we investigated the underpinning molecular mechanism.

6.2 ATG7 is highly conserved across kingdoms

ATG7 is an E1-like enzyme that functions as a homodimer. The protein sequence is highly conserved among yeast, *Arabidopsis* and human sequences (**Fig. 6-2**). ATG7 monomers are comprised of two globular domains connected by a short linker. The unique N-terminal domain (NTD), residues 1–321 in *Arabidopsis*, corresponds to 1-288 in *Saccharomyces cerevisiae* (Noda et al., 2011). The C-terminal domain (CTD) is comprised of the adenylation domain (AD), residues 327-637 in *Arabidopsis*, which corresponds to 294–572 in *S. cerevisiae.* The extreme C-terminal ATG7-specific domain (ECTD), residues 638-697 in *Arabidopsis* corresponds to residues 573–630 in *S. cerevisiae*. The catalytic cysteine residue, Cys558 in

Arabidopsis (Cys507 in *S. cerevisiae*), is located at the long loop region in ATG7^{AD} termed the crossover loop (CL) comprised of residues 511-562 in *Arabidopsis* (residues 473–511 in *S. cerevisiae*) (**Fig. 6-1**) (Noda et al., 2011).

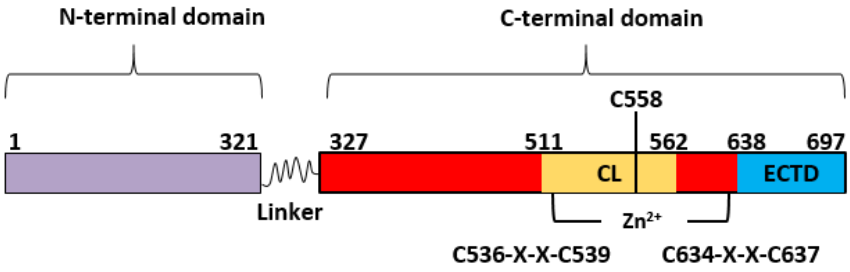

Figure 6-1. A schematic diagram of full-length *Arabidopsis thaliana* ATG7 (AtATG7).

A schematic diagram of AtATG7 showing different domains and parts as indicated. CL, Crossover loop; ECTD, extreme C-terminal domain; Cys-X-X-Cys, Cys motif for Zn^{2+} binding; X, any amino acid.

ATG7^{CTD} also contains two conserved Cys-X-X-Cys motifs at C536-X-X-C539 and C634-X-X-C637. These motifs were found to co-ordinate a single zinc (Zn^{2+}) connecting the CL with the ECTD (**Fig. 6-1**) (Noda et al., 2011). A similar feature is seen in the SUMO E1 heterodimer SAE1/SAE2 (Lois and Lima, 2005). Previous crystallographic studies showed that ATG7^{NTD} is necessary and sufficient for the interaction with ATG3, whereas the ATG7^{CTD} is necessary and sufficient for the interaction with ATG8 and ATG12. In the presence of ATP and Mg^{2+}, ATG7^{CTD} is capable of forming a thioester-linked conjugate with ATG8 and ATG12, and thus is sufficient for the formation of ATG7-ATG8 or ATG7-ATG12 thioester intermediates. It has also been shown that the ATG7 crossover loop (ATG7^{CL}), undergoes a large conformational change to expose a groove during ATG8 or ATG12 binding. ATP is bound in an extension of the ATG8-bound groove but is separated from the core of ATG8 by ATG7^{CL} (Noda et al., 2011).

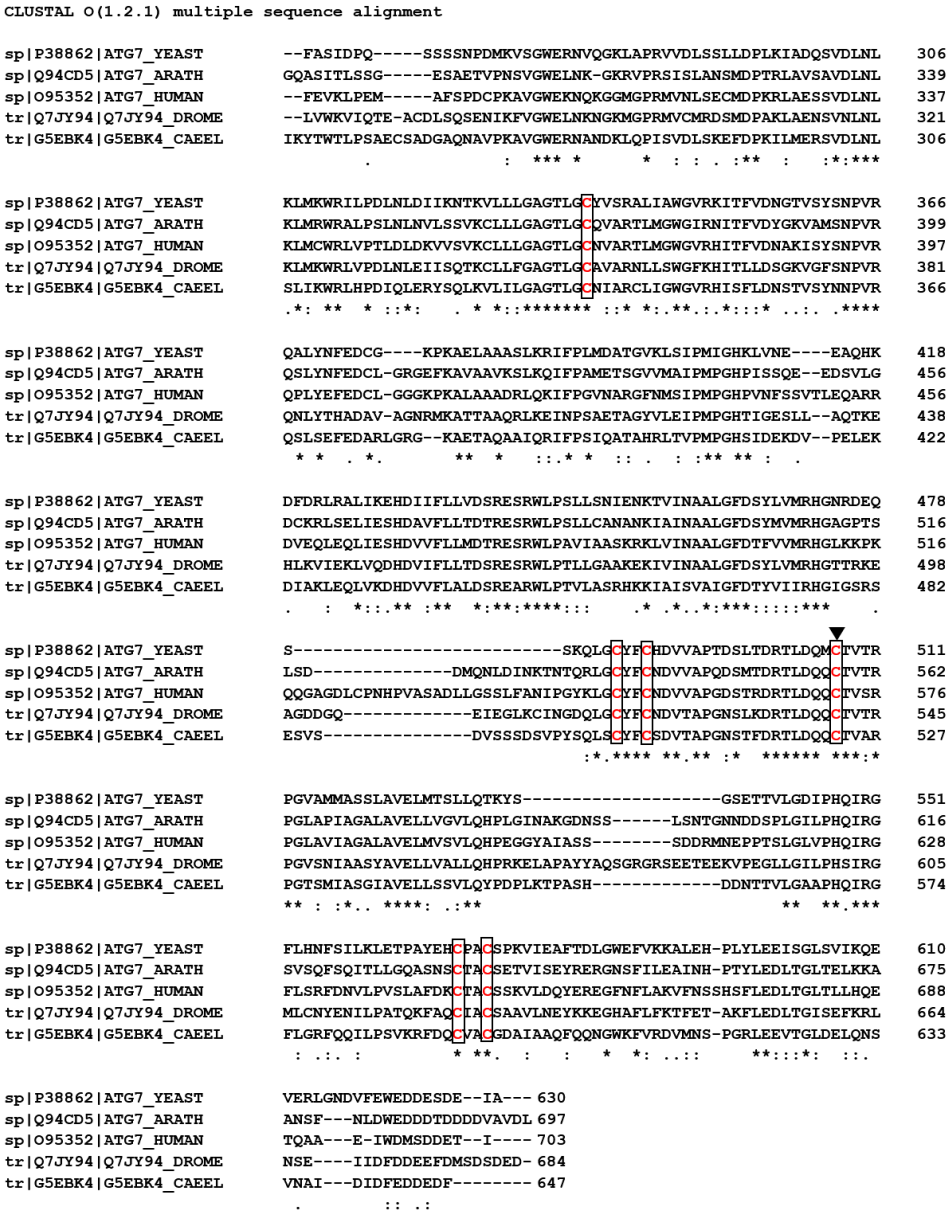

Figure 6-2. Sequence alignment of ATG7^{CTD} from multiple eukaryotes.

Sequences of autophagy E1 enzyme ATG7 from various species were aligned using the CLUSTAL OMEGA (1.2.1) software (http://www.ebi.ac.uk/Tools/msa/clustalo/) (Sievers et al., 2011). Only the aligned C-terminal domain of ATG7 is shown here. Conserved cysteines are shown in red inside the box with the active site residue marked with an arrowhead.

6.3 Recombinant MBP-ATG7^{CTD} and ATG7^{NTD} production and purification

Arabidopsis ATG7 is a 76.52 KDa, 697 residue protein. The full length ATG7 has 16 Cys residues, among which six are conserved across kingdoms and more than one Cys directly takes part in ATG7 function. We hypothesised that ATG7 might be regulated by S-nitrosylation at one of the conserved Cys residues. However, ATG7^{CTD} which contains 10 Cys residues is sufficient for the activation of ATG8 and ATG12, therefore this region was first selected to check possible regulation by S-nitrosylation. The coding sequence from 880-2094 of the *Arabidopsis ATG7* was cloned in-frame with an N-terminal Maltose Binding Protein (MBP) into the *Not*I and *Eco*RI site of pMalC5X vector and expressed in *E. coli* BL21 (DE3) cells. After expression, MBP-ATG7^{CTD} was purified under native conditions by affinity chromatography using amylose resin. The MBP-ATG7^{CTD} (hereafter termed ATG7^{CTD}) was 87.1 KDa **(Fig. 6-3A)**.

Further, to test whether the N-terminal domain of ATG7 is S-nitrosylated, the coding sequence from 1- 879 of the *Arabidopsis ATG7* was cloned in frame with an N-terminal Maltose Binding Protein (MBP) into the pETG40A vector using a GATEWAY™ cloning system and expressed in *E. coli* BL21 (DE3) cells. After expression, MBP-ATG7^{NTD} was purified under native conditions by affinity chromatography using amylose resin. The MBP-ATG7^{NTD} (hereafter termed ATG7^{NTD}) protein was 72.5 KDa (**Fig. 6-3B**). Protein expression optimization for ATG7^{NTD} was undertaken by a MSc project student, Ann-Kathrin Bahlmann.

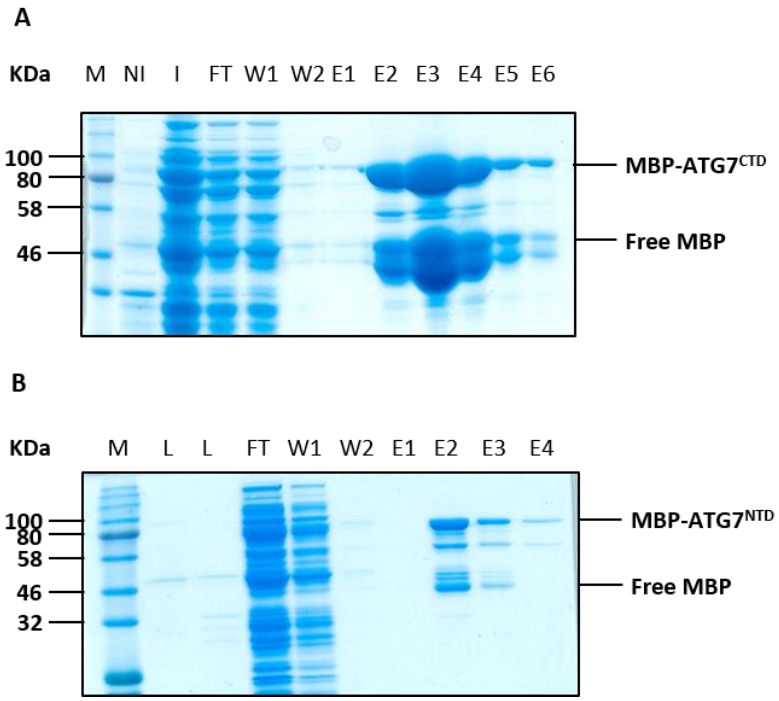

Figure 6-3. Recombinant MBP-ATG^{CTD} and MBP-ATG7^{NTD} purified by amylose affinity chromatography.

A) *E. coli* BL21 (DE3) cells carrying the construct pMalC5X-ATG7^{CTD} were used to express the fusion protein MBP-ATG7^{CTD}. Protein was expressed at 0.5 mM IPTG and four hours incubation at RT. Proteins were run using a 10% reducing SDS-PAGE and stained with InstantBlue™ (Expedeon, Cambridge, UK) following manufacturer's instruction. MBP-ATG7^{CTD} has an estimated molecular mass of 87.1 KDa. **B)** *E. coli* BL21 (DE3) cells carrying the construct pETG40A-ATG7^{NTD} were used to express the fusion protein MBP-ATG7^{NTD}. Protein was expressed, purified, run and visualised using the same method as described in **A**. Final IPTG concentration was 0.5 mM and incubation for expression was performed for three hours at RT. MBP-ATG7^{NTD} has an estimated molecular mass of 72.5 KDa. M, Protein marker; NI, Non-induced; I, Induced lysate; L, lysate; FT, Flow through; W1-W2, Washes; E1-E6, Elutions; LB, Luria-Bertani media; IPTG, Isopropyl β-D-1-thiogalactopyranoside; MBP, Maltose binding protein; RT, Room temperature.

N.B. Data shown in **Fig. 6-3B** was generated by Ann-Kathrin Bahlmann (MSc project student).

6.4 *In vitro* S-nitrosylation of ATG7^{CTD} and ATG7^{NTD}

In order to test if ATG7^{CTD} is S-nitrosylated *in vitro*, recombinant protein was incubated with different NO donors namely GSNO and CysNO in the dark and a biotin switch technique (BST) was performed to monitor SNO formation. Details of the biotin switch technique are given in **chapter 2.11**. The inclusion of CysNO also discriminates between S-nitrosylation and S-glutathionylation. The control sample was treated with reduced glutathione (GSH). Non-reducing SDS-PAGE followed by western blot analysis was carried out, S-nitrosylated protein was detected using an anti-biotin antibody. It was found that ATG7^{CTD} is readily S-nitrosylated *in vitro* **(Fig. 6-4A)**. Since MBP does not have any Cys residues, the signal does not originate from MBP. To test if S-nitrosylation of ATG7^{CTD} protein is GSNO concentration dependent, the protein sample was incubated with different concentrations of GSNO (**Fig. 6-4A**). S-nitrosylation is a reversible process and the specificity of S-nitrosylation can be tested by the addition of a reducing agent, this was verified by adding 20 mM dithiotreitol (DTT). It was found that ATG7^{CTD} S-nitrosylation is clearly GSNO concentration dependent. ATG7^{CTD} is S-nitrosylated by 10 µM GSNO, which suggests the possibility of S-nitrosylation at physiological conditions. The signal intensity substantially increased with an increase in GSNO concentration, reaching a maximum of 500 µM. As expected no signal was seen with GSH or DTT (**Fig. 6-4A**).

Recombinant ATG7^{NTD} was also subjected to BST using two NO-donors GSNO and CysNO. The addition of GSH served as a negative control. SDS was added only to GSNO treatment to unfold the protein during NO-donor incubation to expose all the Cys residues to make them readily available to this NO-donor. It was found that ATG7^{NTD} is also S-nitrosylated *in vitro* **(Fig. 6-4B)**. This experiment as shown in **Fig. 6-4B** was performed by an MSc project student, Ann-Kathrin Bahlmann.

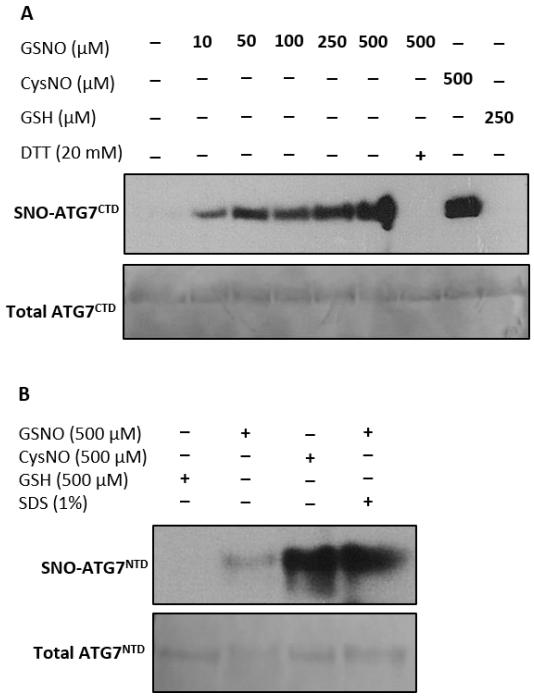

Figure 6-4. ATG7^{CTD} and ATG7^{NTD} are S-nitrosylated *in vitro.*

A) ATG7^{CTD} was subjected to a biotin switch assay after incubation with the stated concentrations of GSNO, GSH, CysNO or DTT followed by non-reducing SDS-PAGE and transferred to nitrocellulose membrane for western blot analyses. Immunodetection was undertaken using an anti-biotin monoclonal HRP conjugated antibody. Ponceau S staining of the total ATG7^{CTD} on nitrocellulose membrane indicated equal loading. A substantial increase in signal intensity was observed with an increase in GSNO concentrations reaching a maximum of 500 µM. Weak signals were obtained at 10 µM GSNO which was the lowest concentration used. ATG7^{CTD} is readily S-nitrosylated by CysNO. No signal was seen in GSH negative control lanes and in the first lane without GSNO. Adding 20 mM DTT reduced the SNOs, therefore, yielding no signal in the last lane. **B)** Recombinant ATG7^{NTD} was also subjected to biotin switch to detect S-nitrosylation with the stated concentration of NO-donors or GSH. ATG7^{NTD} was also S-nitrosylated in presence of 500 µM of GSNO AND 500 µm CysNO. No signal was observed in negative controls. Ponceau S staining of the total ATG7^{NTD} on nitrocellulose membrane indicates equal loading. GSNO, S-nitrosoglutathione; GSH, Glutathione; DTT, Dithiotreitol; HRP, Horseradish peroxidase.

N.B. Data shown in **Fig. 6-4B** was generated by Ann-Kathrin Bahlmann (MSc project student).

6.5 Recombinant His-ATG8a^{G132} production and purification

One of the two substrates of ATG7 enzyme is ATG8. *Arabidopsis* has nine *ATG8* (*ATG8a-ATG8i*) genes with high sequence conservation and identical expression patterns (Yoshimoto et al., 2004; Rose et al., 2006). To test if ATG7 enzyme activity is regulated by S-nitrosylation *in vitro*, an assay for ATG7^{CTD} function utilising its substrate ATG8a was performed. ATG8a was chosen as it lacks any Cys to rule out the potential regulation of ATG8 proteins by S-nitrosylation. The molecular weight of ATG8a is 15.404 KDa. *In vitro,* ATG7^{CTD} can readily activate its substrate ATG8a at the conserved C-terminal glycine (Gly) residue (Noda et al., 2011). Members of ATG8 family are usually synthesised as a longer precursor that requires processing by the cysteine protease ATG4 to expose the C-terminal Gly residue. Mature ATG8 is then activated by ATG7 in an ATP-dependent manner, which subsequently binds ATG8 to the catalytic site Cys in ATG7 via a thioester linkage. The bound ATG8 is then donated from ATG7 to the E2-conjugating enzyme ATG3 by transesterification and finally attached to PE with the aid of an ATG8-specific E3 ligase complex (Ohsumi, 2001). To keep the *in vitro* assay convenient, recombinant ATG8a was produced with the C-terminal Gly exposed. We also omitted the conjugation step since ATG3 also contains a catalytic site Cys thereby might be regulated by S-nitrosylation. The coding sequence from 1-396 of the *Arabidopsis ATG8a* was cloned in frame with an N-terminal 6XHis tag into the *Bam*HI and *Not*I site of pET28a vector and expressed in *E. coli* BL21 (DE3) cells. After expression, His-ATG8a^{G132} was purified under native conditions by immobilized-metal affinity chromatography (IMAC) using Ni-NTA resin. The His-ATG8a^{G132} (hereafter termed ATG8a^{G132}) was 18.5 KDa (**Fig. 6-5**).

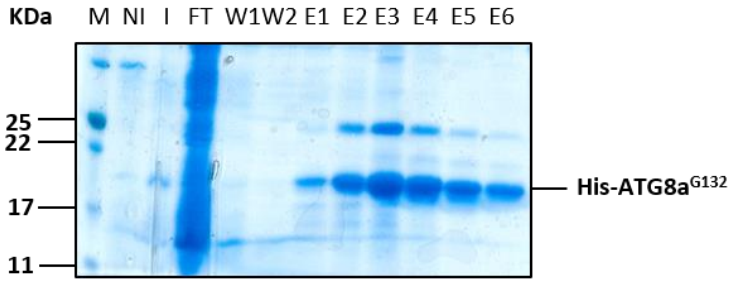

Figure 6-5. Recombinant His-ATG8a^{G132} purified by immobilized-metal affinity chromatography (IMAC).

E. coli BL21 (DE3) cells carrying the construct pET28a-ATG8a^{G132} were used to express the fusion protein 6XHis-ATG8a^{G132}. IPTG was added to a final concentration of 1 mM and after four hours of induction at RT the cells were harvested for protein purification. Protein was run using a 13% reducing SDS-PAGE and stained with InstantBlue™. His-ATG8a^{G132} has an estimated molecular mass of 18.5 KDa. M, Protein marker; NI, Non induced; I, Induced lysate; FT, Flow through; W1-W2, Washes; E1-E6, Elutions. LB, Luria-Bertani media; IPTG, Isopropyl β-D-1-thiogalactopyranoside; RT, Room temperature; 6X, hexa-histidine.

6.6 *In vitro* ATG7^{CTD} function is regulated by NO

In order to explore if the E1 enzymatic activity of ATG7^{CTD} might be regulated by S-nitrosylation, *in vitro* analyses were performed with recombinant proteins using the procedure described in **chapter 2.12**. An *in vitro* charging assay demonstrated that recombinant ATG7^{CTD} is able to activate its substrate ATG8a^{G132} in the presence of ATP and Mg^{2+} and subsequently form ATG7^{CTD}-ATG8a^{G132} thioester intermediates (**Fig. 6-6,** lane 3). To test if S-nitrosylation of ATG7^{CTD} can regulate its activity *in vitro*, the NO donors GSNO and CysNO were added to the reaction in the dark. Both GSNO and CysNO were found to inhibit the formation of ATG7^{CTD}-ATG8a^{G132} thioester intermediates, suggesting an inhibition of the enzymatic activity of ATG7^{CTD} by S-nitrosylation (**Fig. 6-6**, lane 5 & 6). ATG7 forms homodimers and ATG7^{CTD} is sufficient for dimer formation which is seen in the first lane in **Figure 6-6**, and this dimer is not redox regulated since the dimer is stable in the presence of the reducing agent DTT (dithiothreitol) (**Fig. 6-6,** lane 4). Interestingly, in the presence of CysNO less

ATG7^{CTD} monomer was observed whereas in the presence of GSNO more ATG7^{CTD} monomer was seen indicating, CysNO and GSNO might regulate differentially. We added 0.2 mM DTT with CysNO to test if this could rescue ATG7 function as DTT reverses S-nitrosylation. In **Figure 6-6** we can see that in the presence of 0.2 mM DTT, ATG7 function is not rescued probably because the thioester bond is also susceptible to reduction by DTT. Thus, we need to use a mild reductant that will reverse S-nitrosylation but not break a thioester bond.

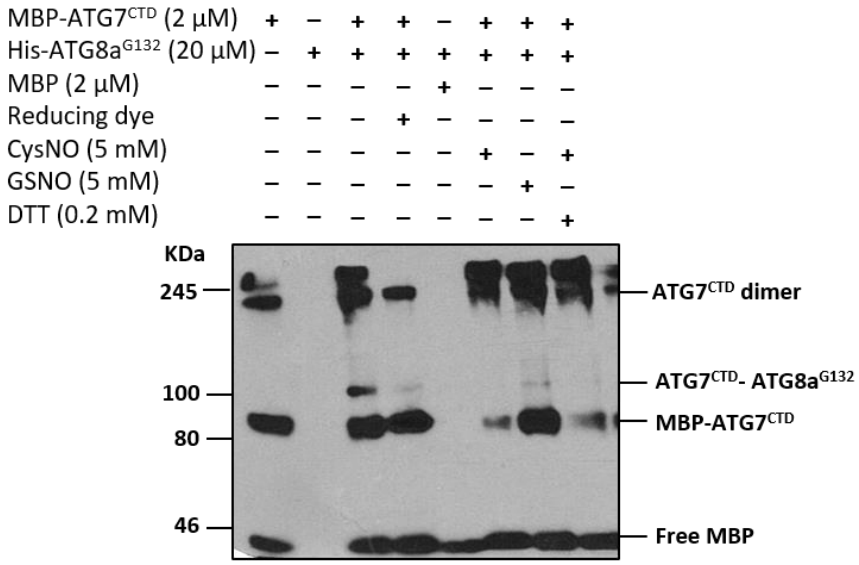

Figure 6-6. *In vitro* substrate binding activity of ATG7^{CTD}.

ATG7^{CTD} was incubated with ATG8a^{G132} in the presence of ATP and Mg^{2+} before subjected to non-reducing SDS-PAGE followed by transfer to a nitrocellulose membrane and then subjected to western blot. An anti-MBP antibody was used to detect the MBP-ATG7^{CTD} protein. An ATG7^{CTD}-ATG8a^{G132} thioester intermediate was detected as a high molecular shift from the size of MBP-ATG7^{CTD} (87.1 KDa). The expected intermediate size is ~105.6 KDa as His-ATG8a^{G132} is 18.5 KDa. The addition of reducing dye breaks down the thioester bond. MBP was added as a control with the substrate to rule out any non-specific interaction between MBP and ATG8a^{G132}. In presence of GSNO or CysNO, the ATG7^{CTD}-ATG8a^{G132} intermediate cannot be detected. The addition of 0.2 mM DTT was not sufficient to rescue ATG7 function. CTD, C-terminal domain; G132, Gly 132 exposed; MBP, maltose binding protein; DTT, dithiothreitol.

6.7 Regulation of ATG7^{CTD} function by S-nitrosylation is reversible

Once it was established that S-nitrosylation of ATG7^{CTD} can regulate its enzymatic activity, it was tested if this inhibition was GSNO concentration dependent. Different concentrations of GSNO were added in the reaction **(Fig. 6-7A**). In the presence of 1 µM GSNO the enzyme is fully active, however, at 50 µM no thioester bond formation with its substrate was detected. To test the specificity and reversibility of this NO-mediated inhibition, a mild reducing agent, sodium ascorbate (NaASC), was added to the reaction as NaASC effectively degrades GSNO and SNO without affecting thioester bonds. As expected NaASC could reverse the effect of S-nitrosylation and recover the enzymatic activity of ATG7^{CTD}. DTT was used as an alternative to sodium ascorbate, however, as DTT is a strong reductant, it affects the thioester bond formation negatively. To determine the GSNO concentration at which the enzymatic activity of ATG7 was inhibited, different concentrations of GSNO were added to the reaction ranging between 1 µM to 50 µM. The enzymatic activity was inhibited in the presence of 20 µM GSNO **(Fig. 6-7B**).

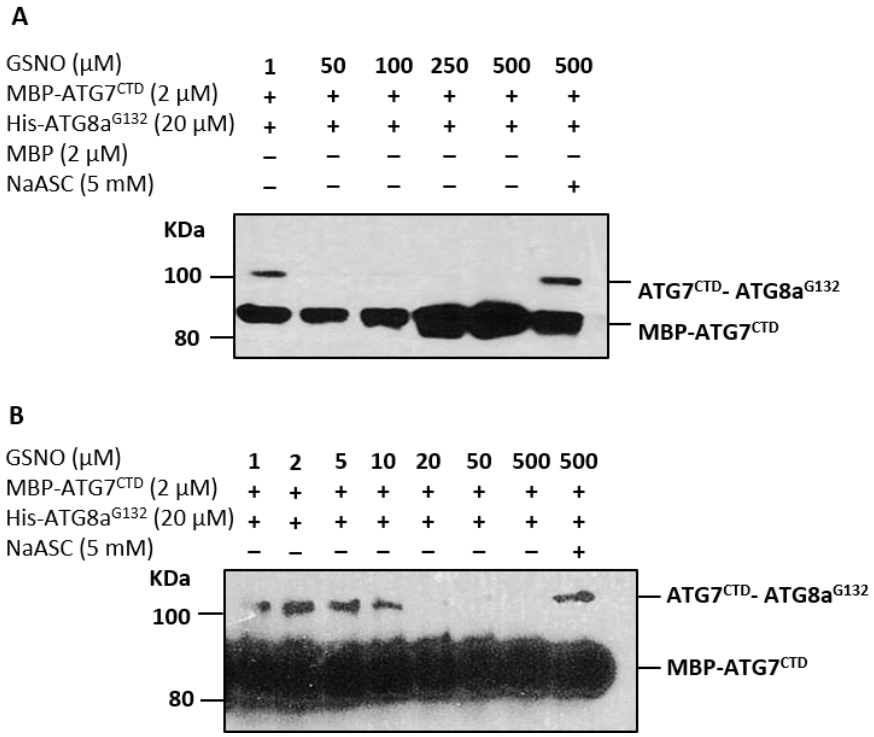

Figure 6-7. ATG7^{CTD} substrate binding activity is inhibited by GSNO in a concentration dependent manner.

ATG7^{CTD} was incubated with ATG8a^{G132} in the presence of ATP and Mg^{2+}. GSNO was added to the reaction at the stated concentrations. **A)** In the presence of 1 µM GSNO, ATG7^{CTD}-ATG8a^{G132} thioester intermediates can still be detected. However, 50 µM GSNO completely abolished the formation of a thioester intermediate. **B)** Inhibition of ATG7^{CTD} activity by the given concentrations of GSNO. The addition of NaASC rescued ATG7^{CTD} activity in the presence of 500 µM GSNO. NaASC; sodium ascorbate.

6.8 Recombinant TRXh5, TRXh5 C42S, NTRA production and purification

The coding sequence from 1-357 of the *Arabidopsis TRXh5* (*Thioredoxin h5*) was cloned in frame with an N-terminal 6XHis tag into the *Bam*HI and *Not*I site of pET28a vector and expressed in *E. coli* BL21 (DE3) cells. After expression, His-TRXh5 was purified under native conditions by immobilized-metal affinity chromatography (IMAC) using Ni-NTA resin. The His-TRXh5 (hereafter termed TRXh5) was 16.7 KDa (**Fig. 6-8A**). Cys 42 of *TRXh5* was mutated to Ser (C42S) using the quickchange lighting site-directed mutagenesis kit following

manufacturer's instructions. His-TRXh5 C42S was also produced in *E. coli* and purified using the same procedure as wild type TRXh5 (**Fig. 6-8B**). *Arabidopsis NTRA* (*thioredoxin reductase A*) was cloned from 1-1134 of the coding sequence keeping in frame with an N-terminal 6XHis and a C-terminal 6XHis tag into the *Bam*HI and *Not*I site of pET28a vector and expressed in *E. coli* BL21 (DE3) cells following purification using similar procedure as all other His tagged proteins (**Fig. 6-8C**). The His-NTRA-His was 45.1 KDa.

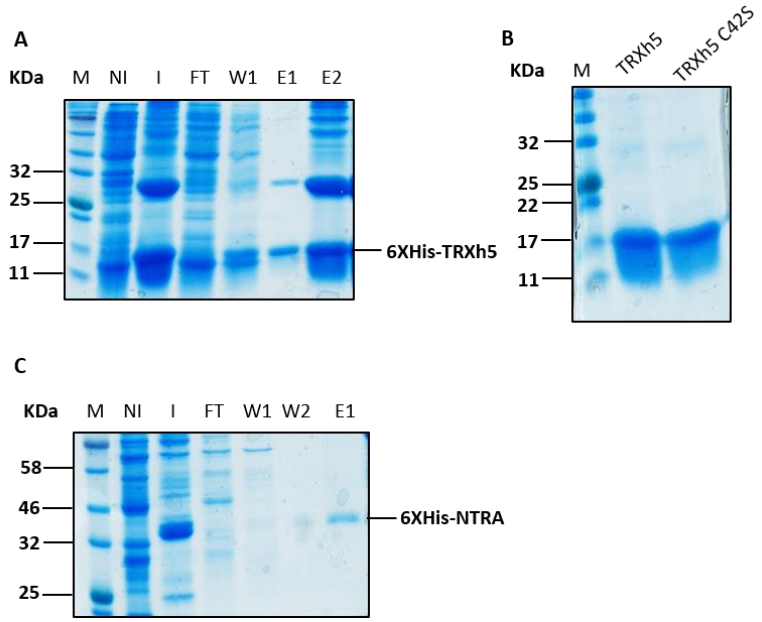

Figure 6-8. Recombinant His-TRXh5, His-TRXh5 C42S and His-NTRA purified by immobilized-metal affinity chromatography (IMAC).

A) *E. coli* BL21 (DE3) cells carrying the construct pET28a-TRXh5 were used to express the fusion protein His-TRXh5. 0.1 mM IPTG was used and after three hours of induction at 37°C, the cells were harvested for purification. Protein was run using a 13% reducing SDS-PAGE and visualised after staining with InstantBlue™. His-TRXh5 has an estimated molecular mass of 16.7 KDa. **B)** Recombinant His-TRXh5 C42S was expressed and purified using the same method as described in **A**. **C)** Recombinant His-NTRA was expressed and purified using pET28a vector and *E. coli* BL21(DE3) strain. 1 mM IPTG was used for induction and after induction, the cells were incubated at RT for two hours before proceeding to purification and visualising using the same method described in **A.** The molecular weight of His-NTRA is 45.1 KDa. M, Protein marker; NI, Non induced lysate; I, Induced lysate; FT, Flow through; W1,

Washes; E1-E2, Elutions; LB, Luria-Bertani media; IPTG, Isopropyl β-D-1-thiogalactopyranoside; RT, Room temperature; 6X, hexa-histidine.

6.9 ATG7^{CTD} is transnitrosylated by TRXh5/NTRA but not by TRXh5 C42S/NTRA *in vitro*

In some instances, S-nitrosylation may be directly reversed by TRX/NTRA denitrosylation (Kneeshaw et al., 2014). Since ATG7^{CTD} is S-nitrosylated *in vitro*, it was next tested whether TRX/NTRA can remove this NO modification. After S-nitrosylating recombinant ATG7^{CTD} with 200mM GSNO, combinations of either TRXh5, TRXh5 C42S, NTRA or both were added to the reaction mixture, which was subsequently left at room temperature for one hour before conducting the BST to detect possible S-nitrosylation. As shown in **Fig. 6-9A & B**, neither TRXh5 nor TRXh5 C42S in combination with NTRA was capable of denitrosylating ATG7^{CTD} *in vitro*. Interestingly, increased S-nitrosylation was observed when wild type TRXh5/NTRA was assayed. It is well established that the TRX/NTRA system has both denitrosylation and transnitrosylation activity (Wu et al., 2010; Kneeshaw et al., 2014; Benhar et al., 2008; Wu et al., 2011). Thereby, in our case, ATG7^{CTD} acts as a substrate for transnitrosylation by the TRXh5/NTRA system.

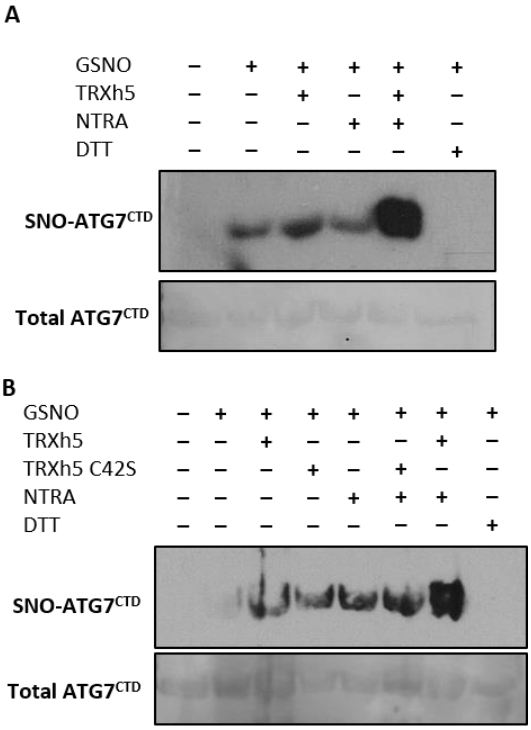

Figure 6-9. ATG7^{CTD} is transnitrosylated by TRXh5/NTRA *in vitro.*

A) Recombinant ATG7^{CTD} was incubated with 200 µM GSNO for 20 minutes before, the described combinations of recombinant TRXh5, and NTRA were added to total reaction volumes of 100µl. After biotin switch, proteins were analysed by non-reducing SDS-PAGE and western blot against biotin for SNO-ATG7^{CTD}. Total ATG7^{CTD} was detected by Ponceau S staining of the membrane. **B)** A similar experiment as in **A** was performed using both TRX5 and TRXh5 C42S.

6.10 ATG7^{CTD} substrate binding activity is negatively regulated by TRXh5/NTRA but not by TRXh5 C42S/NTRA

Next, we wanted to test whether ATG7^{CTD} substrate binding activity is regulated by the TRXh5/NTRA system. We performed the ATG7^{CTD} assay following the same procedure as described in **chapter 2.12** with or without adding a different combination of TRXh5/NTRA enzymes. As expected, the ATG7^{CTD}-ATG8a^{G132} thioester bond does not form in the presence of TRXh5/NTRA as shown in **Figure 6-10A** since TRXh5 has disulphide reductase activity. Next,

we used the TRXh5 C42S/NTRA hypothesising that the thioester bond will be stabilised due to the C42S mutation of TRXh5. The ATG7^{CTD}-ATG8a^{G132} thioester bond is stabilised in the presence of TRXh5 C42S/NTRA, however, the enzyme couple is unable to denitrosylate ATG7^{CTD} in the presence of GSNO, thereby the ATG7^{CTD} activity cannot be rescued by TRXh5 C42S/NTRA (**Fig. 6-10B**).

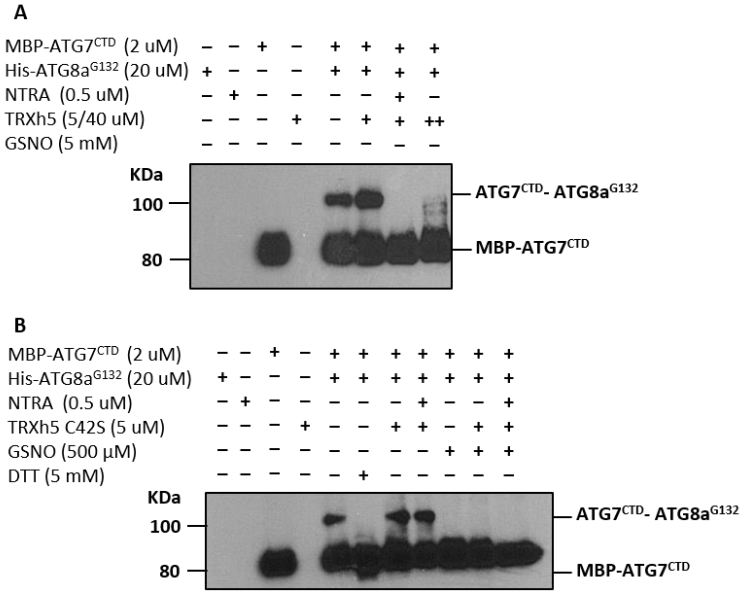

Figure 6-10. ATG7^{CTD} function is negatively regulated by TRX *in vitro*.

Substrate binding activity of ATG7^{CTD} was performed as in **Figure 6-6. A)** In the presence of TRXh5/NTRA, the ATG7^{CTD}-ATG8a^{G132} intermediate cannot be detected. **B)** In the presence of TRXh5 C42S/NTRA the ATG7^{CTD}-ATG8a^{G132} intermediate is detected however it does not rescue the enzyme activity in the presence of GSNO. The addition of DTT cannot rescue the enzyme.

6.11 Full-length ATG7 is S-nitrosylated *in vivo*

To further investigate whether ATG7 is S-nitrsylated *in vivo* and this modification is a biologically relevant process during plant salt stress, salt stressed and non-stressed wild type *Arabidopsis* (Col-0) and *gsnor1-3* plants were subjected to the BST following the procedure described in **chapter 2.11**. Streptavidin was used to pulldown biotinylated proteins and anti-

ATG7 antibody was used to detect the presence of ATG7 among the biotinylated proteins. As input controls, 20 µL aliquots were taken from the total protein extracts before streptavidin pulldowns. As seen in **Figure 6-11,** ATG7 is S-nitrosylated in both wild type and *gsnor1-3* plants. The level of S-nitrosylation in both wild type and *gsnor1-3* plants under non-stressed conditions is similar which is consistent with the level of autophagosome formation in both lines as shown as in **Figure 5-1, 5-2 & 5-3**. Interestingly, under salt stressed conditions, in *gsnor1-3* plants, the level of ATG7 S-nitrosylation is strikingly increased compared to than that of wild type plants.

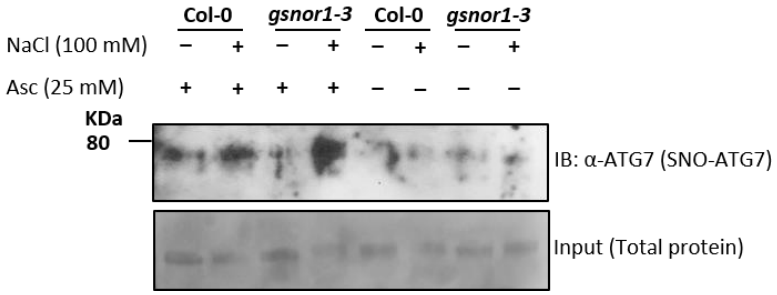

Figure 6-11. ATG7 is S-nitrosylated *in vivo* and the modification is regulated by salt stress.

Wild type (Col-0) and *gsnor1-3* plants were grown on ½ MS agar plates for five days before transferring them to control plates or plates containing 100 mM NaCl. Samples were collected after five days of stress. Total protein extracts from 100 mg seedlings were submitted to the BST followed by streptavidin pulldown and western blots with an anti-ATG7 antibody. 25mM sodium ascorbate (NaASC) was used to reduce SNOs. NaASC was omitted from the reaction as a negative control for the assay. To confirm that similar amounts of total protein were being compared, sample aliquots were taken before the pulldown step and used in parallel.

6.12 Discussion

Autophagy is a catabolic process highly conserved across the kingdoms which is required for degradation and recycling of cellular components during stressed and non-stressed conditions. In the previous chapter, it was shown that autophagy is regulated by S-

nitrosylation during plant salt stress. In this chapter, the mechanism of this regulation was studied using a molecular approach. We posit based on our data in **chapter 5** that molecular component(s) in autophagy may be regulated by redox based PTMs. Remarkably, many of the proteins involved during autophagy contain cysteine residue(s) in their catalytic or regulatory sites. One of the central components of autophagy are the ubiquitin-like ATG8/ATG12 conjugation pathways that involve autophagosome expansion and maturation. Both ATG8and ATG12 conjugation pathways require a single E1-like activating enzyme ATG7. Previous results from our lab have suggested that machinery involved in ubiquitination or SUMOylation in plants may be regulated by redox regulation specifically S-nitrosylation (Manda Yu, unpublished data & Michael Skelly, unpublished data). A deeper investigation of the ATG8/ATG12 conjugation pathway revealed ATG7 as a potential target. In this chapter, we sought to investigate any possible regulation of ATG7 by S-nitrosylation.

The C-terminal domain of ATG7, the activation domain, has 10 Cys residues and the N-terminal domain contains six Cys residues. Therefore, our primary goal was to investigate if the C-terminal domain of ATG7 can be regulated by S-nitrosylation. A biotin switch assay of recombinant $ATG7^{CTD}$ and $ATG7^{NTD}$ revealed that both domains are S-nitrosylated *in vitro* in a concentration dependent manner. Subsequently, we investigated the biological effect of this S-nitrosylation by an activity assay for $ATG7^{CTD}$ in the presence of its substrate $ATG8a^{G132}$ and ATP and Mg^{2+}. $ATG7^{CTD}$ retained its activity *in vitro,* however, activity was completely abolished in the presence of NO donors (GSNO, CysNO) in a concentration-dependent fashion. $ATG7^{CTD}$ loses activity completely in the presence of GSNO as low as 20 µM, thus suggesting possible regulation by S-nitrosylation *in vivo*. $ATG7^{CTD}$ inhibition was found to be reversible in the presence of the mild reductant sodium ascorbate, implying a possible reversible modification *in vivo* corresponding to the cellular redox status. It would be interesting to further investigate whether $ATG7^{NTD}$ S-nitrosylation also modifies ATG7

function.

TRX/NTRA is an important system for redox based protein modification conserved across kingdoms. TRX selectively reduces disulphide bonds in target proteins resulting in a disulphide bond formation within the two catalytic Cys residues in TRX. Subsequently, the catalytic Cys disulphide bond in TRX is resolved to free thiols by NADPH dependent NTRA (Wu et al., 2011). The TRX/NTRA system also has denitrosyltion and transnitrosylation activities (Wu et al., 2011, 2010). Recently, it has been shown that mutation in one of the TRX catalytic sites abolishes its disulphide reductase activity while retaining the denitrosylation function (we used TRXh5 C42S in this study) (Kneeshaw et al., 2014). Consequently, we tested if ATG7 S-nitrosylation can be reversed by TRX. In this context, we performed the biotin switch assay after incubating S-nitrosylated $ATG7^{CTD}$ with TRXh5/NTRA and TRXh5 C42S/NTRA for denitrosylation. Interestingly, $ATG7^{CTD}$ appears to be transnitrosylated by wild type TRXh5 while TRXh5 C42S does not denitrosylate $ATG7^{CTD}$ suggesting $ATG7^{CTD}$ may not be a substrate for TRXh5 denitrosylation. We also tested if TRXh5/NTRA or TRXh5 C42S/NTRA can rescue $ATG7^{CTD}$ enzyme activity in the presence of NO. Neither of the enzyme couples can alleviate the inhibition of $ATG7^{CTD}$ enzyme activity mediated by S-nitrosylation. Nevertheless, in our system, ATG7 is found to be a substrate for transnitrosylation by TRX/NTRA system suggesting a possible regulation may also exist *in vivo.* Thereby, we showed that ATG7 is negatively regulated by NO. It would be interesting to analyse the salt stress response in mutants associated with the TRX/TRX reductase system. We can achieve this by crossing an *Arabidopsis TRXh3/TRXh5* knockout mutant and/or overexpression lines with *gsnor1-3* plants to generate double mutants. Since we showed ATG7 is reversibly modified by S-nitrosylation, this suggests the existence of a possible denitrosylation mechanism *in vivo.* In this context, it would be interesting to investigate whether increasing the levels of antioxidant molecules, for example, ascorbate or glutathione in plants could suppress the *gsnor1-3* phenotype

during salt stress. Thus, the application of overexpression or loss-of-function lines of antioxidant pathways may provide additional insight into this mechanism of regulation. For example, loss-of-function mutants such as *vtc2-1* (*vitamin C2-1*) and *pad2-1* (*phytoalexin deficient2-1*) with lower cellular ascorbate and glutathione levels (Glazebrook and Ausubel, 1994; Conklin et al., 1996, 2000; Schlaeppi et al., 2008) respectively could be utilized to create *gsnor1-3* double mutants, which might exhibit enhanced NaCl sensitivity relative to *gnsor1-3* plants.

Finally, we performed the BST to potentially detect endogenously S-nitrosylated ATG7 in stressed and non-stressed plants. We found that ATG7 is endogenously S-nitrosylated in both conditions. The levels of S-nitrosylation under basal conditions in wild type and *gsnor1-3* plants is similar. However, under NaCl stress, the level of this modification in *gsnor1-3* plants is highly increased compared to wild type plants. This data is consistent with our previous data shown in **chapter 5**. The underlying mechanism of reduced autophagosome formation in *gsnor1-3* plants under salt stress might be due to the excessive S-nitrosylation of ATG7 inhibiting the activity of this enzyme, thus impairing the ATG8-PE and ATG12-ATG5 conjugation systems. Work presented in this chapter, thereby, provides a new insight into the autophagy regulation by S-nitrosylation at the molecular level. In this context, another important question arises, how this modification regulates ATG7 function in wild type plants. We have demonstrated that S-nitrosylation negatively regulates ATG7 function and in the absence of GSNOR1 function autophagy is impaired which leads us to speculate *GSNOR1* is a positive regulator of autophagy. Our data also showed that ATG7 is highly S-nitrosylated in a high S-nitrosylation background suggesting, ATG7 S-nitrosylation occurs at a point above to a critical NO and SNO levels. As autophagy is an energy-consuming cellular degradation process, this pathway needs to be under robust regulatory control to avoid excessive cellular material degradation under normal conditions. It is possible that the TRX/TRX reductase

system negatively control autophagy to achieve this. Further, GSNOR1 may indirectly regulate autophagy positively by maintaining cellular redox balance. On the other hand, during stress conditions, autophagy is induced to degrade damaged cellular materials. However, during prolonged stress, an accumulation of NO and S-nitrosothiols (SNOs) can affect autophagy negatively. We hypothesised that prolonged stress can lead to a build-up of NO above a critical point leading to S-nitrosylation of ATG7 resulting in impaired autophagy, therefore, causing salt sensitivity over time. This is also supported by the concentration dependent inhibition of ATG7 function (**Fig. 6-7**). Monitoring NO and SNO accumulation over time during stress and correlating ATG7 S-nitrosylation and function will provide us a deeper insight of this regulation. Collectively, we have demonstrated that GSNOR1 is a positive regulator of autophagy while the accumulation of endogenous NO during stress over time leading to ATG7 S-nitrosylation may function as one of the negative feedback mechanisms to regulate autophagy.

Ubiquitin (Ub) and ubiquitination like (Ubl) conjugation systems are an important regulatory mechanism in eukaryotes which involve activating enzyme(s) (E1), conjugating enzyme(s) (E2) and ligase enzyme(s) (E3) (Welchman et al., 2005). ATG8 and ATG12 conjugation pathways contain components similar to classical Ub/Ubl conjugation systems including ATG7 as an E1-like activating enzyme (Xie and Klionsky, 2007). All members of E1, E2 and E3 function via a catalytic Cys residue and the particular sensitivity of Cys residues to oxidation make them a target of redox regulation. Interestingly, though all E1s contain a catalytic Cys and could be potentially regulated by redox, this area of research is not well explored. Recently, S-nitrosylation of a SUMO conjugating enzyme (SCE1) at a highly conserved but previously uncharacterized Cys residue has been reported to regulate efficient immunity against the bacterial pathogen (Michael Skelly, unpublished data). From our data, we proposed that Ub/Ubl conjugation systems containing catalytic Cys residues might be

targets of reversible regulation by S-nitrosylation and other oxidative modifications.

Autophagy plays important roles in both biotic and abiotic stress in plants. Interestingly, both of these stresses are known to result in reactive oxygen/nitrogen burst (Yu et al., 2012, 2014; Spoel and Loake, 2011). Previous studies have shown that the autophagy deficient *atg7* and *atg9* mutants are compromised in early bacterial growth restriction (Hofius et al., 2009). In addition, high S-nitrosylation was reported to negatively regulate plant immunity (Feechan et al., 2005; Yun et al., 2011). Consequently, our data provides evidence that autophagy might be regulated by S-nitrosylation and a similar mechanism may be involved in plant-pathogen interaction.

Autophagy is implicated in neurodegenerative disorders such as Alzheimer's and Parkinson's diseases and neuronal injury in mammals and the absence or reduction of autophagy is often responsible for disease progression and severity (Hensley and Harris-White, 2015). Autophagy deficient *atg7* knock out flies (*Drosophila melanogaster*) were shown to accumulate ubiquitin-positive aggregates in degenerating neurons (Juhász et al., 2007). Interestingly, NO and S-nitrosothiols are also linked to neurodegenerative diseases (Wang et al., 2010). By extension, we can hypothesise from our data that, S-nitrosylation of ATG7 might play a significant role in autophagy inhibition during neurodegenerative diseases.

Collectively, in this chapter, we have described a novel mechanism for autophagy regulation by S-nitrosylation. We showed that E1-like activating enzyme ATG7 is modified by S-nitrosylation *in vitro* and *in vivo* regulating plant salt tolerance. In the next chapter, we will investigate the target Cys residue for S-nitrosylation in $ATG7^{CTD}$ and the possible biological implication of that modification.

Chapter 7

7 Mutational analysis to reveal the biological role of Cys residue in ATG7^{CTD}

7.1 Introduction

Cysteine (Cys for three letter code; C for one letter code) is a small amino acid containing a nucleophilic thiol side chain that often takes part in redox modifications and enzymatic reactions. A Cys thiol group normally has a high pKa (~8.5) so it is expected that at physiological pH, the vast majority of Cys residue within cytoplasmic proteins are protonated and are not much reactive to oxidants (Roos et al., 2013). However, proteins with active-site or regulatory Cys residues rely on the deprotonated (thiolate) form of the Cys for activity and reactivity towards oxidants. This is normally achieved by the microenvironment which can reduce the pKa of Cys lower than the physiological pH leading to the fully ionised thiolate form. One such example is the disulphide bond of oxidoreductase DsbA where the pKa of Cys drops to 3.5 (Klomsiri et al., 2011). Cys residues also show high affinities towards zinc (Zn), the second most biologically relevant metal second to only iron (Fe) in abundance within the cell. Cys-Zn^{2+} complexes contribute to protein structure, catalysis, regulation and Zn^{2+} storage. However, Cys reactivity highly depends on the microenvironment thereby the affinity for Zn^{2+} varies accordingly (Pace and Weerapana, 2014). Cys being a potential redox active residue, also plays an important role in cellular signalling by redox-based, post-translational modifications (Spadaro et al., 2010). Therefore, Cys plays an important role in protein function due to its unique biological characteristics.

Previous results in **chapter 6** have shown that S-nitrosylation of ATG7^{CTD} inhibits cognate enzyme activity *in vitro*. The identification of one or more Cys residues and their biological role will be investigated in this chapter using molecular methods such as mass-

spectrometry (MS) and mutation and computational structural biology.

7.2 Mass-spectrometry reveals NO-dependent ATG7 Cys modification

Mass-spectrometry (MS) is a powerful technique to identify post-translational modifications. Recombinant $ATG7^{CTD}$ was subjected to a modified biotin switch technique before analysis by MS. Recombinant $ATG7^{CTD}$ was incubated with NO donor (500 µM GSNO) in the dark for 20 min. After removing excess NO donor, free thiols were alkylated using 20 mM NEM. After alkylation, proteins were precipitated and washed with acetone. Protein samples were then resuspended and in-solution trypsin digestion was carried out before analysis of the sample by nESI (nano-electrospray ionisation) on FT-ICR (fourier transform-ion cyclotron resonance). The protein digestion and MS analysis was carried out by Dr. David Clarke, School of Chemistry, University of Edinburgh. MS could detect 76% of the protein sequence. Five out of 10 Cys were detected (**Fig. 7-1**). This is probably due to the size of the fragments containing the remaining residues. Thus, further analysis using a different peptidase or a combination of peptidases to digest ATG7 should be employed to try to increase the sequence detection coverage and capture all Cys residues in the peptide mixture. However, all five of these were NEM modified indicating that these residues were not modified by NO donor (**Table 7-1**). Though we could not detect all the Cys in this experiment, the result rules out five Cys thus the rest of the five Cys were subjected to mutational analysis.

>MBP-ATG7^{CTD}
MKIEEGKLVIWINGDKGYNGLAEVGKKFEKDTGIKVTVEHPDKLEEKFPQVAATGDGP
DIIFWAHDRFGYAQSGLLAEITPDKAFQDKLYPFTWDAVRYNGKLIAYPIAVEALSLI
YNKDLLPNPPKTWEEIPALDKELKAKGKSALMFNLQEPYFTWPLIAADGGYAFKYENG
KYDIKDVGVDNAGAKAGLTFLVDLIKNKHMNADTDYSIAEAAFNKGETAMTINGPWAW
SNIDTSKVNYGVTVLPTFKGQPSKPFVGVLSAGINAASPNKELAKEFLENYLLTDEGL
EAVNKDKPLGAVALKSYEEELVKDPRIAATMENAQKGEIMPNIPQMSAFWYAVRTAVI
NAASGRQTVDEALKDAQTNSSSNNNNNNNNNLGIEGRISHMSMGGRSGESAETVPNS
VGWELNKGKRVPRSISLANSMDPTRLAVSAVDLNLKLMRWRALPSLNLNVLSSVK**C360**
LLLGAGTLG**C370**QVARTLMGWGIRNITFVDYGKVAMSNPVRQSLYNFEDC408LGRGEF
KAVAAVKSLKQIFPAMETSGVVMAIPMPGHPISSQEEDSVLGD**C458**KRLSELIESHDA
VFLLTDTRESRWLPSLLC488ANANKIAINAALGFDSYMVMRHGAGPTSLSDDMQNLDI
NKTNTQRLG**C536**YF**C539**NDVVAPQDSMTDRTLDQQC558TVTRPGLAPIAGALAVELLV
GVLQHPLGINAKGDNSSLSNTGNNDDSPLGILPHQIRGSVSQFSQITLLGQASNSC634
TAC637SETVISEYRERGNSFILEAINHPTYLEDLTGLTELKKAANSFNLDWEDDDTDD
DDVAVDL

Figure 7-1. Protein sequence of MBP-ATG7^{CTD} showing sites detected by mass spectrometry (MS).

Recombinant and purified MBP-ATG7^{CTD} was subjected to biotin switch with few modifications before analysing by MS. Blue text showing sequence of MBP. Black text showing sequence for ATG7^{CTD}. Cysteine (C) residues observed as NEM modified are shown in green indicating they are not sensitive to oxidation by GSNO. Cysteine residues that were not detected by MS are shown in gray. Cysteine residue numbers are given according to their position in *Arabidopsis* ATG7 full-length protein.

Table 7-1. Table showing the cysteine (C) sites detected by MS and their modification status.

Position	Modification	Modification by S-nitrosylation
C360	NEM modified	Not susceptible
C370	NEM modified	Not susceptible
C408	Not detected	Not detected
C458	NEM modified	Not susceptible
C488	Not detected	Not detected
C536	NEM modified	Not susceptible
C539	NEM modified	Not susceptible
C558	Not detected	Not detected
C634	Not detected	Not detected
C637	Not detected	Not detected

7.3 Site-directed mutagenesis of Cys residues of ATG7^{CTD} reveals C558 and C637 are the sites of S-nitrosylation

Having ruled out five Cys out of 10, we subjected the remaining Cys residues to mutational analysis. Before substitution, we used GPS-SNO (version 1.0) (Xue et al., 2010), to predict the target site for S-nitrosylation. The GPS-SNO program was run on a medium threshold according to the method described in (Xue et al., 2010). The predicted sites were then ranked as previously described (Chaki et al., 2014). The most probable Cys site for S-nitrosylation in ATG7^{CTD} was predicted to be C637 (**Table 7-2**), while C558 was the second ranked site for S-nitrosylation. The third ranked, C360, was found not to be S-nitrosylated by MS (**Fig. 7-1**). Therefore, we decided to mutate C558 and C637. We also chose to mutate C634 because of its proximity to C637, though it was not predicted to form an SNO by the GPS-SNO programme. C558 is the catalytic site residue in ATG7 which forms a transient thio-ester bond with the C-terminal glycine (Gly) residue of ATG8 or ATG12 (Thompson et al., 2005; Noda et al., 2011). C634 and C637 reside near the ECTD at the hinge of CL (**Fig. 6-1A**). These two Cys are part of a Cys tetrad motif that includes C536 and C539. This Cys tetrad coordinates a zinc ion in the vicinity of the CL hinge region connecting one end of CL to the ECTD (**Fig. 6-1A**) that helps the CL hinge to undergo a conformational change (Noda et al., 2011; Lee and Schindelin, 2008).

Previous studies have shown that the catalytic site Cys substitution with Ser generates a stable complex between the ATG7 and its substrate ATG8 or ATG12 due to the formation of an O-ester bond instead of an intermediate complex by a thio-ester bond (Ichimura et al., 2004). Therefore, C558 was substituted with alanine (Ala) (C558A) as this has been reported to abolish the enzyme activity (Tanida et al., 1999). The other Cys residues were substituted with serine (Ser/S) due to this residue being isosteric to Cys. We also generated different

combinations of Cys mutations within ATG7. A QuickChange Lightning Site-Directed Mutagenesis kit was used to mutate nucleotides to generate the desired codon and the mutation was confirmed by sequencing. The mutated ATG7^{CTD} fragment was then cloned into the pETG40A vector using a GATEWAY™ cloning system. The recombinant protein was expressed in *E. coli* BL21(DE3) and purified using an MBP-tag purification system following the procedure described in **chapter 2.10** and **Figure 6-3A**. Recombinant protein containing the C558A or C637S mutation were stable and same size as wild type ATG7. Interestingly, we could not purify the C558A+C637S double mutant instead we used C558A+C637A double mutant. We also produced C634S+C637S double mutant and C558A+C634S+C647S triple mutant.

Table 7-2. Table showing the predicted cysteine (C) sites for S-nitrosylation by GPS-SNO program.

Rank	Position	Peptide	Domain	Score	Cutoff	Score/ Cutoff	Cluster	Threshold
1	637	SCTACSETV	CTD	4.272	2.443	1.7	B	High
2	558	LDQQCTVTR	CTD	22.679	20.743	1.1	C	Medium
3	360	SSVKCLLLG	CTD	21.022	20.743	1.0	C	Medium
4	87	NRNKCPVPG	NTD	21.292	20.743	1.0	C	Medium

7.4 Multiple Cys targets for S-nitrosylation in ATG7^{CTD}

Next, we applied the BST using the Cys mutant to detect S-nitrosylation following the procedure described in **chapter 2.11**. We used C558A and C558A+C637A mutant proteins for BST. Interestingly, both mutant proteins gave us a positive signal in the presence of GSNO indicating that there are multiple Cys targets for S-nitrosylation in ATG7^{CTD} (**Fig. 7-2)**. Data presented in **Figure 7-2** was undertaken by an MSc project student, Ann-Kathrin Bahlmann.

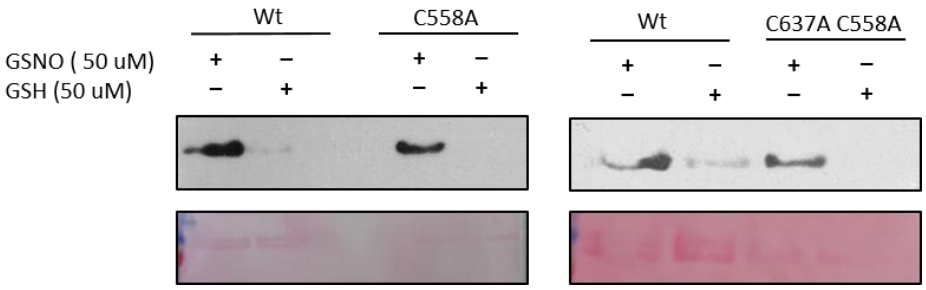

Figure 7-2. BST of mutant ATG7^{CTD} reveals there are multiple target sites for S-nitrosylation.

Cys mutant ATG7^{CTD} proteins were subjected to a biotin switch assay after incubation with the stated concentrations of GSNO or GSH followed by non-reducing SDS-PAGE and transferred to a nitrocellulose membrane for western blot analysis. Immunodetection was undertaken by an anti-biotin monoclonal HRP conjugated antibody. Ponceau S staining of the total ATG7^{CTD} on nitrocellulose membrane indicated equal loading. Wild type, C558A and C558A+C637A double mutant were S-nitrosylated in the presence of GSNO indicating that there are more than these two target Cys sites that are subjected to S-nitrosylation.

N.B. Data shown in **Fig. 7-2** was generated by Ann-Kathrin Bahlmann (MSc project student).

7.5 S-nitrosylation of C588 and C637 regulates ATG7^{CTD} enzyme activity

We carried out the ATG7 substrate binding assay using the Cys mutant proteins following the same procedure as described in **chapter 2.12**. We hypothesised that S-nitrosylation of redox-regulated Cys residue(s) inhibits ATG7 function, mutation of which should make ATG7, independent of NO modification. **Figure 7-3** shows that among all the ATG7^{CTD} Cys mutants, C558A, C637S, C634S+C637S and C558A+C637A can bind to the substrate, ATG8a^{G132}, forming a high molecular complex, in the absence of NO indicating that the overall structure of the enzyme and substrate specificity is not abolished by these mutations. C558A and C558A+C637A, therefore, only lost their thio-esterification activity due to a mutation in the catalytic site Cys while retaining the substrate binding activity (**Fig. 7-3**

lane 1 & 9 respectively). Though weakly, C637S was also able to form a complex with the substrate ATG8a^{G132} (**Fig. 7-3 lane 3**). This demonstrates that C637 is important for efficient substrate binding which is supported by the fact that it is part of a Cys tetrad core that co-ordinates a Zn^{2+} providing stability to the otherwise flexible CL (**Fig 6-1**). A similar effect was observed in the C634S+C637S double mutant, indicating that both residues are important for structural stability (**Fig. 7-3 lane 5**). In C637S and C634S+C637S double mutant, substrate binding is reduced, probably due to the charge present in the -OH (hydroxyl) side chain of Ser which will change the environment of the Zn^{2+} binding core whereas C558A+C637A efficiently binds to the substrate due to the neutrality of Ala. C558A+C634S+C637S triple mutant does not bind to the substrate, hence, is not biologically active due to the abolishment of both the catalytic site Cys and two Cys from the tetrad core (**Fig. 7-3 lane 7**).

Next, we tested ATG7^{CTD} activity of all the Cys mutants in the presence GSNO. **Figure 7-3** shows that C558A, C637S and C634S+C637S double mutant lost enzyme activity in the presence of GSNO indicating these mutants still formed SNO. C558A does not bind substrate in the presence of GSNO, suggesting that S-nitrosylation might affect the structural conformation of this protein and hence substrate specificity of ATG7^{CTD} (**Fig. 7-3 lane 2**). A similar effect was observed in the C637S and C634S+C637S double mutant suggesting that C558 and C634 might be regulated by S-nitrosylation, thus impacting enzyme activity in the presence of NO. C637S and C634S+C637S double mutant also seemed to be destabilised upon the addition of GSNO (**Fig. 7-3 lane 4 & 6**).

Interestingly, C558A+C637A double mutant binds to the substrate in the presence of GSNO implying that this mutant does not lose its substrate binding ability due to the mutation of C637, suggesting this residue is subjected to S-nitrosylation (**Fig. 7-3 lane 10**). It is possible that the ATG7^{CTD} C558A+C637A double mutant can still co-ordinate the Zn^{2+} in the hinge

region of CL due to the neutrality of Ala even in the presence of NO.

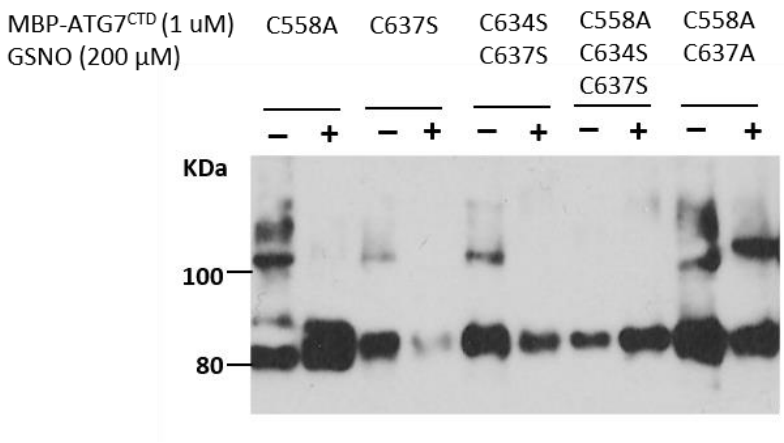

Figure 7-3. Effect of cysteine mutations on ATG7^{CTD} substrate binding activity.

ATG7^{CTD} Cys mutant proteins were (as indicated) incubated with ATG8a^{G132} in the presence of ATP and Mg^{2+} with or without the addition of NO donor (GSNO). ATG7^{CTD}-ATG8a^{G132} formation can be seen as a high molecular weight shift around 105 KDa.

7.6 Modelling of *Arabidopsis* ATG7 helps to identify target Cys residue

Bioinformatics and computational biology have become a powerful tool to predict structure, function and post-translational modifications in protein biology. We have also taken advantage of computational prediction programmes to detect the target Cys residues for S-nitrosylation in ATG7. To understand whether S-nitrosylation of the target Cys residues can modulate the activity of ATG7, we first computationally modelled the structure of this protein. For this, we have used the intensive mode in Phyre2 (http://www.sbg.bio.ic.ac.uk/phyre2) which applies advanced remote homology detection methods to build 3D models. The homology detection method involves both searching for sequence-based homology and known structure-based homology (Kelley et al., 2015). Since the crystal and NMR structure for *Saccharomyces cerevisiae* is already available in the database and *Arabidopsis* ATG7 shares significant sequence similarity with ScATG7, the

resulting predicted structure will be largely accurate. Full length *Arabidopsis thaliana* ATG7 protein sequence (http://www.uniprot.org/; UniProt ID: Q94CD5) was submitted for modelling. At least 606 residues (87%) were modelled at >90% accuracy. **Figure 7-4 is** showing both AtATG7 (**A**) and ScATG7 (**B**). There are 10 Cys residues present in the C-terminal domain of ATG7 (**Fig. 7-4C**). Among these three were predicted as a potential target for S-nitrosylation (**Table 7-2**). Next, we generated the surface model using PyMOL™ (v. 1.7.4.4. Educational build, Schrödinger**,** LLC) to visualise the solvent accessibility of Cys residues (**Fig. 7-5**). However, the predicted site C360 was not solvent accessible making it unlikely to be a site of S-nitrosylation. This was also supported by the MS data (**Fig. 7-1 and Table 7-1**) as C360 was found to be NEM modified and thereby not S-nitrosylated. This left two other potential target residues, C558 and C637. Interestingly, BST data (**Fig. 7-2**) showed that there may be other targets for S-nitrosylation though the Cys residue(s) may not be biologically relevant since $ATG7^{CTD}$ C558A+C637A substrate binding was not inhibited by GSNO (**Fig. 7-3**). Nonetheless, we tried to predict the other target Cys residue(s). From the surface model it was observed that C408 is fully solvent accessible, thus we hypothesised that C408 might also be S-nitrosylated without a significant impact on protein function (**Fig. 7-5**). However, this would need to be further verified by both MS data and mutational analysis. From the surface model, it is implied that the Cys tetrad for Zn^{2+} binding is also solvent accessible making these Cys residues likely to be regulated by S-nitrosylation (**Fig. 7-5A**).

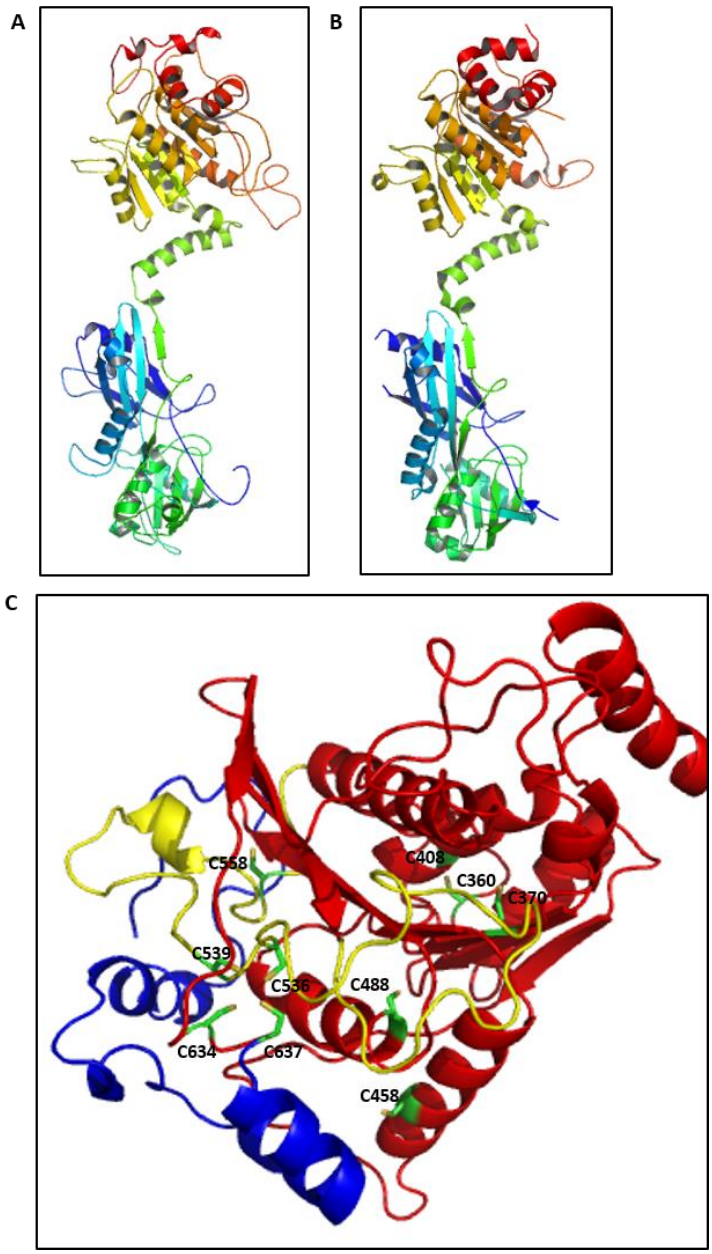

Figure 7-4. Modelling of *Arabidopsis thaliana* ATG7 (AtATG7) using Phyre2 shows significant structural similarity to *Saccharomyces cerevisiae* ATG7 (ScATG7).

The web server Phyre2 was used to generate a model for AtATG7 based on the structural template of ScATG7. **A)** Full-length AtATG7. **B)** Full-length ScATG7 structure (PDB ID: 3VH2) **C)** C-terminal domain of AtATG7 showing all 10 Cys residues present in this domain. Crossover loop (CL) is coloured in yellow. Extended C-terminal domain ECTD is coloured in blue. Sulphur atoms in Cys residues are shown in golden. All structures were visualised by the PyMOL™ molecular graphics system (v. 1.7.4.4. Educational build, Schrödinger**,** LLC).

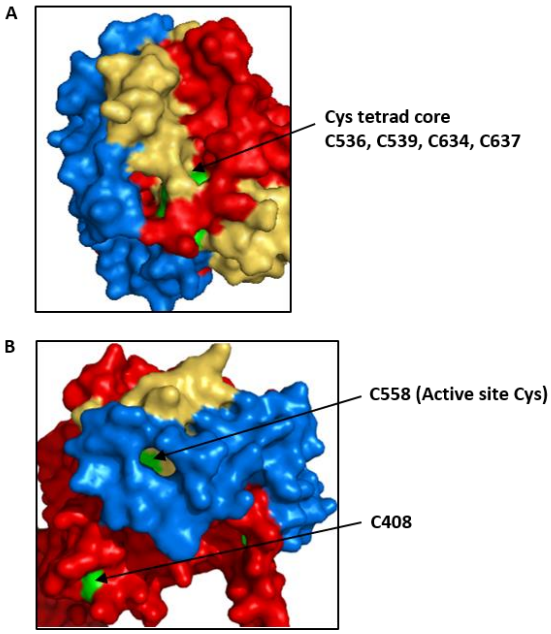

Figure 7-5. Surface structure showed solvent accessible Cys residues in the ATG7^{CTD}.

The PyMOL™ molecular graphics system (v. 1.7.4.4. Educational build, Schrödinger, LLC) was used to generate the surface model to visualise solvent accessible Cys residues. Among 10 Cys residues, six were solvent accessible including C408, C536, C539, C558, C634, C637. Cys residues are shown in green. The crossover loop is shown in yellow and the ECTD is shown in blue.

Noda et al. (2011) also analysed the crystal structure of ScATG7^{CTD} bound to ScATG8a, ATP and Mg^{2+}. We then used the structural template based one-to-one threading function of Phyre2 (expert mode) to model AtATG7^{CTD} bound to AtATG8a^{G132} (**Fig. 7-6**). Our predicted structure is significantly similar to the template. Next, we aligned the free AtATG7^{FL} (FL, full-length) structure with the AtATG7^{CTD}-AtATG8a^{G132} complex structure using PyMOL™ and the built-in align function. Aligning these two structures showed that the CL undertakes a significant structural change upon substrate (ATG8a) binding (**Fig. 7-7**), indicating that the model was highly accurate since a similar change was also seen in the crystal and NMR

structure of ScATG7 (Noda et al., 2011). Interestingly, the Cys tetrads in both structures aligned almost perfectly indicating that this tetrad might work as a hinge that provides structural stability to the otherwise flexible CL in ATG7. Since C637 is part of the tetrad, S-nitrosylation of this particular Cys residue might abolish Zn^{2+} binding thereby inhibiting ATG7 activity (**Fig. 7-8**). Interestingly, substituting C637 to Ala eliminates the effect of S-nitrosylation. It is evident that Zn^{2+} binding residues in a motif can range from two to four of Cys and/or His. The bond can also be stabilised with a water molecule or Asp and Glu residues (Pace and Weerapana, 2014). It is possible that abolishing just one Cys from the tetrad (C637A) does not fully destabilise the CL structure while preventing S-nitrosylation at this position.

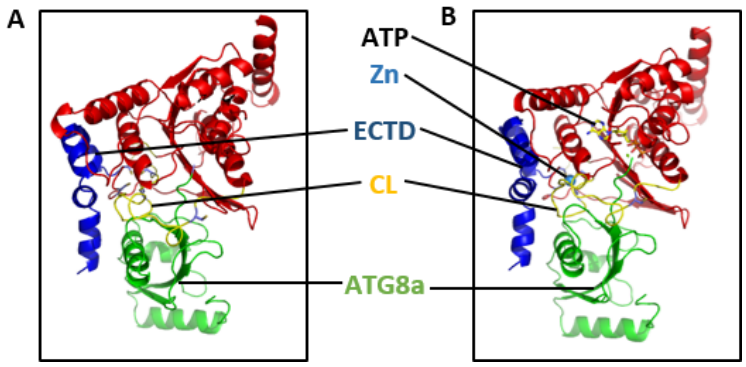

Figure 7-6. Modelling of AtATG7^{CTD} bound to AtATG8a^{G132} using Phyre2 shows significant structural similarity to the ScATG7^{CTD}-ATG8 complex.

Employing the web server Phyre2, one-to-one threading was used to generate a model for AtATG7^{CTD}-AtATG8a^{G132} complex formation based on the structural template of ScATG7. **A)** AtATG7^{CTD}-AtATG8a^{G132}. **B)** ScATG7^{CTD}-ScATG8 (PDB ID: 3VH4). All structures were aligned and visualised by the PyMOL™ molecular graphics system (v. 1.7.4.4. Educational build, Schrödinger, LLC).

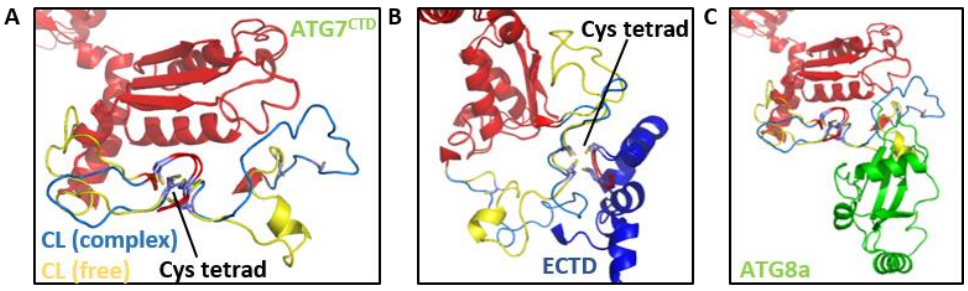

Figure 7-7. Aligning free AtATG7^{CTD} with AtATG7^{CTD}-AtATG8a^{G132} complex shows the conformational change in the crossover loop (CL).

Structures were aligned and visualised by the PyMOL™ molecular graphics system (v. 1.7.4.4. Educational build, Schrödinger, LLC). Aligning reveals that the CL undergoes a dramatic conformational change upon binding to ATG8a^{G132}, however, the Cys tetrad position is not significantly changed. **(A, B)** AtATG7^{CTD}-AtATG8a^{G132} complex aligned with free AtATG7^{CTD}, AtATG8a^{G132} is not shown for clarity **A)** Front view of the complex, **B)** Side view of the complex, **C)** AtATG7^{CTD}-AtATG8a^{G132} complex aligned with free AtATG7^{CTD}, AtATG8a^{G132} is shown in green.

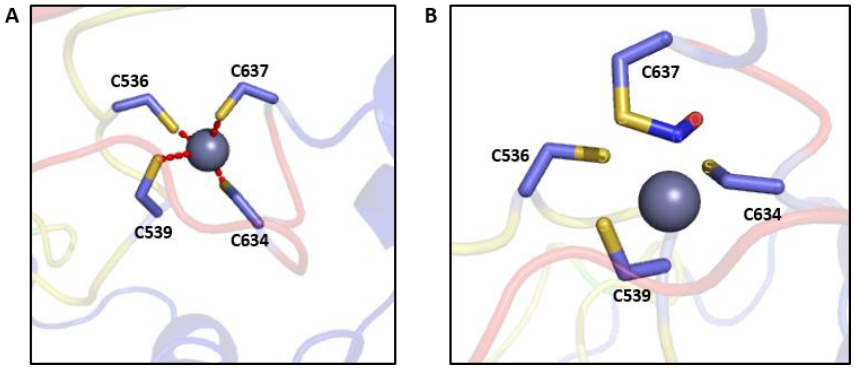

Figure 7-8. Computational modelling reveals the impact of SNO formation at C637 on ATG7^{CTD} structure.

A) Model showing the site of Cys tetrad including C637. The tetrad holds a single Zn^{2+} by forming a tetrahedral structure. **B)** S-nitrosylation of C637 may change the reduced environment to more an oxidised environment, thereby probably resulting in Zn^{2+} release.

Zn^{2+} is shown as a blue sphere. Sulphur atom is in golden yellow, Nitrogen in blue and Oxygen in red. An NO group was added using the build function in PyMOL™.

7.7 Discussion

In this chapter, we adopted molecular analysis, mass-spectrometric analysis and computational prediction to investigate the potential target cysteine residues for S-nitrosylation in ATG7 and the possible effect of this modification on protein function. BST analysis of the mutant protein revealed that there are possibly more than two target sites for S-nitrosylation including C558 and C637. Another potential site for S-nitrosylation might be C408 due to its solvent accessibility. However, no significant biological function was assigned to this particular Cys. Moreover, C408 is not evolutionarily conserved across kingdoms making it less likely to be a site of regulation (**Fig. 6-1**). However, more MS analysis supported by mutational analysis is required to confirm the modification and its possible effect. MS data failed to detect the most important Cys residues in the C-terminal domain of ATG7 including the active site C558 and also C634 and C637. Interestingly, two other Cys residues in the Cys tetrad were detected by MS: C536 and C539. These two Cys were not modified by S-nitrosylation. C360 was also highlighted as a possible site of S-nitrosylation by the prediction software GPS-SNO but C360 was detected by MS as NEM modified thus indicating it is not S-nitrosylated. The other undetected Cys in MS was C488, however, this residue was not predicted as a site for S-nitrosylation neither it is evolutionarily conserved. Further, C488 is deeply buried within ATG7 making it highly improbable to be S-nitrosylated. Collectively, we hypothesise the most likely Cys targets are C558 and C637. Two other potential Cys targets are C634 and C408 for this modification.

Next, we have shown in the substrate binding assay using the Cys mutant ATG7 proteins that $ATG7^{CTD}$ C558A+C637A was still able to bind substrate. Though this mutant protein will

not be able to activate the substrate ATG8a because of the active site Cys mutation but the mutant is able to bind the substrate in the presence of GSNO due to the C637A mutation, thereby precluding S-nitrosylation.

We also used computational and structural biology to predict the potential target site(s) for S-nitrosylation and the effect of that modification. C558 is the active site residue, S-nitrosylation of this residue will inhibit enzyme activity of $ATG7^{CTD}$. Furthermore, C637 and C634 are part of the Cys tetrad which co-ordinates a Zn^{2+} near the hinge region of CL connecting to ECTD. This is supported by previous research on SUMO E1-like activating enzyme SAE1/SAE2 where a similar Cys tetrad core is formed by two Cys-X-X-Cys motifs (X; any amino acids) (Lois and Lima, 2005). A similar feature was observed in the antecedent of the E1-like activating enzyme MoeB-MoaD complex (Lake et al., 2001). Interestingly, this Cys tetrad motif was absent in the UBA1 and all Ub-E1s (ubiquitin E1 activating enzymes) probably because the Ub-E1 requires only a smaller conformational change to allow the thio-esterification (Lee and Schindelin, 2008).

The zinc binding motif is responsible for one of the three functions: structural support, regulatory and catalytic roles (Pace and Weerapana, 2014). Zn^{2+} binding Cys motifs can play different roles depending on the position of the Cys residue and the mode of interaction between Cys and Zn^{2+}. The most classical interaction between Cys and Zn^{2+} is the zinc finger domain consisting of Cys_4 or Cys_2His_2 coordination environments which support structural stability. The Cys-Zn^{2+} complex is an important regulatory mechanism for enzymes. Usually, Cys has a pKa close to physiological pH converting the thiol group to fully reduced unmodified form that is suitable for binding Zn^{2+}. Cellular redox status can be coupled with the Cys-Zn^{2+} complex where an oxidising environment can cause Zn^{2+} release. Betain-homocysteine methyltransferase (BHMT) is a metabolic enzyme in multiple amino acid biosynthetic

pathways which is regulated by a redox switch Cys-Zn^{2+} complex. In the reducing environment, the active form of BHMT co-ordinates a Zn^{2+} by C217, C299 and C300. In an oxidising condition, C217 and C299 form a disulphide bond, inducing the release of Zn^{2+}, rendering the enzyme inactive (Pace and Weerapana, 2014).

Collectively, our data suggests that ATG7 is redox regulated and in an oxidising environment this enzyme is inhibited. S-nitrosylation plays an important role in modulating enzyme activity by promoting an oxidising environment. S-nitrosylation possibly inhibits enzyme activity by S-nitrosylating both the active site C558 and also C637, which is present in the Zn^{2+} binding Cys tetrad, thereby modulating the structural stability of ATG7.

Chapter 8

8 General Discussion

8.1 S-nitrosylation plays role in plant salt stress

Plants have evolved to adopt a plethora of mechanisms during biotic and abiotic stresses. A reactive nitrogen species burst is one of the common features in stress signalling. One of the ways NO exerts its biological effects is through S-nitrosylation, the covalent attachment of an NO molecule to a reactive cysteine (Cys) thiol (-SH) group to form an S-nitrosothiol. S-nitrosylation is a crucial redox-based post-translational mechanism conserved across species (Yu et al., 2014). *GSNOR* plays central roles in regulating global SNO levels (Feechan et al., 2005). Previous studies have indicated that *GSNOR* might be involved in plant abiotic stress as GSNOR activity was found to be increased under salinity, high temperature, low temperature and arsenic stress (Ziogas et al., 2013; Airaki et al., 2012; Corpas et al., 2011; Camejo et al., 2013; Leterrier et al., 2011). *GSNOR* knock down tomato (*Solanum lycopersicum*) plants were shown to be sodic alkaline stress sensitive (Gong et al., 2015). Further, the absence of *GSNOR* was shown to convey reduced heat acclimation in *Arabidopsis* (Hong et al., 2003). However, direct regulation of salt stress by *GSNOR* has not been previously explored. In this work, we investigated the role of S-nitrosylation in plant salt tolerance. We have shown in chapter 3 that *gsnor1-3* plants are more sensitive to salt and osmotic stress compared to wild type *Arabidopsis* plants in various stages of the life cycle. Plants lacking *GSNOR1* showed reduced germination in the presence of NaCl, KCl and mannitol suggesting a possible regulation by salt and osmotic stress. Survival was also reduced for both media and soil grown plants under salt treatment. Further, *gsnor1-3* plants showed higher fresh weight loss compared to wild type plants in the presence of NaCl.

Together, these data suggest that in the absence of *GSNOR* function plants are more sensitive to salt stress, implying underlying regulation by S-nitrosylation.

8.2 Classical salt stress signalling pathways are not impaired in *gsnor1-3* plants

To determine the underlying mechanisms of salt sensitivity in *gsnor1-3* plants, we studied whether the classical salt stress signalling pathways are regulated by S-nitrosylation. Maintenance of ion homoeostasis is one of the classical salt tolerance mechanisms that involves class I *HKT* and *salt overly sensitive* (*SOS*) pathway during salt stress (Munns and Tester, 2008). Any defects in ion homoeostasis are known to increase Na^+ levels in the photosynthetic organs of plants (Shi et al., 2002b; Munns and Tester, 2008). NO is also known to enhance plant salt tolerance by attenuating the elevation of the Na^+/K^+ ration (Zhao et al., 2007). Thereby, we tested ion contents during salt stress in wild type and *gsnor1-3* plants. We have found that *gsnor1-3* plants accumulate similar levels of Na^+ ions relative to wild type plants, suggesting that ion homoeostasis pathways are not disrupted in the absence of *GSNOR1* function.

S-nitrosylation is known to regulate biosynthetic pathways and signalling of several plant hormones including salicylic acid (SA) and possibly auxin (Feechan et al., 2005; Shi et al., 2015; Malik et al., 2011). Further, *gsnor1-3* plants showed impaired abscisic acid (ABA) induced stomatal closure (Wang et al., 2015). In this context, ABA is known to be involved in salt and water stress signalling (Zhu, 2002). Therefore, we investigated whether abscisic acid (ABA) biosynthesis is regulated by S-nitrosylation. Interestingly, we have found that *gsnor1-3* plants have increased ABA levels upon salt stress indicating ABA biosynthetic pathways are not impaired in *gsnor1-3* plants. In addition, we studied whether the ABA signalling pathway can be regulated by S-nitrosylation. We checked the transcripts levels of salt and osmotic stress related marker genes including ABA-dependent and ABA-independent signalling

pathways. Interestingly, none of the genes was found to be directly affected by S-nitrosylation at least at the level of transcription. This data demonstrates that ABA signalling pathways are not compromised in the absence of *GSNOR1* in *Arabidopsis.* Collectively, our data imply that classical salt stress signalling pathways are functional in *gsnor1-3* plants.

8.3 Autophagy is impaired in *gsnor1-3* plants

Autophagy is a conserved catabolic process which was shown to be involved mostly with starvation and nutritional stress. Nevertheless, autophagy also regulates plant abiotic stresses including salt, drought and oxidative stress (Liu et al., 2009; Zhou et al., 2013; Kirkin et al., 2009). Thereby, we studied autophagy in response to salt stress in *gsnor1-3* plants. We have found that during salt stress autophagy is induced in wild type plants as seen by an increase in autophagosomes, while in *gsnor1-3* plants, there was no increase. Application of concanamycin A, a vacuolar ATPase inhibitor, showed that reduced autophagosome formation is not due to a high turnover rate. Our data suggests the impairment in autophagy in *gsnor1-3* plants is upstream of autophagosome formation as even in the presence of concanamycin A the autophagic bodies are substantially less in quantity compared to wild type plants.

Autophagy deficient mutants are known to accumulate higher levels of basal NBR1 (Next to BRCA1), a selective autophagy marker, compared to wild type plants (Svenning et al., 2011). We have found that *gsnor1-3* plants contain higher basal levels of NBR1 compared to wild type which further increases in the presence of NaCl. Interestingly, the basal NBR1 levels are restored with the withdrawal of stress. Therefore, cytoplasmic accumulation of the NBR1 also supports the impairment in autophagy in *gsnor1-3* plants during salt stress.

Autophagy degrades unwanted and damaged cellular materials to recycle cellular nutrients during normal and stressed conditions. Autophagy was also shown to degrade

ubiquitinylated proteins during stress (Zhou et al., 2013; Kirkin et al., 2009). We propose that in a high S-nitrosylation background autophagy is impaired during salt stress leading to accumulation of damaged and oxidised proteins. A failure in the clearance and recycling of nutrients results in stress susceptibility. Thus, work presented in this thesis has provided new insight into autophagy regulation during salt stress.

8.4 ATG7 is regulated by S-nitrosylation

Data presented in **chapter 5** suggests that S-nitrosylation regulates a function(s) upstream of autophagosome formation. Remarkably, many proteins involved in autophagy contain regulatory and/or catalytic cysteine residues. Thus, it is possible that S-nitrosylation regulates multiple points of autophagy signalling. A deeper investigation searching for possible targets of S-nitrosylation within autophagy components pointed to ATG7 as a potential candidate. ATG7 plays a central role in autophagosome formation by regulating two ubiquitin-like conjugation pathways. An absence of ATG7 activity will lead to impaired autophagosome formation. Biotin switch assays revealed that both the N-terminal and C-terminal domain of ATG7 are S-nitrosylated *in vitro.* We further investigated the effects of this modification on ATG7 function. The activity of ATG7 was found to be inhibited in the presence of NO donors in a concentration-dependent fashion. In addition, reversal of this modification was shown to restore the function of ATG7. TRX/NTRA is an important cellular denitrosylation/transnitrosylation mechanism. To determine if TRXh5/NTRA can regulate ATG7, we performed a modified biotin switch assay. Interestingly, ATG7 was found to be transnitrosylated by TRXh5/NTRA. Further, the TRXh5 C42S/NTRA couple was unable to denitrosylate ATG7 at least *in vitro*. Interestingly, $ATG7^{CTD}$ activity was abolished in the presence of TRXh5/NTRA even in the absence of NO donors which suggests that the thioester bond between $ATG7^{CTD}$ and $ATG8^{G132}$ is reduced by the TRX. $ATG7^{CTD}$ forms a stable complex

with ATG8^{G132} in the presence of TRXh5 C42S/NTRA which lacks disulphide reductase activity but this is abolished in the presence of an NO donor. From this evidence, we hypothesised that TRX/NTRA negatively regulates ATG7 function at least *in vitro* and similar mechanisms might also exist *in planta.* A deeper investigation using TRX/TRX reductase system associated mutants will provide more insight on the regulation of ATG7.

Finally, ATG7 was found to be S-nitrosylated *in vivo* which is regulated by salt stress. Interestingly, ATG7 was found to be S-nitrosylated in both wild type and *gsnor1-3* plants in non-stressed conditions, whereas, the level of this modification increased in *gsnor1-3* plants upon salt stress. One potential question arises, how S-nitrosylation regulates ATG7 in wild type plants with a low S-nitrosylation background. We hypothesised that being a core component of autophagy pathway, ATG7 remains under strong regulatory control and S-nitrosylation could be necessary to keep the protein less active and avoid over-responsiveness during control conditions. On the contrary, ATG7 is highly S-nitrosylated in a high S-nitroslation background suggesting, ATG7 S-nitrosylation occurs at a point above to a critical NO and SNO levels. As autophagy is an energy-consuming cellular degradation process, this pathway needs to be under robust regulatory control to avoid excessive cellular material degradation under normal conditions. It is possible that the TRX/TRX reductase system negatively control autophagy to achieve this. We have demonstrated that S-nitrosylation negatively regulates ATG7 function and in the absence of GSNOR1 function autophagy is impaired which leads us to speculate *GSNOR1* is a positive regulator of autophagy. Further, GSNOR1 may indirectly regulate autophagy positively by maintaining cellular redox balance. On the other hand, during stress conditions, autophagy is induced to degrade damaged cellular materials. However, during prolonged stress, an accumulation of NO and S-nitrosothiols (SNOs) can affect autophagy negatively. We hypothesised that prolonged stress can lead to a build-up of NO above a critical point leading to S-nitrosylation

of ATG7 resulting in impaired autophagy, therefore, causing salt sensitivity over time. Monitoring NO and SNO accumulation over time during stress and correlating ATG7 S-nitrosylation and function will provide us a deeper insight of this regulation. It would also be interesting to investigate whether cellular antioxidant molecules such as ascorbate and glutathione (GSH) can regulate ATG7 denitrosylation *in planta.* Collectively, we have demonstrated that GSNOR1 is a positive regulator of autophagy while the accumulation of endogenous NO during stress over time leading to ATG7 S-nitrosylation may function as one of the negative feedback mechanisms to regulate autophagy.

Next, we investigated the target of S-nitrosylation using mass-spectrometry, mutational and computational prediction analysis. Mass-spectrometry and mutational analysis narrowed down our target cysteine (Cys) residues for S-nitrosylation to the C-terminal domain residues of ATG7: C558 and C637. C558 is the catalytic Cys residue that activates the enzyme substrates before transferring to a conjugation enzyme. Thereby, a modification of this Cys is likely to affect the enzyme function. On the other hand, C637 is part of a Cys tetrad motif which co-ordinates a Zn^{2+} providing structural stability to the crossover loop in the adenylation domain of ATG7. Oxidation of C637 by S-nitrosylation is likely to change the Cys tetrad environment making it unable to bind the Zn^{2+}, thereby reducing the structural stability. Collectively, we hypothesised that S-nitrosylation of C558 and/or C637 inhibits ATG7 enzyme function, consequently, inhibiting autophagy during salt stress.

Though we showed that ATG7 is regulated by S-nitrosylation leading to impaired autophagy, other possible mechanisms of autophagy regulation by NO cannot be ruled out. Autophagy is regulated by ROS, specifically hydrogen peroxide (H_2O_2), though it is still not clear if ROS work as an inducer of inhibitor. Starvation-induced ROS is essential for the

induction of autophagy by regulating ATG4, an important cysteine protease required for delipidation of ATG8 (Scherz-Shouval et al., 2007). On the contrary, NADPH oxidase-dependent ROS production was also shown to result in the activation of the autophagy repressor, mammalian target of rapamycin (mTOR) (Pal, 2014). Interestingly, autophagy is known to be regulated differentially under salt and osmotic stresses. Autophagy is most likely regulated by NADPH oxidase-dependent and independent pathway in salt and osmotic stress respectively (Liu et al., 2009). Yun et al. (2011) showed that S-nitrosylation of RBOHD inhibits its function reducing ROS production in pathogen challenged condition (Yun et al., 2011). It would be interesting to see if this regulation is also involved during salt stress in *gsnor1-3* plants.

Another important node of regulation in autophagy is SnRK1/SNF1/AMPK. SnRK1/SNF1/AMPK activation leads to the induction of autophagy. Interestingly, H_2O_2 exposure leads to the oxidation of C299 and C304 of AMPK resulting in increased kinase activity while mutation of these two cysteines prevents H_2O_2-mediated AMPK activation (Zmijewski et al., 2010). Though, direct evidence of AMPK regulation by S-nitrosylation is still not found in animal systems, recently, another member of SnRK family protein, SnRK2.6, involved in the ABA signalling pathway, was shown to be S-nitrosylated *in vitro* and *in vivo* resulting in the inactivation of its catalytic activity (Wang et al., 2015). Therefore, investigating if such regulation exists in SnRK1/SNF1/AMPK function may provide further insights into the control of autophagy.

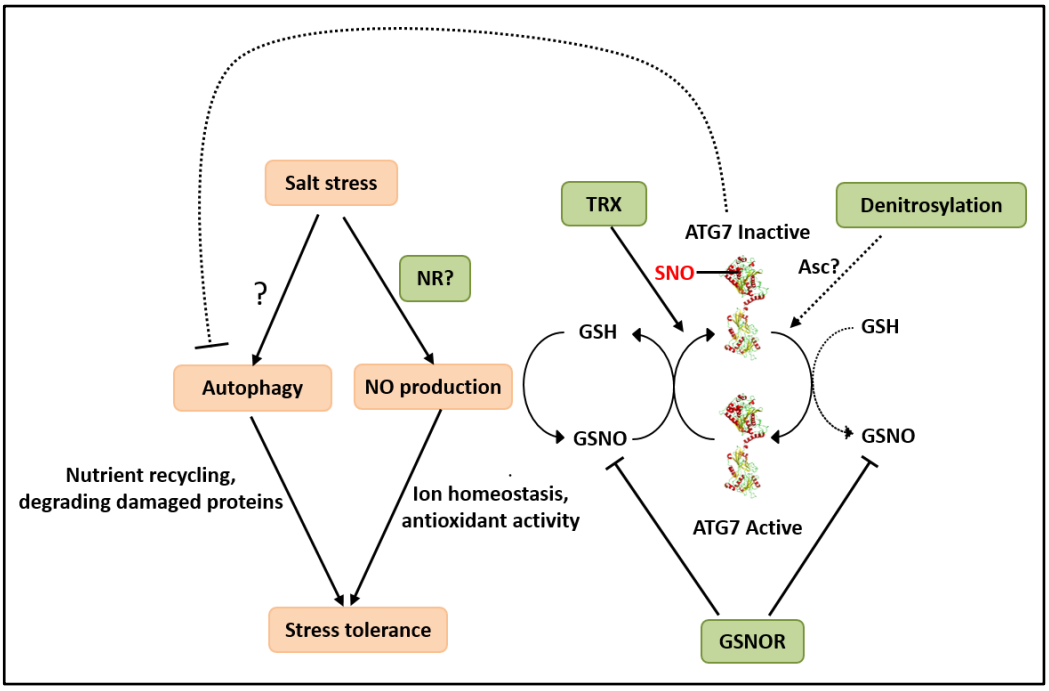

Figure 8-1. A schematic model for redox regulation of ATG7 in *Arabidopsis* salt stress.

Autophagy is involved in plant salt stress tolerance by nutrient recycling. Nitric oxide (NO) production, possibly by nitrate reductase (NR), also provides salt stress tolerance by maintaining ion homoeostasis and antioxidant activity. Glutathione (GSH) forms S-nitrosoglutathione (GSNO) through the attachment of NO. GSNO acts as a stable store for NO and contributes to NO bioactivity. GSNO levels are negatively regulated by S-nitrosoglutathione reductase (GSNOR). GSNO S-nitrosylates ATG7 resulting in an inhibition of enzyme function subsequently inhibiting autophagy. Endogenously produced NO may function as a negative feedback mechanism for autophagy. GSNOR function as a positive regulator of autophagy and salt tolerance while thioredoxin (TRX) transnitrosylates ATG7 implying negative regulation of autophagy. Asc, ascorbate.

Collectively, we hypothesise a possible mechanism of salt stress regulation based on our data presented in this thesis. **Figure 8-1** schematically shows that salt stress can induce NO production and autophagy though the mode of induction is still not yet clear. Autophagy conveys stress tolerance probably by nutrient recycling and degrading damaged and/or oxidised proteins. On the other hand, NO provides stress tolerance by maintaining ion homoeostasis and antioxidant activity. GSNOR negatively regulates GSNO levels hence

indirectly regulating global S-nitrosothiols. ATG7 can be S-nitrosylated by NO, GSNO or TRX resulting in an inhibition of its function. Consequently, inhibition of ATG7 by S-nitrosylation leads to impaired autophagy. In wild type plants, autophagy is active during salt stress because both GSNOR and TRX can function synergistically. It is possible that in wild type plants, ATG7 is transiently regulated by S-nitrosylation which is important to keep the protein inactive and avoid over-responsiveness. Further, accumulation of endogenous NO above a critical level over time during prolonged stress leads to excessive S-nitrosylation of ATG7 impairing autophagy. Hence, GSNOR1 indirectly functions as a positive regulator for autophagy and salt tolerance whereas TRX/TRX reductase system regulates negatively. S-nitrosylation of ATG7 regulates autophagy in a negative feedback mechanism.

8.5 Conclusion, impact and future work

In **Chapter 1.13**, we hypothesised that dysregulation in NO/SNO pathway may alter salt tolerance. We found our results in **Chapter 3** to agree with our hypothesis as *gsnor1-3* plants showed NaCl sensitivity and *nox1* plants showed NaCl sensitivity in some stages of life cycle. Our second hypothesis was that post-translational modification may occur in the proteins involved in salt stress signalling pathways. Interestingly, the classical salt stress signalling pathways seem to be unaltered in *gsnor1-3* plants. However, our results from **Chapter 5** to **Chapter 7** showed that autophagy is involved during salt stress and this pathway is inhibited in *gsnor1-3* plants. Further, an important protein in autophagy pathway is S-nitrosylated leading to the inhibition of autophagy in *gsnor1-3* plants which also supports our second hypothesis.

As outlined above, work presented in this thesis has uncovered several novel mechanisms which involve autophagy and S-nitrosylation. The findings are summarised below:

1) *Arabidopsis GSNOR1* positively regulates salt tolerance.
2) Classical salt tolerance mechanisms are functioning in the absence of *GSNOR1.*
3) Autophagy is positively regulated by *GSNOR1* through the control of the cellular SNO levels.
4) S-nitrosylation of ATG7 causes functional inhibition leading to impaired autophagy.
5) The TRX/TRX reductase system negatively regulates ATG7 function *in vitro.*
6) Endogenous NO accumulation may function as a negative feedback mechanism to regulate autophagy.

Future work will involve identification and confirmation of the target cysteine residues for S-nitrosylation and the mode of the ATG7 inhibition and to test whether substituting those residues can alleviate the effect of S-nitrosylation *in planta*. It will also be interesting to see how the TRX/TRX reductase system regulates autophagy *in planta* during salt stress. The role of cellular antioxidant compounds, for example, ascorbate and glutathione in the regulation of ATG7 function can be explored. Salinity tolerance is a complex trait which involves a plethora of response mechanisms, however, a detailed understanding of autophagy regulation may provide novel insights to help guide the design and/or breeding of salt tolerant crops. Further, *GSNOR1* is a master regulator of S-nitrosylation and was found to be a positive regulator for both biotic and abiotic stress tolerance. Our work further confirms the role of *GSNOR1* in salt tolerance. *GSNOR1* thus can be a good target for genetic modification in the development of salt tolerant plant variety.

Our work has shed significant light on the regulation of salt tolerance by S-nitrosylation. However, there are certain issues need to be addressed in future researches. Salt tolerance is a complex trait and salinity stress affects many aspects of plant physiology making it difficult to study without appropriate experimental systems. A recent review on how to evaluate

physiological responses of plants to salinity stress discussed guidelines for the selection of appropriate experimental systems, the imposition of salinity stress and obtaining and analysing relevant physiological data using appropriate indices (Negrão et al., 2016). This guideline will be an appropriate starting point for future researches on salinity tolerance. However, if we were to start this study from the beginning, some future recommendation involves the use of multiple mutant alleles for a single gene and use of a complementation line if available for the phenotypic studies to confirm the effects of the gene mutation. Use of a suitable growth media is also very important. From the experiences, we have from our study, we believe the use of both agar plate and soil-filled pot systems should be used to test the phenotypic response to stress. Further, appropriate concentrations for stress components should be considered depending on plant species and a good choice of the appropriate growth measurement is also required, for example, the relative decrease in plant biomass is an important index for growth measurement. Lastly, we would also use mannitol in all the experiments along with NaCl to test the osmotic stress effect on *gsnor1-3* plants which was done only in **Chapter 3.5.**

Our work may also be relevant for plant immunity. Whether autophagy functions as a pro-death or pro-survival mechanism in plant immunity is still under a considerable debate. Nevertheless, autophagy is believed to be a regulator of hypersensitive cell death (HR) (Coll et al., 2014; Liu et al., 2015; Hofius et al., 2009; Patel and Dinesh-Kumar, 2008). Therefore, it would be interesting to explore if autophagy is regulated by S-nitrosylation during plant immunity.

This study might also impact biomedicine. For example, points (3) and (4) may provide clues as to how the activities of ATG7 and other ubiquitin or ubiquitin-like activating enzymes and associated PTMs are regulated in mammals. Since autophagy, ubiquitination and

SUMOylation have been implicated in many human diseases including, cancer, Alzheimer's and Parkinson's. Designing drugs that interfere with or exploit regulatory mechanisms uncovered in this thesis might provide novel therapeutic strategies.

Bibliography

Abat, J.K. and Deswal, R. (2009). Differential modulation of S-nitrosoproteome of *Brassica juncea* by low temperature: Change in S-nitrosylation of Rubisco is responsible for the inactivation of its carboxylase activity. Proteomics **9**: 4368–4380.

Abogadallah, G.M. (2010). Antioxidative defense under salt stress. Plant Signal. Behav. **5**: 369–374.

Affenzeller, M.J., Darehshouri, A., Andosch, A., Lütz, C., and Lütz-Meindl, U. (2009). Salt stress-induced cell death in the unicellular green alga *Micrasterias denticulata*. J. Exp. Bot. **60**: 939–54.

Ahmad, P., Abdel Latef, A.A., Hashem, A., Abd_Allah, E.F., Gucel, S., and Tran, L.-S.P. (2016). Nitric oxide mitigates salt stress by regulating levels of osmolytes and antioxidant enzymes in chickpea. Front. Plant Sci. **7**: 1–11.

Airaki, M., Leterrier, M., Mateos, R.M., Valderrama, R., Chaki, M., Barroso, J.B., del Río, L. a., Palma, J.M., and Corpas, F.J. (2012). Metabolism of reactive oxygen species and reactive nitrogen species in pepper (*Capsicum annuum* L.) plants under low temperature stress. Plant, Cell Environ. **35**: 281–295.

Al-Shehbaz, I.A. and O'Kane, S.L. (2002). Taxonomy and phylogeny of Arabidopsis (Brassicaceae).

Anand, P., Hausladen, A., Wang, Y.-J., Zhang, G.-F., Stomberski, C., Brunengraber, H., Hess, D.T., and Stamler, J.S. (2014). Identification of S-nitroso-CoA reductases that regulate protein S-nitrosylation. Proc. Natl. Acad. Sci. U. S. A. **111**: 18572–18577.

Apse, M.P., Aharon, G.S., Snedden, W. a, and Blumwald, E. (1999). Salt tolerance conferred by overexpression of a vacuolar Na+/H+ antiport in *Arabidopsis*. Science **285**: 1256–1258.

Apse, M.P. and Blumwald, E. (2002). Engineering salt tolerance in plants. Curr. Opin. Biotechnol. **13**: 146–150.

Arasimowicz, M. and Floryszak-Wieczorek, J. (2007). Nitric oxide as a bioactive signalling molecule in plant stress responses. Plant Sci. **172**: 876–887.

Athar, H. and Ashraf, M. (2009). Strategies for Crop Improvement Against Salinity and Drought Stress: An Overview. In Salinity and water stress;Improving crop efficiency, M. Ashraf, M. Ozturk, and H.R. Athar, eds, pp. 1–17.

Barroso, J.B., Corpas, F.J., Carreras, A., Sandalio, L.M., Valderrama, R., Palma, J.M., Lupiáñez, J.A., and del Río, L.A. (1999). Localization of nitric-oxide synthase in plant peroxisomes. J. Biol. Chem. **274**: 36729–36733.

Bartels, D. and Sunkar, R. (2005). Drought and Salt Tolerance in Plants. CRC. Crit. Rev. Plant Sci. **24**: 23–58.

Bechtold, N. and Pelletier, G. (1998). *In planta Agrobacterium*-mediated transformation of adult *Arabidopsis thaliana* plants by vacuum infiltration. Methods Mol. Biol. **82**: 259–66.

Begara-Morales, J.C., Sánchez-Calvo, Beatriz, Chaki, M., Valderrama, R., Mata-Pérez, C., López-Jaramillo, J., Padilla, M.N., Carreras, A., Corpas, F.J., and Barroso, J.B. (2014). Dual regulation of cytosolic ascorbate peroxidase (APX) by tyrosine nitration and S-nitrosylation. J. Exp. Bot. **65**: 527–538.

Begara-Morales, J.C., Sánchez-Calvo, B., Chaki, M., Mata-Pérez, C., Valderrama, R., Padilla, M.N., López-Jaramillo, J., Luque, F., Corpas, F.J., and Barroso, J.B. (2015). Differential molecular response of monodehydroascorbate reductase and glutathione reductase by nitration and S-nitrosylation. J. Exp. Bot. **66**: 5983–5996.

Benhar, M., Forrester, M.T., Hess, D.T., and Stamler, J.S. (2008). Regulated protein denitrosylation by cytosolic and mitochondrial thioredoxins. Science (80-.). **320**: 1050–1054.

Berthomieu, P. et al. (2003). Functional analysis of *AtHKT1* in *Arabidopsis* shows that Na+ recirculation by the phloem is crucial for salt tolerance. EMBO J. **22**: 2004–2014.

Bohnert, H.J. and Jensen, R.G. (1996). Strategies for engineering water-stress tolerance in plants. Trends Biotechnol. **14**: 89–97.

Boyer, J.S. (1982). Plant productivity and environment. Science **218**: 443–448.

Bright, J., Desikan, R., Hancock, J.T., Weir, I.S., and Neill, S.J. (2006). ABA-induced NO generation and stomatal closure in *Arabidopsis* are dependent on H2O2 synthesis. Plant J. **45**: 113–122.

Camejo, D., Romero-Puertas, M.D.C., Rodríguez-Serrano, M., Sandalio, L.M., Lázaro, J.J., Jiménez, A., and Sevilla, F. (2013). Salinity-induced changes in S-nitrosylation of pea mitochondrial proteins. J. Proteomics **79**: 87–99.

Chaki, M., Kovacs, I., Spannagl, M., and Lindermayr, C. (2014). Computational prediction of candidate proteins for S-nitrosylation in *Arabidopsis thaliana*. PLoS One **9**: 1–12.

Chaki, M., Valderrama, R., Fernández-Ocaña, A.M., Carreras, A., Gómez-Rodríguez, M. V., López-Jaramillo, J., Begara-Morales, J.C., Sánchez-Calvo, B., Luque, F., Leterrier, M., Corpas, F.J., and Barroso, J.B. (2011). High temperature triggers the metabolism of S-nitrosothiols in sunflower mediating a process of nitrosative stress which provokes the inhibition of ferredoxin-NADP reductase by tyrosine nitration. Plant, Cell Environ. **34**: 1803–1818.

Chen, R., Sun, S., Wang, C., Li, Y., Liang, Y., An, F., Li, C., Dong, H., Yang, X., Zhang, J., and Zuo, J. (2009a). The *Arabidopsis PARAQUAT RESISTANT2* gene encodes an S-nitrosoglutathione reductase that is a key regulator of cell death. Cell Res. **19**: 1377–1387.

Chen, Y., Azad, M.B., and Gibson, S.B. (2009b). Superoxide is the major reactive oxygen species regulating autophagy. Cell Death Differ. **16**: 1040–1052.

Clough, S.J. and Bent, A.F. (1998). Floral dip: a simplified method for Agrobacterium-mediated transformation of *Arabidopsis thaliana*. Plant J. **16**: 735–743.

Coll, N.S., Smidler, A., Puigvert, M., Popa, C., Valls, M., and Dangl, J.L. (2014). The plant metacaspase *AtMC1* in pathogen-triggered programmed cell death and aging: functional linkage with autophagy. Cell Death Differ. **21**: 1–10.

Conklin, P.L., Saracco, S.A., Norris, S.R., and Last, R.L. (2000). Identification of Ascorbic Acid-Deficient *Arabidopsis thaliana* Mutants. Genetics **154**: 847–856.

Conklin, P.L., Willlams, E.H., and Last, R.L. (1996). Environmental stress sensitivity of an ascorbic acid-deficient *Arabidopsis* mutant. Proc. Natl. Acad. Sci. **93**: 9970–9974.

Conn, S.J., Hocking, B., Dayod, M., Xu, B., Athman, A., Henderson, S., Aukett, L., Conn, V., Shearer, M.K., Fuentes, S., Tyerman, S.D., and Gilliham, M. (2013). Protocol : optimising hydroponic growth systems for nutritional and physiological analysis of Arabidopsis thaliana and other plants. Methodology **9**: 1–11.

Contento, A.L., Xiong, Y., and Bassham, D.C. (2005). Visualization of autophagy in *Arabidopsis* using the fluorescent dye monodansylcadaverine and a GFP-AtATG8e fusion protein. Plant J. **42**: 598–608.

Conti, L., Kioumourtzoglou, D., O'Donnell, E., Dominy, P., and Sadanandom, A. (2009). OTS1 and OTS2 SUMO proteases link plant development and survival under salt stress. Plant Signal. Behav. **4**: 225–227.

Cooper, C.E. (1999). Nitric oxide and iron proteins. Biochim. Biophys. Acta - Bioenerg. **1411**: 290–309.

Corpas, F. et al. (2004). Cellular and subcellular localization of endogenous nitric oxide in young and senescent pea plants. Plant Physiol **136**: 2722–2733.

Corpas, F.J., Chaki, M., Fernández-Ocaña, A., Valderrama, R., Palma, J.M., Carreras, A., Begara-Morales, J.C., Airaki, M., del Río, L.A., and Barroso, J.B. (2008). Metabolism of reactive nitrogen species in pea plants under abiotic stress conditions. Plant Cell Physiol. **49**: 1711–1722.

Corpas, F.J., Leterrier, M., Valderrama, R., Airaki, M., Chaki, M., Palma, J.M., and Barroso, J.B. (2011). Nitric oxide imbalance provokes a nitrosative response in plants under abiotic stress. Plant Sci. **181**: 604–611.

Crawford, N.M. (1995). Nitrate: nutrient and signal for plant growth. Plant Cell **7**: 859–868.

Cueto, M., Hernández-Perera, O., Martín, R., Bentura, M.L., Rodrigo, J., Lamas, S., and Golvano, M.P. (1996). Presence of nitric oxide synthase activity in roots and nodules of *Lupinus albus*. FEBS Lett. **398**: 159–164.

Cutler, S.R., Rodriguez, P.L., Finkelstein, R.R., and Abrams, S.R. (2010). Abscisic acid: emergence of a core signaling network.

Davenport, R.J., Muñoz-Mayor, A., Jha, D., Essah, P.A., Rus, A., and Tester, M. (2007). The Na+ transporter AtHKT1;1 controls retrieval of Na+ from the xylem in *Arabidopsis*. Plant, Cell Environ. **30**: 497–507.

Dean, J. V. and Harper, J.E. (1988). The conversion of nitrite to nitrogen oxide(s) by the constitutive NAD(P)H-nitrate reductase enzyme from soybean. Plant Physiol. **88**: 389–395.

Deinlein, U., Stephan, A.B., Horie, T., Luo, W., Xu, G., and Schroeder, J.I. (2014). Plant salt-tolerance mechanisms. Trends Plant Sci. **19**: 371–379.

Delledonne, M., Xia, Y., Dixon, R.A., and Lamb, C. (1998). Nitric oxide functions as a signal in plant disease resistance. Nature **394**: 585–588.

Delledonne, M., Zeier, J., Marocco, a, and Lamb, C. (2001). Signal interactions between nitric oxide and reactive oxygen intermediates in the plant hypersensitive disease resistance response. Proc. Natl. Acad. Sci. U. S. A. **98**: 13454–13459.

Derakhshan, B., Hao, G., and Gross, S.S. (2007). Balancing reactivity against selectivity : The evolution of protein S -nitrosylation as an effector of cell signaling by nitric oxide. Cardiovasc. Res. **75**: 210–219.

Derelle, E. et al. (2006). Genome analysis of the smallest free-living eukaryote *Ostreococcus tauri* unveils many unique features. Proc. Natl. Acad. Sci. U. S. A. **103**: 11647–11652.

Doelling, J.H., Walker, J.M., Friedman, E.M., Thompson, A.R., and Vierstra, R.D. (2002). The APG8/12-activating enzyme APG7 is required for proper nutrient recycling and senescence in *Arabidopsis thaliana*. J. Biol. Chem. **277**: 33105–33114.

Dubos, C., Stracke, R., Grotewold, E., Weisshaar, B., Martin, C., and Lepiniec, L. (2010). MYB transcription factors in *Arabidopsis*. Trends Plant Sci. **15**: 573–581.

Fan, H.F., Du, C.X., Ding, L., and Xu, Y.L. (2013). Effects of nitric oxide on the germination of cucumber seeds and antioxidant enzymes under salinity stress. Acta Physiol. Plant. **35**: 2707–2719.

Fancy, N.N., Bahlmann, A.-K., and Loake, G.J. (2016). Nitric oxide function in plant abiotic stress. Plant. Cell Environ.: 1–11.

Fares, A., Rossignol, M., and Peltier, J.B. (2011). Proteomics investigation of endogenous S-nitrosylation in *Arabidopsis*. Biochem. Biophys. Res. Commun. **416**: 331–336.

Fatma, M., Masood, A., Per, T.S., and Khan, N.A. (2016). Nitric oxide alleviates salt stress inhibited photosynthetic performance by interacting with sulfur assimilation in mustard. Front. Plant Sci. **7**: 1–16.

Feechan, a, Kwon, E., Yuri, B., Wang, Y., Pallas, J., and Loake, G. (2005). A central role for S-nitrosothiols in plant disease resistance. **102**: 8054–8059.

Foresi, N., Correa-Aragunde, N., Parisi, G., Caló, G., Salerno, G., and Lamattina, L. (2010). Characterization of a nitric oxide synthase from the plant kingdom: NO generation from the green alga *Ostreococcus tauri* is light irradiance and growth phase dependent. Plant Cell **22**: 3816–3830.

Foster, M.W., Hess, D.T., and Stamler, J.S. (2009). Protein S-nitrosylation in health and disease: a current perspective. J. Mol. Med. **15**: 391–404.

Frungillo, L., Skelly, M.J., Loake, G.J., Spoel, S.H., and Salgado, I. (2014). S-nitrosothiols regulate nitric oxide production and storage in plants through the nitrogen assimilation pathway. Nat. Commun. **5**: 5401–5420.

Fu, J., Chu, J., Sun, X., Wang, J., and Yan, C. (2012). Simple, rapid, and simultaneous assay of multiple carboxyl containing phytohormones in wounded tomatoes by UPLC-MS/MS using single SPE purification and isotope dilution. Anal. Sci. **28**: 1081–1087.

Gibeaut, D.M., Hulett, J., Cramer, G.R., and Seemann, J.R. (1997). Maximal biomass of *Arabidopsis thaliana* using a simple, low-maintenance hydroponic method and favorable environmental conditions. Plant Physiol. **115**: 317–319.

Glazebrook, J. and Ausubel, F.M. (1994). Isolation of phytoalexin-deficient mutants of *Arabidopsis thaliana* and characterization of their interactions with bacterial pathogens. Proc. Natl. Acad. Sci. **91**: 8955–8959.

Gong, B., Wen, D., Wang, X., Wei, M., Yang, F., Li, Y., and Shi, Q. (2015). S-nitrosoglutathione reductase modulated redox signaling controls sodic alkaline stress responses in *Solanum lycopersicum* L. Plant Cell Physiol. **1**: 790–802.

Gorren, A.C.F., Schrammel, A., Schmidt, K., and Mayer, B. (1996). Decomposition of S - nitrosoglutathione in the presence of copper ions and glutathione. Arch. Biochem. Biophys. **330**: 219–228.

Gould, K.S., Lamotte, O., Klinguer, a., Pugin, a., and Wendehenne, D. (2003). Nitric oxide production in tobacco leaf cells: A generalized stress response? Plant, Cell Environ. **26**: 1851–1862.

Gu, Z., Nakamura, T., and Lipton, S.A. (2010). Redox reactions induced by nitrosative stress mediate protein misfolding and mitochondrial dysfunction in neurodegenerative diseases. Mol. Neurobiol. **41**: 55–72.

Guillaumot, D., Guillon, S., Déplanque, T., Vanhee, C., Gumy, C., Masquelier, D., Morsomme, P., and Batoko, H. (2009). The *Arabidopsis* TSPO-related protein is a stress and abscisic acid-regulated, endoplasmic reticulum-golgi-localized membrane protein. Plant J. **60**: 242–256.

Guo, F.-Q., Okamoto, M., and Crawford, N.M. (2003). Identification of a plant nitric oxide synthase gene involved in hormonal signaling. Science **302**: 100–103.

Gupta, K.J., Fernie, A.R., Kaiser, W.M., and van Dongen, J.T. (2011). On the origins of nitric oxide. Trends Plant Sci. **16**: 160–168.

Hackenberg, T. et al. (2013). Catalase and *NO CATALASE ACTIVITY1* promote autophagy-dependent cell death in *Arabidopsis*. Plant Cell **25**: 4616–4626.

Halfter, U., Ishitani, M., and Zhu, J.K. (2000). The *Arabidopsis* SOS2 protein kinase physically interacts with and is activated by the calcium-binding protein SOS3. Proc. Natl. Acad. Sci. U. S. A. **97**: 3735–3740.

Hara, M.R. et al. (2005). S-nitrosylated GAPDH initiates apoptotic cell death by nuclear translocation following Siah1 binding. Nat. Cell Biol. **7**: 665–674.

He, Y., Tang, R., Yi Hao, R.D.S., and Charles W. Cook, Sun M. Ahn, Liufang Jing, Zhongguang Yang, Longen Chen, Fangqing Guo, Fabio Fiorani, Robert B. Jackson, Nigel M. Crawford, Z.-M.P. (2004). Nitric oxide represses the *Arabidopsis* floral transition. Science **305**: 1968–1971.

Hensley, K. and Harris-White, M.E. (2015). Redox regulation of autophagy in healthy brain and neurodegeneration. Neurobiol. Dis. **84**: 50–59.

Herder, G. Den, Keyser, A. De, Rycke, R. De, Rombauts, S., Velde, W. Van de, Clemente, M.R., Verplancke, C., Mergaert, P., Kondorosi, E., Holsters, M., and Goormachtig, S. (2008). Seven in absentia proteins affect plant growth and nodulation in *Medicago truncatula*. Plant Physiol. **148**: 369–382.

Hofius, D., Schultz-Larsen, T., Joensen, J., Tsitsigiannis, D.I., Petersen, N.H.T., Mattsson, O., Jørgensen, L.B., Jones, J.D.G., Mundy, J., and Petersen, M. (2009). Autophagic components contribute to hypersensitive cell death in *Arabidopsis*. Cell **137**: 773–783.

Hong, J.K., Yun, B.W., Kang, J.G., Raja, M.U., Kwon, E., Sorhagen, K., Chu, C., Wang, Y., and Loake, G.J. (2008). Nitric oxide function and signalling in plant disease resistance. J. Exp. Bot. **59**: 147–154.

Hong, S.-W., Lee, U., and Vierling, E. (2003). *Arabidopsis hot* mutants define multiple functions required for acclimation to high temperatures. Plant Physiol. **132**: 757–767.

Hu, W.J., Chen, J., Liu, T.W., Liu, X., Wu, F.H., Wang, W.H., He, J.X., Xiao, Q., and Zheng, H.L. (2014). Comparative proteomic analysis on wild type and *nitric oxide-overproducing mutant* (*nox1*) of *Arabidopsis thaliana*. Nitric Oxide - Biol. Chem. **36**: 19–30.

Huss, M., Ingenhorst, G., König, S., Gaßel, M., Dröse, S., Zeeck, A., Altendorf, K., and Wieczorek, H. (2002). Concanamycin A, the specific inhibitor of V-ATPases, binds to the Vo subunit c. J. Biol. Chem. **277**: 40544–40548.

Ichimura, Y., Imamura, Y., Emoto, K., Umeda, M., Noda, T., and Ohsumi, Y. (2004). *In vivo* and *in vitro* reconstitution of Atg8 conjugation essential for autophagy. J. Biol. Chem. **279**: 40584–40592.

Jaffrey, S.R., Erdjument-Bromage, H., Ferris, C.D., Tempst, P., and Snyder, S.H. (2001). Protein S-nitrosylation: a physiological signal for neuronal nitric oxide. Nat. Cell Biol. **3**: 193–197.

Jaffrey, S.R. and Snyder, S.H. (2001). The biotin switch method for the detection of S-nitrosylated proteins. Sci. STKE **2001**: pl1.

Jeandroz, S., Wipf, D., Stuehr, D.J., Lamattina, L., Melkonian, M., Tian, Z., Zhu, Y., Carpenter, E.J., Wong, G.K., and Wendehenne, D. (2016). Occurrence , structure , and evolution of nitric oxide synthase – like proteins in the plant kingdom. Sci. Signal. **9**: 1–9.

Jiang, Z., Zhu, S., Ye, R., Xue, Y., Chen, A., An, L., and Pei, Z.M. (2013). Relationship between NaCl- and H2O2-Induced Cytosolic Ca2+ Increases in Response to Stress in *Arabidopsis*. PLoS One **8**: 1–10.

Johansen, T. and Lamark, T. (2011). Selective autophagy mediated by autophagic adapter proteins. Autophagy **7**: 279–296.

Juhász, G., Érdi, B., Sass, M., and Neufeld, T.P. (2007). Atg7-dependent autophagy promotes neuronal health, stress tolerance, and longevity but is dispensable for metamorphosis in *Drosophila*. Genes Dev. **21**: 3061–3066.

Kelley, L.A., Mezulis, S., Yates, C.M., Wass, M.N., and Sternberg, M.J.E. (2015). The Phyre2 web portal for protein modeling, prediction and analysis. Nat. Protoc. **10**: 845–858.

Khan, M. a. and Duke, N.C. (2001). Halophytes - A resource for the future. Wetl. Ecol. Manag. **9**: 455–456.

Kim, J., Kundu, M., Viollet, B., and Guan, K.-L. (2011). AMPK and mTOR regulate autophagy through direct phosphorylation of Ulk1. Nat. Cell Biol. **13**: 132–141.

Kirkin, V. et al. (2009). A role for NBR1 in autophagosomal degradation of ubiquitinated substrates. Mol. Cell **33**: 505–516.

Klomsiri, C., Karplus, P.A., and Poole, L.B. (2011). Cysteine-based redox switches in enzymes. Antioxid. Redox Signal. **14**: 1065–1077.

Kneeshaw, S., Gelineau, S., Tada, Y., Loake, G.J., and Spoel, S.H. (2014). Selective protein denitrosylation activity of *Thioredoxin-h5* modulates plant immunity. Mol. Cell **56**: 153–162.

Knight, H., Trewavas, a J., and Knight, M.R. (1997). Calcium signalling in *Arabidopsis thaliana* responding to drought and salinity. Plant J. **12**: 1067–1078.

Koornneef, M. and Meinke, D. (2010). The development of *Arabidopsis* as a model plant. Plant J. **61**: 909–921.

Kopyra, M. and Gwóźdź, E.A. (2003). Nitric oxide stimulates seed germination and counteracts the inhibitory effect of heavy metals and salinity on root growth of *Lupinus luteus*. Plant Physiol. Biochem. **41**: 1011–1017.

Kreps, J.A., Wu, Y., Chang, H.-S., Zhu, T., Wang, X., and Harper, J.F. (2002). Transcriptome changes for *Arabidopsis* in response to salt, osmotic, and cold stress. Plant Physiol. **130**: 2129–2141.

Lake, M.W., Wuebbens, M.M., Rajagopalan, K. V, and Schindelin, H. (2001). Mechanism of ubiquitin activation revealed by the structure of a bacterial MoeB-MoaD complex. Nature **414**: 325–329.

Lam, M.A., Pattison, D.I., Bottle, S.E., Keddie, D.J., and Davies, M.J. (2008). Nitric oxide and nitroxides can act as efficient scavengers of protein-derived free radicals. chem. res. toxicol **21**: 2111–2119.

Läuchli, A. and Grattan, S. (2007). Plant growth and development under salinity stress. Adv. Mol. Breed. Towar. drought salt Toler.: 1–32.

Lee, I. and Schindelin, H. (2008). Structural insights into E1-catalyzed ubiquitin activation and transfer to conjugating enzymes. Cell **134**: 268–278.

Lee, U., Wie, C., Fernandez, B.O., Feelisch, M., and Vierling, E. (2008). Modulation of nitrosative stress by S-nitrosoglutathione reductase is critical for thermotolerance and plant growth in *Arabidopsis*. Plant Cell **20**: 786–802.

Leterrier, M., Airaki, M., Palma, J.M., Chaki, M., Barroso, J.B., and Corpas, F.J. (2012). Arsenic triggers the nitric oxide (NO) and S-nitrosoglutathione (GSNO) metabolism in *Arabidopsis*. Environ. Pollut. **166**: 136–143.

Leterrier, M., Chaki, M., Airaki, M., Valderrama, R., Palma, J.M., Barroso, J.B., and Corpas, F.J. (2011). Function of S-nitrosoglutathione reductase (GSNOR) in plant development and under biotic/abiotic stress. Plant Signal. Behav. **6**: 789–793.

Levine, B. and Klionsky, D.J. (2004). Development by self-digestion: molecular mechanisms and biological functions of autophagy. Dev. Cell **6**: 463–477.

Li, F. and Vierstra, R.D. (2012). Autophagy: A multifaceted intracellular system for bulk and selective recycling. Trends Plant Sci. **17**: 526–537.

Li, H., Culligan, K., Dixon, R., and Chory, J. (1995). CUE1: A Mesophyll Cell-Specific Positive Regulator of Light-Controlled Gene Expression in Arabidopsis. Plant Cell **7**: 1599–1610.

Li, J., Hu, L., Zhang, L., Pan, X., and Hu, X. (2015). Exogenous spermidine is enhancing tomato tolerance to salinity-alkalinity stress by regulating chloroplast antioxidant system and chlorophyll metabolism. BMC Plant Biol. **15**: 1–17.

Liu, H.B., Wang, X.D., Zhang, Y.Y., Dong, J.J., Ma, C., and Chen, W.L. (2015). NADPH oxidase RBOHD contributes to autophagy and hypersensitive cell death during the plant defense response in *Arabidopsis thaliana*. Biol. Plant. **59**: 570–580.

Liu, J., Ishitani, M., Halfter, U., Kim, C.S., and Zhu, J.K. (2000). The *Arabidopsis thaliana* SOS2 gene encodes a protein kinase that is required for salt tolerance. Proc. Natl. Acad. Sci. U. S. A. **97**: 3730–3734.

Liu, Y. and Bassham, D.C. (2012). Autophagy: Pathways for self-eating in plant cells. Annu. Rev. Plant Biol. **63**: 215–237.

Liu, Y. and Bassham, D.C. (2010). TOR is a negative regulator of autophagy in Arabidopsis thaliana. PLoS One **5**: 1–9.

Liu, Y., Burgos, J.S., Deng, Y., Srivastava, R., Howell, S.H., and Bassham, D.C. (2012). Degradation of the endoplasmic reticulum by autophagy during endoplasmic reticulum stress in *Arabidopsis*. Plant Cell **24**: 4635–4651.

Liu, Y., Schiff, M., Czymmek, K., Tallóczy, Z., Levine, B., and Dinesh-Kumar, S.P. (2005). Autophagy regulates programmed cell death during the plant innate immune response. Cell **121**: 567–577.

Liu, Y., Xiong, Y., and Bassham, D.C. (2009). Autophagy is required for tolerance of drought and salt stress in plants. Autophagy **5**: 954–963.

Lois, L.M. and Lima, C.D. (2005). Structures of the SUMO E1 provide mechanistic insights into SUMO activation and E2 recruitment to E1. EMBO J. **24**: 439–51.

Mahajan, S., Pandey, G.K., and Tuteja, N. (2008). Calcium- and salt-stress signaling in plants: Shedding light on SOS pathway. Arch. Biochem. Biophys. **471**: 146–158.

Malik, S.I., Hussain, A., Yun, B.W., Spoel, S.H., and Loake, G.J. (2011). GSNOR-mediated de-nitrosylation in the plant defence response. Plant Sci. **181**: 540–544.

Mäser, P., Eckelman, B., Vaidyanathan, R., Horie, T., Fairbairn, D.J., Kubo, M., Yamagami, M., Yamaguchi, K., Nishimura, M., and Uozumi, N. (2002). Altered shoot/root Na+ distribution and bifurcating salt sensitivity in *Arabidopsis* by genetic disruption of the Na+ transporter *AtHKT1*. FEBS Lett **531**: 157–161.

Mason, M.G., Jha, D., Salt, D.E., Tester, M., Hill, K., Kieber, J.J., and Eric Schaller, G. (2010). Type-B response regulators ARR1 and ARR12 regulate expression of *AtHKT1;1* and accumulation of sodium in *Arabidopsis* shoots. Plant J. **64**: 753–763.

Mayer, B. and Hemmens, B. (1997). Biosynthesis and action of nitric oxide in mammalian cells. Trends Biochem. Sci. **22**: 477–481.

Merkulova, E.A., Guiboileau, A., Naya, L., Masclaux-Daubresse, C., and Yoshimoto, K. (2014). Assessment and optimization of autophagy monitoring methods in *Arabidopsis* roots indicate direct fusion of autophagosomes with vacuoles. Plant Cell Physiol. **55**: 715–726.

Millar, a H. and Day, D. a (1996). Nitric oxide inhibits the cytochrome oxidase but not the alternative oxidase of plant mitochondria. FEBS Lett. **398**: 155–158.

Mittler, R. (2006). Abiotic stress, the field environment and stress combination. Trends Plant Sci. **11**: 15–19.

Mittler, R. (2002). Oxidative stress, antioxidants and stress tolerance. Trends Plant Sci. **7**: 405–410.

Moreau, M., Lee, G.I., Wang, Y., Crane, B.R., and Klessig, D.F. (2008). AtNOS/AtNOA1 is a functional *Arabidopsis thaliana* cGTPase and not a nitric-oxide synthase. J. Biol. Chem. **283**: 32957–32967.

Moriyasu, Y., Hattori, M., Jauh, G.-Y., and Rogers, J.C. (2003). Alpha tonoplast intrinsic protein is specifically associated with vacuole membrane involved in an autophagic process. Plant Cell Physiol. **44**: 795–802.

Munns, R. (2002). Comparative physiology of salt and water stress. Plant, Cell Environ. **25**: 239–250.

Munns, R., Schachtman, D., and Condon, A. (1995). The significance of a two-phase growth response to salinity in wheat and barley. Aust. J. Plant Physiol. **22**: 561–569.

Munns, R. and Tester, M. (2008). Mechanisms of salinity tolerance. Annu. Rev. Plant Biol. **59**: 651–81.

Mur, L.A.J., Mandon, J., Persijn, S., Cristescu, S.M., Moshkov, I.E., Novikova, G. V, Hall, M.A., Harren, F.J.M., Hebelstrup, K.H., and Gupta, K.J. (2012). Nitric oxide in plants: an assessment of the current state of knowledge. AoB Plants **5**: 1–17.

Nakashima, K., Ito, Y., and Yamaguchi-Shinozaki, K. (2009). Transcriptional regulatory networks in response to abiotic stresses in *Arabidopsis* and grasses. Plant Physiol. **149**: 88–95.

Negrão, S., Schmöckel, S.M., and Tester, M. (2016). Evaluating physiological responses of plants to salinity stress. Ann. Bot.: mcw191.

Neill, S., Barros, R., Bright, J., Desikan, R., Hancock, J., Harrison, J., Morris, P., Ribeiro, D., and Wilson, I. (2008). Nitric oxide, stomatal closure, and abiotic stress. J. Exp. Bot. **59**: 165–176.

Neto, B.N.M., Saturnino, S.M., Bomfim, D.C., and Custódio, C.C. (2004). Water stress induced by mannitol and sodium chloride in soybean cultivars. Brazilian Arch. Biol. Technol. An Int. J. **47**: 521–529.

Noda, N.N., Satoo, K., Fujioka, Y., Kumeta, H., Ogura, K., Nakatogawa, H., Ohsumi, Y., and Inagaki, F. (2011). Structural basis of Atg8 activation by a homodimeric E1, Atg7. Mol. Cell **44**: 462–475.

Ohsumi, Y. (2001). Molecular dissection of autophagy: two ubiquitin-like systems. Nat. Rev. Mol. Cell Biol. **2**: 211–216.

Pace, N.J. and Weerapana, E. (2014). Zinc-binding cysteines: diverse functions and structural motifs. Biomolecules **4**: 419–434.

Pal, R. (2014). NADPH oxidase: the culprit in impaired autophagy and lysosomal biogenesis ? SOJ Biochem. **1**: 1–2.

Parihar, P., Singh, S., Singh, R., Singh, V.P., and Prasad, S.M. (2015). Effect of salinity stress on plants and its tolerance strategies: a review. Environ. Sci. Pollut. Res. **22**: 4056–4075.

Patel, S. and Dinesh-Kumar, S.P. (2008). *Arabidopsis ATG6* is required to limit the pathogen-associated cell death response. Autophagy **4**: 20–27.

Pérez-Pérez, M.E., Zaffagnini, M., Marchand, C.H., Crespo, J.L., and Lemaire, S.D. (2014). The yeast autophagy protease Atg4 is regulated by thioredoxin. Autophagy **10**: 1953–1964.

Pigliucci, M. (2002). Ecology and evolutionary biology of Arabidopsis.

Platten, J.D. et al. (2006). Nomenclature for *HKT* transporters, key determinants of plant salinity tolerance. Trends Plant Sci. **11**: 372–374.

Pu, Y. and Bassham, D.C. (2013). Links between ER stress and autophagy in plants. Plant Signal. Behav. **8**.

Radi, R. (2004). Nitric oxide, oxidants, and protein tyrosine nitration. Proc. Natl. Acad. Sci. U. S. A. **101**: 4003–4008.

Robaglia, C., Thomas, M., and Meyer, C. (2012). Sensing nutrient and energy status by SnRK1 and TOR kinases. Curr. Opin. Plant Biol. **15**: 301–307.

Rockel, P., Strube, F., Rockel, A., Wildt, J., and Kaiser, W.M. (2002). Regulation of nitric oxide (NO) production by plant nitrate reductase *in vivo* and *in vitro*. J. Exp. Bot. **53**: 103–110.

Rodríguez-Navarro, A. and Benito, B. (2010). Sodium or potassium efflux ATPase. A fungal, bryophyte, and protozoal ATPase. Biochim. Biophys. Acta - Biomembr. **1798**: 1841–1853.

Roos, G., Foloppe, N., and Messens, J. (2013). Understanding the pK(a) of redox cysteines: the key role of hydrogen bonding. Antioxid. Redox Signal. **18**: 94–127.

Rose, T.L., Bonneau, L., Der, C., Marty-Mazars, D., and Marty, F. (2006). Starvation-induced expression of autophagy-related genes in *Arabidopsis*. Biol. Cell **98**: 53–67.

Rubbo, H. and Radi, R. (2008). Protein and lipid nitration: Role in redox signaling and injury. Biochim. Biophys. Acta **1780**: 1318–1324.

Rubbo, H., Radi, R., Anselmi, D., Kirk, M., Barnes, S., Butler, J., Eiserich, J.P., and Freeman, B.A. (2000). Nitric oxide reaction with lipid peroxyl radicals spares alpha-Tocopherol during lipid peroxidation. **275**: 10812–10818.

Rümer, S., Gupta, K.J., and Kaiser, W.M. (2009). Plant cells oxidize hydroxylamines to NO. J. Exp. Bot. **60**: 2065–2072.

Rus, A., Yokoi, S., Sharkhuu, A., Reddy, M., Lee, B.H., Matsumoto, T.K., Koiwa, H., Zhu, J.K., Bressan, R. a, and Hasegawa, P.M. (2001). AtHKT1 is a salt tolerance determinant that controls Na(+) entry into plant roots. Proc. Natl. Acad. Sci. U. S. A. **98**: 14150–14155.

Sarkar, S. et al. (2011). Complex inhibitory effects of nitric oxide on autophagy. Mol. Cell **43**: 19–32.

Scherz-Shouval, R. et al. (2007). Reactive oxygen species are essential for autophagy and specifically regulate the activity of Atg4. EMBO J. **26**: 1749–1760.

Schlaeppi, K., Bodenhausen, N., Buchala, A., Mauch, F., and Reymond, P. (2008). The glutathione-deficient mutant pad2-1 accumulates lower amounts of glucosinolates and is more susceptible to the insect herbivore Spodoptera littoralis. Plant J. **55**: 774–786.

Seki, M. et al. (2002). Monitoring the expression profiles of 7000 Arabidopsis genes under drought, cold and high-salinity stresses using a full-length cDNA microarray. Plant J. **31**: 279–292.

Shaw, A.W. and Vosper, A.J. (1977). Solubility of nitric oxide in aqueous and nonaqueous solvents. J. Chem. Soc. Faraday Trans. 1 **73**: 1239–1244.

Shi, H., Lee, B., Wu, S.-J., and Zhu, J.-K. (2003). Overexpression of a plasma membrane Na+/H+ antiporter gene improves salt tolerance in *Arabidopsis thaliana*. Nat. Biotechnol. **21**: 81–85.

Shi, H., Quintero, F.J., Pardo, J.M., and Zhu, J. (2002a). The Putative Plasma Membrane Na+ / H+ Antiporter SOS1 Controls Long-Distance Na+ Transport in Plants. **14**: 465–477.

Shi, H., Xiong, L., Stevenson, B., Lu, T., and Zhu, J.-K. (2002b). The Arabidopsis salt overly sensitive 4 mutants uncover a critical role for vitamin B6 in plant salt tolerance. Plant Cell **14**: 575–588.

Shi, Q., Ding, F., Wang, X., and Wei, M. (2007). Exogenous nitric oxide protect cucumber roots against oxidative stress induced by salt stress. Plant Physiol. Biochem. **45**: 542–550.

Shi, Y.-F., Wang, D., Wang, C., Culler, A.H., Kreiser, M. a., Suresh, J., Cohen, J.D., Pan, J., Baker, B., and Liu, J.-Z. (2015). Loss of *GSNOR1* function leads to compromised auxin signaling and polar auxin transport. Mol. Plant **8**: 1350–1365.

Shin, J.-H., Yoshimoto, K., Ohsumi, Y., Jeon, J.-S., and An, G. (2009). OsATG10b, an autophagosome component, is needed for cell survival against oxidative stresses in rice. Mol. Cells **27**: 67–74.

Shinozaki, K. and Yamaguchi-Shinozaki, K. (2007). Gene networks involved in drought stress response and tolerance. J. Exp. Bot. **58**: 221–227.

Shinozaki, K., Yamaguchi-Shinozaki, K., and Seki, M. (2003). Regulatory network of gene expression in the drought and cold stress responses. Curr. Opin. Plant Biol. **6**: 410–417.

Shkolnik-Inbar, D., Adler, G., and Bar-Zvi, D. (2013). ABI4 downregulates expression of the sodium transporter *HKT1;1* in *Arabidopsis* roots and affects salt tolerance. Plant J. **73**: 993–1005.

Shpilka, T., Weidberg, H., Pietrokovski, S., and Elazar, Z. (2011). Atg8: an autophagy-related ubiquitin-like protein family. Genome Biol. **12**: 1–11.

Sievers, F., Wilm, A., Dineen, D., Gibson, T.J., Karplus, K., Li, W., Lopez, R., McWilliam, H., Remmert, M., Söding, J., Thompson, J.D., and Higgins, D.G. (2011). Fast, scalable generation of high-quality protein multiple sequence alignments using Clustal Omega. Mol. Syst. Biol. **7**: 539.

Slavikova, S., Shy, G., Yao, Y., Glozman, R., Levanony, H., Pietrokovski, S., Elazar, Z., and Galili, G. (2005). The autophagy-associated Atg8 gene family operates both under favourable growth conditions and under starvation stresses in *Arabidopsis* plants. J. Exp. Bot. **56**: 2839–2849.

Smith, J.N. and Dasgupta, T.P. (2000). Kinetics and mechanism of the decomposition of S-nitrosoglutathione by L-ascorbic acid and copper ions in aqueous solution to produce nitric oxide. Nitric Oxide **4**: 57–66.

Spadaro, D., Yun, B.-W., Spoel, S.H., Chu, C., Wang, Y.-Q., and Loake, G.J. (2010). The redox switch: dynamic regulation of protein function by cysteine modifications. Physiol. Plant. **138**: 360–71.

Spoel, S.H. and Loake, G.J. (2011). Redox-based protein modifications: The missing link in plant immune signalling. Curr. Opin. Plant Biol. **14**: 358–364.

Stamler, J.S., Singel, D.J., and Loscalzo, J. (1992). Biochemistry of nitric oxide and its redox-activated forms. Science **258**: 1898–1902.

Stamler, J.S., Toone, E.J., Lipton, S. a., and Sucher, N.J. (1997). (S)NO signals: Translocation, regulation, and a consensus motif. Neuron **18**: 691–696.

Svenning, S., Lamark, T., Krause, K., and Johansen, T. (2011). Plant NBR1 is a selective autophagy substrate and a functional hybrid of the mammalian autophagic adapters NBR1 and p62/SQSTM1. Autophagy **7**: 993–1010.

Tada, Y., Spoel, S.H., Pajerowska-Mukhtar, K., Mou, Z., Song, J., Wang, C., Zuo, J., and Dong, X. (2008). Plant immunity requires conformational changes of NPR1 via S-nitrosylation and Thioredoxins. **321**: 952–955.

Tanida, I., Mizushima, N., Kiyooka, M., Ohsumi, M., Ueno, T., Ohsumi, Y., and Kominami, E. (1999). Apg7p/Cvt2p: A novel protein-activating enzyme essential for autophagy. Mol. Biol. Cell **10**: 1367–1379.

Tanou, G., Job, C., Rajjou, L., Arc, E., Belghazi, M., Diamantidis, G., Molassiotis, A., and Job, D. (2009). Proteomics reveals the overlapping roles of hydrogen peroxide and nitric oxide in the acclimation of citrus plants to salinity. Plant J. **60**: 795–804.

Tester, M. and Davenport, R. (2003). Na+ tolerance and Na+ transport in higher plants. Ann. Bot. **91**: 503–527.

The Arabidopsis Genome Initiative (2000). Analysis of the genome sequence of the flowering plant Arabidopsis thaliana. Nature **408**: 796–815.

Tholakalabavi, A., Zwiazek, J.J., and Thorpe, T.A. (2013). Effect of mannitol and glucose-induced osmotic stress on growth, water relations, and solute composition of cell suspension cultures of Poplar (Populus deltoides var. occidentals) in relation to anthocyanin. Vitr. Cell. Dev. Biol. plant **30**: 164–170.

Thompson, A.R., Doelling, J.H., Suttangkakul, A., and Vierstra, R.D. (2005). Autophagic nutrient recycling in *Arabidopsis* directed by the ATG8 and ATG12 conjugation pathways. Plant Physiol. **138**: 2097–2110.

Toledo, J.C. and Augusto, O. (2012). Connecting the chemical and biological properties of nitric oxide. Chem. Res. Toxicol. **25**: 975–989.

Tran, L.-S.P., Urao, T., Qin, F., Maruyama, K., Kakimoto, T., Shinozaki, K., and Yamaguchi-Shinozaki, K. (2007). Functional analysis of AHK1/ATHK1 and cytokinin receptor histidine kinases in response to abscisic acid, drought, and salt stress in Arabidopsis. Proc. Natl. Acad. Sci. **104**: 20623–20628.

Tun, N.N., Santa-Catarina, C., Begum, T., Silveira, V., Handro, W., Segal Floh, E.I., and Scherer, G.F.E. (2006). Polyamines induce rapid biosynthesis of nitric oxide (NO) in *Arabidopsis thaliana* seedlings. Plant Cell Physiol. **47**: 346–354.

Tuteja, N. and Sopory, S.K. (2008). Chemical signaling under abiotic stress environment in plants. Plant Signal. Behav. **3**: 525–536.

Uchida, A., Jagendorf, A.T., Hibino, T., Takabe, T., and Takabe, T. (2002). Effects of hydrogen peroxide and nitric oxide on both salt and heat stress tolerance in rice. Plant Sci. **163**: 515–523.

Urao, T., Yakubov, B., Satoh, R., Yamaguchi-Shinozaki, K., Seki, M., Hirayama, T., and Shinozaki, K. (1999). A transmembrane hybrid-type histidine kinase in *Arabidopsis* functions as an osmosensor. Plant Cell **11**: 1743–54.

Valderrama, R., Corpas, F.J., Carreras, A., Fernández-Ocaña, A., Chaki, M., Luque, F., Gómez-Rodríguez, M. V., Colmenero-Varea, P., del Río, L.A., and Barroso, J.B. (2007). Nitrosative stress in plants. FEBS Lett. **581**: 453–461.

Vanhee, C., Guillon, S., Masquelier, D., Degand, H., Deleu, M., Morsomme, P., and Batoko, H. (2011). A TSPO-related protein localizes to the early secretory pathway in *Arabidopsis*, but is targeted to mitochondria when expressed in yeast. J. Exp. Bot. **62**: 497–508.

Vitecek, J., Reinohl, V., and Jones, R.L. (2008). Measuring NO production by plant tissues and suspension cultured cells. Mol. Plant **1**: 270–284.

Walden, H., Podgorski, M.S., Huang, D.T., Miller, D.W., Howard, R.J., Minor, D.L., Holton, J.M., and Schulman, B.A. (2003). The structure of the APPBP1-UBA3-NEDD8-ATP complex reveals the basis for selective Ubiquitin-like protein activation by an E1. Mol. Cell **12**: 1427–1437.

Wang, P., Du, Y., Hou, Y.-J., Zhao, Y., Hsu, C.-C., Yuan, F., Zhu, X., Tao, W.A., Song, C.-P., and Zhu, J.-K. (2015). Nitric oxide negatively regulates abscisic acid signaling in guard cells by S-nitrosylation of OST1. Proc. Natl. Acad. Sci. **112**: 613–618.

Wang, Y., Chen, C., Loake, G.J., and Chu, C. (2010). Nitric oxide: Promoter or suppressor of programmed cell death? Protein Cell **1**: 133–142.

Wang, Z.Y., Xiong, L., Li, W., Zhu, J.K., and Zhu, J. (2011). The plant cuticle is required for osmotic stress regulation of abscisic acid biosynthesis and osmotic stress tolerance in *Arabidopsis*. Plant Cell **23**: 1971–1984.

Wawer, I., Bucholc, M., Astier, J., Anielska-Mazur, A., Dahan, J., Kulik, A., Wysłouch-Cieszynska, A., Zareba-Kozioł, M., Krzywinska, E., Dadlez, M., Dobrowolska, G., and Wendehenne, D. (2010). Regulation of *Nicotiana tabacum* osmotic stress-activated protein kinase and its cellular partner GAPDH by nitric oxide in response to salinity. Biochem. J. **429**: 73–83.

Welchman, R.L., Gordon, C., and Mayer, R.J. (2005). Ubiquitin and ubiquitin-like proteins as multifunctional signals. Nat. Rev. Mol. Cell Biol. **6**: 599–609.

Wilkinson, J.Q. and Crawford, N.M. (1991). Identification of the Arabidopsis CHL3 gene as the nitrate reductase structural gene *NIA2*. Plant Cell **3**: 461–471.

Wink, D.A., Miranda, K.M., Espey, M.G., Pluta, R.M., Hewett, S.J., Colton, C., Vitek, M., Feelisch, M., and Grisham, M.B. (2001). Mechanisms of the antioxidant effects of nitric oxide. Antioxid. redox Signal. **3**: 203–221.

Wright, C., Iyer, A.K. V., Kulkarni, Y., and Azad, N. (2016). S-Nitrosylation of Bcl-2 negatively affects autophagy in lung epithelial cells. J. Cell. Biochem. **117**: 521–532.

Wu, C. et al. (2011). Thioredoxin 1-mediated post-translational modifications: reduction, transnitrosylation, denitrosylation, and related proteomics methodologies. Antioxid. Redox Signal. **15**: 2565–604.

Wu, C., Liu, T., Chen, W., Oka, S., Fu, C., Jain, M.R., Parrott, A.M., Baykal, A.T., Sadoshima, J., and Li, H. (2010). Redox regulatory mechanism of transnitrosylation by thioredoxin. Mol. Cell. Proteomics **9**: 2262–2275.

Xie, Z. and Klionsky, D.J. (2007). Autophagosome formation: core machinery and adaptations. Nat. Cell Biol. **9**: 1102–1109.

Xiong, Y., Contento, A.L., and Bassham, D.C. (2005). AtATG18a is required for the formation of autophagosomes during nutrient stress and senescence in *Arabidopsis thaliana*. Plant J. **42**: 535–46.

Xiong, Y., Contento, A.L., Nguyen, P.Q., and Bassham, D.C. (2007). Degradation of oxidized proteins by autophagy during oxidative stress in *Arabidopsis*. Plant Physiol. **143**: 291–299.

Xue, Y., Liu, Z., Gao, X., Jin, C., Wen, L., Yao, X., and Ren, J. (2010). GPS-SNO: Computational prediction of protein S-nitrosylation sites with a modified GPS algorithm. PLoS One **5**: 1–7.

Yang, H., Mu, J., Chen, L., Feng, J., Hu, J., Li, L., Zhou, J.-M., and Zuo, J. (2015). S-Nitrosylation positively regulates ascorbate peroxidase activity during plant stress responses. Plant Physiol. **167**: 1604–1615.

Yang, Y., Xu, S., An, L., and Chen, N. (2007). NADPH oxidase-dependent hydrogen peroxide production, induced by salinity stress, may be involved in the regulation of total calcium in roots of wheat. J. Plant Physiol. **164**: 1429–1435.

Yang, Z. and Klionsky, D.J. (2009). An overview of the molecular mechanism of autophagy. Curr Top Microbiol Immunol. **335**: 1–32.

Yoshimoto, K., Hanaoka, H., Sato, S., Kato, T., Tabata, S., Noda, T., and Ohsumi, Y. (2004). Processing of ATG8s, ubiquitin-like proteins, and their deconjugation by ATG4s are essential for plant autophagy. Plant Cell **16**: 2967–2983.

Yu, M., Lamattina, L., Spoel, S.H., and Loake, G.J. (2014). Nitric oxide function in plant biology: A redox cue in deconvolution. New Phytol. **202**: 1142–1156.

Yu, M., Yun, B.W., Spoel, S.H., and Loake, G.J. (2012). A sleigh ride through the SNO: Regulation of plant immune function by protein S-nitrosylation. Curr. Opin. Plant Biol. **15**: 424–430.

Yuan, F. et al. (2014). OSCA1 mediates osmotic-stress-evoked Ca2+ increases vital for osmosensing in <i>Arabidopsis<i>. Nature **514**: 367–71.

Yun, B.-W., Feechan, A., Yin, M., Saidi, N.B.B., Le Bihan, T., Yu, M., Moore, J.W., Kang, J.-G., Kwon, E., Spoel, S.H., Pallas, J. a., and Loake, G.J. (2011). S-nitrosylation of NADPH oxidase regulates cell death in plant immunity. Nature **478**: 264–268.

Zemojtel, T., Fröhlich, A., Palmieri, M.C., Kolanczyk, M., Mikula, I., Wyrwicz, L.S., Wanker, E.E., Mundlos, S., Vingron, M., Martasek, P., and Durner, J. (2006). Plant nitric oxide synthase: a never-ending story? Trends Plant Sci. **11**: 524-5-8.

Zhang, A., Zhang, J., Zhang, J., Ye, N., Zhang, H., Tan, M., and Jiang, M. (2011). Nitric oxide mediates brassinosteroid-induced ABA biosynthesis involved in oxidative stress tolerance in maize leaves. Plant Cell Physiol. **52**: 181–192.

Zhang, C., He, P., Yu, Z., Du, D., and Wei, P. (2010). Effect of exogenous Ca2+ and NO donor SNP on seed germination and antioxidase activities of <i>Perilla frutescens<i> seedlings under NaCl stress. J. Chinese Mater. medica **35**: 3114–3119.

Zhang, F., Wang, Y., Yang, Y., Wu, H., Wang, D., and Liu, J. (2007). Involvement of hydrogen peroxide and nitric oxide in salt resistance in the calluses from *Populus euphratica*. Plant, Cell Environ. **30**: 775–785.

Zhang, Y., Wang, L., Liu, Y., Zhang, Q., Wei, Q., and Zhang, W. (2006). Nitric oxide enhances salt tolerance in maize seedlings through increasing activities of proton-pump and Na+/H+ antiport in the tonoplast. Planta **224**: 545–555.

Zhao, L., Zhang, F., Guo, J., Yang, Y., Li, B., and Zhang, L. (2004). Nitric oxide functions as a signal in salt resistance in the calluses from two ecotypes of reed. Plant Physiol. **134**: 849–857.

Zhao, M.-G., Tian, Q.-Y., and Zhang, W.-H. (2007). Nitric oxide synthase-dependent nitric oxide production is associated with salt tolerance in Arabidopsis. Plant Physiol. **144**: 206–217.

Zheng, C., Jiang, D., Liu, F., Dai, T., Liu, W., Jing, Q., and Cao, W. (2009). Exogenous nitric oxide improves seed germination in wheat against mitochondrial oxidative damage induced by high salinity. Environ. Exp. Bot. **67**: 222–227.

Zhou, J., Wang, J., Cheng, Y., Chi, Y.J., Fan, B., Yu, J.Q., and Chen, Z. (2013). NBR1-mediated selective autophagy targets insoluble ubiquitinated protein aggregates in plant stress responses. PLoS Genet. **9**: 1–19.

Zhou, J., Wang, J., Yu, J.-Q., and Chen, Z. (2014a). Role and regulation of autophagy in heat stress responses of tomato plants. Front. Plant Sci. **5**: 174.

Zhou, J., Zhang, Y., Qi, J., Chi, Y., Fan, B., Yu, J.Q., and Chen, Z. (2014b). E3 Ubiquitin ligase CHIP and NBR1-mediated selective autophagy protect additively against proteotoxicity in plant stress responses. PLoS Genet. **10**: 1–18.

Zhu, J.K. (2001). Plant salt tolerance. Trends Plant Sci. **6**: 66–71.

Zhu, J.K. (2002). Salt and drought stress signal transduction in plants. Annu. Rev. Plant Biol. **53**: 247–273.

Ziogas, V., Tanou, G., Filippou, P., Diamantidis, G., Vasilakakis, M., Fotopoulos, V., and Molassiotis, A. (2013). Nitrosative responses in citrus plants exposed to six abiotic stress conditions. Plant Physiol. Biochem. **68**: 118–126.

Zmijewski, J.W., Banerjee, S., Bae, H., Friggeri, A., Lazarowski, E.R., and Abraham, E. (2010). Exposure to hydrogen peroxide induces oxidation and activation of AMP-activated protein kinase. J. Biol. Chem. **285**: 33154–33164.